Beatriz Gomes
da Silva Aleixo

Modelação do Jet Lag e Otimização da Fototerapia para a Recuperação do Jet Lag

Modelling Jet Lag and Light Therapy Optimisation for Jet Lag Recovery

Universidade de Aveiro
2023

Beatriz Gomes
da Silva Aleixo

Modelação do Jet Lag e Otimização da Fototerapia para a Recuperação do Jet Lag

Modelling Jet Lag and Light Therapy Optimisation for Jet Lag Recovery

"*Science is not limited to laboratories and equations; it is a way of seeing and understanding the world, and its wonders are accessible to all.*"

— Rachel Carson

Universidade de Aveiro
2023

Beatriz Gomes da Silva Aleixo

Modelação do Jet Lag e Otimização da Fototerapia para a Recuperação do Jet Lag

Modelling Jet Lag and Light Therapy Optimisation for Jet Lag Recovery

Dissertação apresentada à Universidade de Aveiro para cumprimento dos requisitos necessários à obtenção do grau de Mestre em Engenharia Computacional, realizada sob a orientação científica do Doutor José Mendes, Professor Catedrático do Departamento de Física da Universidade de Aveiro, e do Doutor Alexander Goltsev, Investigador Auxiliar do Departamento de Física da Universidade de Aveiro.

Dedico este trabalho ao João, desejando que a sua paixão pela neurociência o motive para seguir os seus sonhos.

o júri / the jury

presidente / president

Professor Doutor Luis Filipe Mesquita Nero Moreira Alves
Professor Auxiliar, Departamento de Eletrónica, Telecomunicações e Informática, Universidade de Aveiro

vogais / examiners committee

Doutora Joana Ribeiro Barbosa Cabral
Investigadora Auxiliar, Instituto de Investigação em Ciências da Vida e Saúde, Universidade do Minho

Professor Doutor José Fernando Ferreira Mendes
Professor Catedrático, Departamento de Física, Universidade de Aveiro

agradecimentos / acknowledgements

I would like to thank my supervisors, José Mendes, Alexander Goltsev and Sooyeon Yoon for accepting me to be a part of this fantastic project. Namely, a thank you to Sooyeon, for the long discussions about the core-shell model and the simulations, and for the reassurance and guidance when I felt lost. A thank you to José Mendes and Alexander Goltsev for the numerous discussions of my results and doubts, as well as for giving me opportunities to share my work with the public, meet researchers in my area and advise me on my talks. All of you showed me an incredible availability, even from miles away.

This project also gave me new friends as I was included in the group of complex systems. I would like to especially thank Guilherme for letting me use his lab computer for my simulations and for the patient explanations. Chaoyang, Filipe, Guilherme and Hanieh, thanks for the companionship and funny moments. Wherever I end up working in the future, I hope I can find the same heart-warming environment as you gave me.

Agradeço à minha família por me dar sempre o conforto necessário para viver uma vida sem preocupações. Agradeço, também, pelos seus grandes conselhos e motivação. Agradeço, especialmente, à minha mãe, pelos ensinamentos sobre a escrita científica e estrutura da dissertação. Se não fosse ela, ainda agora estaria a stressar com os capítulos e as referências.

Queria agradecer, também, ao João, pelo apoio incondicional e pelas constantes palavras de motivação e amor.

Por fim, agradeço aos meus amigos, Ana, Catarinas, Mendonça, Bernardo e João pelos galões no DEMaC, pelos piqueniques, pelo mútuo apoio nesta última fase dos nossos estudos e pelos bons momentos. Agradeço, também, à Dalila e à Rita, amigas de longa data, que mesmo longe estão sempre perto.

Palavras Chave

regra de Aschoff, ritmos circadianos, *entrainment*, *jet lag*, modelo de Kuramoto, fototerapia, tempo de recuperação, núcleo supraquiasmático, sincronização

Resumo

O núcleo supraquiasmático (SCN) do cérebro mamífero gera os nossos ritmos circadianos e sincroniza os nossos processos biológicos com as variações diárias de luz. No entanto, viagens rápidas para diferentes fusos horários podem dessincronizar os neurónios do SCN e perturbar os ritmos circadianos, causando sintomas de *jet lag*. O mecanismo do *jet lag* e o papel das duas regiões do SCN, o *core*, região ventral, e o *shell*, região dorsal, continuam por esclarecer e o seu estudo é crucial para encontrar novos tratamentos para o *jet lag*. A exposição à luz intensa (fototerapia) é uma terapia eficaz contra o *jet lag*, mas o seu impacto no SCN ainda não foi totalmente compreendido. Para resolver estas questões, o *jet lag* foi modelado com o modelo *core-shell* do SCN, baseado no modelo de Kuramoto. Assumiu-se que a recuperação do *jet lag* é equivalente à ressincronização do SCN ao ciclo de luz exterior. Verificou-se que o *core* do SCN recupera mais rapidamente do que o *shell*. Ao analisar o espaço de estados dos osciladores do SCN, foi encontrada uma região de dinâmica lenta. Uma vez nesta zona, o sistema demora muito tempo a deixá-la. Esta região é, portanto, responsável por uma longa adaptação após viagens para este, particularmente através de 8 fusos horários, em comparação com viagens para oeste. De seguida, a fototerapia foi também modelada para deslocações através de 6/8 fusos horários para este/oeste. Foi demonstrado que uma intensidade ou duração dos períodos de luz suficientemente longas podem ser mais prejudiciais do que benéficas para acelerar a recuperação do SCN. Os resultados sugerem que a fototerapia com intensidade ou duração moderada da luz diminui o tempo de recuperação após uma deslocação para este, mas não para oeste. Dois protocolos de terapia (uma sessão e várias sessões) foram também considerados. Assim, os protocolos com os parâmetros ótimos de intensidade da luz, duração e número de sessões para a obtenção do mínimo tempo de recuperação foram obtidos. Concluiu-se que a fototerapia é personalizável, assegurando que o indivíduo pode escolher os seus parâmetros de acordo com as suas necessidades. Os resultados deste estudo alinham-se qualitativa e quantitativamente com os dados existentes para humanos e ratinhos. Concluindo, este estudo é uma contribuição relevante para o estudo do *jet lag*, abrindo caminho para o uso generalizado da fototerapia nos cuidados de saúde modernos.

Keywords Aschoff's rule, circadian rhythms, entrainment, jet lag, Kuramoto model, light therapy, recovery time, suprachiasmatic nucleus, synchronisation

Abstract

The suprachiasmatic nucleus (SCN) in the mammalian brain generates our circadian rhythms and synchronises our biological processes with daily light variations. However, rapid time zone travelling can desynchronise the SCN neurons and disrupt the circadian rhythms, causing jet lag symptoms. The mechanism of jet lag and the role of the two regions of the SCN, the core and shell, remain unclear and its study is crucial to find new jet lag treatments. Bright light exposure is an efficient jet lag therapy, but its impact on the SCN is not yet fully understood. To solve these issues, jet lag was modelled with the core-shell model of the SCN, based on the Kuramoto model. It was assumed that jet lag recovery is equivalent to the resynchronisation of the SCN to the exterior light cycle. It was found that the core region of the SCN recovers faster than the shell region. While analysing the space of states of the SCN oscillators, it was found a region of slow dynamic states. Once in this area, the system takes a long time to leave it. This region is, thus, responsible for a long adaptation after eastward travelling, particularly across 8 time zones, compared to westward travelling. Then, light therapy was also modelled, considering the 6/8h eastward/westward time shifts. It was shown that a sufficiently long duration or high intensity of light pulses can be more detrimental than beneficial for speeding up the recovery of the SCN. The findings suggest that light therapy with moderate duration or intensity decreases the recovery time after travelling east but not west. Two light treatment protocols (one-session and multi-session) were also considered. Thus, the protocols with optimal light intensity, duration and number of sessions giving the lowest recovery time were obtained. It was concluded that light therapy is customisable, ensuring the individual can choose the light therapy parameters according to their needs. The results of this study align qualitatively and quantitatively with existing data for humans and mice. All in all, this work is a relevant contribution to jet lag research, paving the way for the widespread use of light therapy in modern healthcare.

Contents

List of Figures

List of Tables

Glossary

AVP	arginine vasopressin
BMAL1	brain and muscle ARNT-like 1
CBTmin	minimum core body temperature
CLOCK	circadian locomotor output cycles kaput
CRY	cryptochrome
DD	dark-dark
DLMO	dim light melatonin onset
GABA	gamma-aminobutyric acid
ipRGC	intrinsically photosensitive retinal ganglion cell
LD	light-dark
LL	light-light
LT	light therapy
Per	period
PRC	phase-response curve
R2	R-squared
RHT	retinohypothalamic tract
SAD	seasonal affective disorder
SCN	suprachiasmatic nucleus
VIP	vasoactive intestinal peptide

CHAPTER 1

Introduction

The Earth's rotation takes approximately 24 h to complete, resulting in unique conditions such as light and dark, humidity, and temperature cycles. To ensure habitability on this special planet, living organisms have evolved to be capable of almost "predicting the future" by anticipating changes in the environment and actively adapting to them. This property derives from a developed sense of time that optimises biological processes, from the cellular machinery to sleep, within 24 h. This periodic biological variation is referred to as "circadian rhythm" (Evans and Silver, 2015; Karatsoreos and Silver, 2017; Silver, 2018).

In mammals, the circadian rhythms are mainly dictated by a master biological clock. Since the brain is the central hub for information integration and control, it is not surprising that our master clock is located in this extraordinary organ. Indeed, the suprachiasmatic nucleus (SCN), one of the nuclei of the hypothalamus in the mammalian brain, is the main structure responsible for the regulation of circadian rhythms. In perspective, the size of the human SCN is about 1 mm, the same size as a poppy seed, and it has approximately $100,000$ neurons (Hofman, 2009; T. Nakamura et al., 2016). The number of neurons in the human brain is about 100 billion (Herculano-Houzel, 2009). Therefore, the human SCN has only $10^{-4}\%$ of the total number of neurons. Despite this small size, the SCN coordinates the rhythms of the cells in the human body!

1.1 How the Body Keeps Track of Time

The neurons of the SCN exhibit the remarkable property of producing endogenous rhythms, that is, self-sustained oscillations of the molecular processes that keep them alive and functioning properly. These oscillations are driven by rhythmic changes in gene expression. That is, circadian rhythms are encoded in our DNA. Each SCN neuron has its own rhythm, close to 24 h, although our physiological and behavioural processes exhibit a single rhythm. Its generation is achieved through the coupling between SCN neurons, as they communicate signals via synapses, synchronising the cellular rhythms in the SCN neuronal network. These signals are then communicated with the whole organism (Figure 1.1) (Evans and Silver, 2015; Herzog, 2007; Silver, 2018).

The SCN is a bilateral structure that has two lobes, each one having a ventral or core region enclosed by a dorsal or shell region. The functional separation between core and shell comes from neurochemical and anatomical differences, for example, the core receives signals about the exterior light-dark (LD) cycle from the retina (Evans and Silver, 2015)).

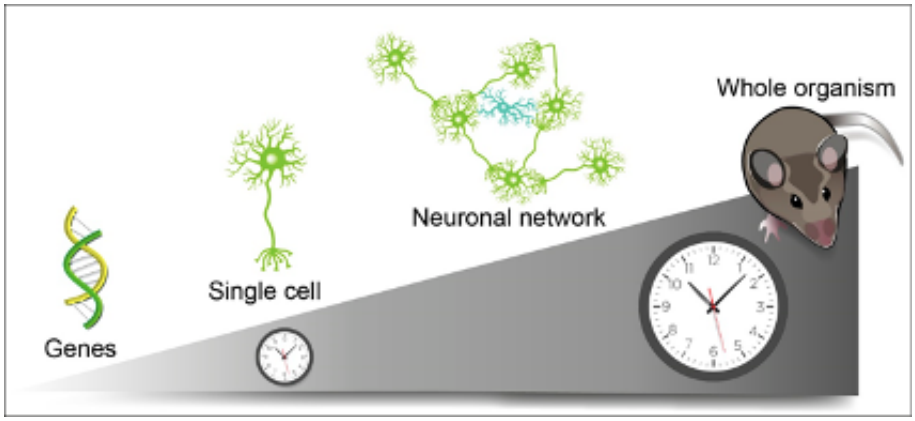

Figure 1.1: Within each cell, self-sustaining circadian rhythmicity emerges from a genetically encoded clock. Intercellular coupling in the SCN results in a robust and precise circadian pacemaker that influences circadian rhythms throughout the body. Green and blue cells represent SCN neurons and astrocytes, respectively. Adapted from Hussein et al., 2019.

Thus, the role of the core in the SCN is to send signals synchronised by external light cues to the shell, having a leading role in the synchronisation of the SCN. Regarding the role of the shell, there is significant experimental evidence that, after SCN desynchronisation, peripheral tissues maintain synchronisation with the shell, but not the core. This suggests that the shell communicates with downstream tissues, allowing them to synchronise their processes with the LD cycles (Evans et al., 2015; Nagano et al., 2003).

After the discovery of the mechanism of circadian rhythm generation, mathematicians and physicists began to develop models that could represent these neurons as self-sustaining oscillators and the network-emerging synchronisation processes (Asgari-Targhi and Klerman, 2019; Lara-Aparicio et al., 2006). By being able to model circadian rhythms, one could finally understand how synchronisation of the circadian system occurs, and, in particular, the role of light on the SCN neuronal network properties (Forger et al., 1999; Goltsev et al., 2022; Kronauer et al., 1982), the coupling differences within the SCN (Gu et al., 2016; Taylor et al., 2017), as well as how this nucleus adapts after a phase shift in the LD cycle, e.g., when people travel to different time zones (Lu et al., 2016) or when they work in shifts.

1.2 Jet Lag Disrupts the Circadian Rhythms

It is noteworthy that light is the main external cue that sets the pace of our internal functions. The synchronisation process to an external cue, such as external light, is called entrainment (Evans and Silver, 2015; Li and Androulakis, 2021). After a phase shift in the LD cycle, the circadian system becomes desynchronised in relation to it. Namely, when individuals travel across multiple time zones, work in shifts at night, or even when there is a change from summer to winter timing and vice-versa, the body initiates an effort to reentrain. This reentrainment is reflected in the amount of time that the body takes to resynchronise with the external light (Nagano et al., 2003), leading to the jet lag condition, i.e., the experience of symptoms like gastrointestinal distress, fatigue, sleeping disturbances and cognitive dysfunction (Eastman and Burgess, 2009; Karatsoreos and Silver, 2017).

Jet lag is a major concern for people who travel constantly, such as pilots, athletes, business people, politicians and even astronauts. Continuous jet lag can lead to increased risk of cancer, type II diabetes, obesity, stroke and all-cause mortality, making it a major public health concern (Evans and Silver, 2015; Karatsoreos and Silver, 2017). Therefore, it is critical to develop treatments that fully or partially reduce the recovery time.

Jet lag treatments should take into account that one normally recovers from jet lag after eastward travels through phase advancing one's circadian system. This is because eastward time zones are advanced in time in relation to the traveller. In contrast, from jet lag after westward travels, one normally recovers through phase delaying since westward time zones are delayed in time in relation to the traveller. It should also be considered that eastward travels yield longer jet lag than westward travels (Eastman and Burgess, 2009; Lu et al., 2016). This is very commonly reported by travellers and might be due to the fact that our circadian clock has a periodicity larger than 24 h - 24.2 h, approximately - which means that the human's circadian system slightly delays each day, making it harder to advance than to delay (Eastman and Burgess, 2009). This east-west asymmetry in recovery times has been reproduced by mathematical models (Diekman and Bose, 2018; Gundel and Spencer, 1999; Lu et al., 2016). Unfortunately, these models do not take into account the SCN anatomical and functional division in the core and shell regions.

Some already-developed treatments rely on melatonin ingestion, a sleep-related hormone or performing physical exercise at certain times of the day. Because light is the most influential external cue in the circadian system, it is not surprising that light can also be a form of jet lag therapy (Arendt, 2018; Morgenthaler et al., 2007; Roach and Sargent, 2019).

Fortunately, nowadays, after bridging a few gaps in the knowledge of jet lag's mechanism, research in modern chronobiology and experimental and computational neuroscience will be able to devise creative and trustworthy strategies to reduce jet lag symptoms.

1.3 Light as an Effective Jet Lag Therapy

Light therapy is the use of bright light at a specific time of the day and for a predetermined duration to effectively shift the phase of the circadian system. It can be used to reduce the winter blues, or, more scientifically, the seasonal affective disorder (SAD), improve sleep patterns and minimise jet lag (Lucimed, 2023; Philips, 2023). It is the promise of these goals that has driven the commercialisation of light therapy in the form of light boxes, visors or lamps (Lucimed, 2023; ORTOREX, n.d.; Philips, 2023). Even mobile applications have been developed with the sole purpose of providing the best light therapy protocol for a user's specific travelling needs (Ng, 2023; Sleepopolis Team, 2023; Timeshifter, 2023). These light therapy applications are based on some experimental studies of how light intensity, duration and timing affect the circadian rhythms. Despite this, the number of experimental studies of light therapy is still reduced, and they have only tested a small range of light intensities and durations since the experiments are very time-consuming and expensive. Therefore, although the commercialised treatments may work, it is hard to believe that the optimal parameters are being used - there is a clear lack of studies on a wide range of light therapy parameters. Furthermore, there is an absolute need for standardised light therapy procedures that are specialised to treat jet lag since the majority of the commercialised light therapy objects do not exist to specifically treat this condition. This is where mathematical and computational modelling can help: a wide range of parameters can be tested by applying light therapy to accurate models of the human circadian system.

To find the optimal parameters of light therapy to minimise jet lag, it is also important to understand what the effect of bright light on our circadian system is. Fortunately, this issue has been brought into question a long time ago by Aschoff (1960), one of the fathers of chronobiology. He created a set of three rules which he derived from his experimental observations. The Aschoff's first rule is of great importance in understanding the potential role of bright light as a jet lag therapy: in diurnal animals, like humans, constant light increases the frequency of the circadian rhythms when in the absence of external cues and, the brighter the light, the larger that increase is (Beaulé, 2008). Curiously, few studies aiming

at understanding the molecular mechanisms of this rule have been developed (Muñoz et al., 2005; Prabhat et al., 2020).

Mathematical modelling is very important in the context of understanding light therapy since the system in hands demonstrates complex multi-cellular dynamics and emergent properties (Kori et al., 2017). The generation of hypothetical light treatments might lead to further experimental tests and raise other theoretical hypotheses about the role of light in the entrainment of our biological rhythms to the environment. The formulation of light treatments may also help in the interpretation of further biomedical data. The most important goal is, perhaps, aiding the medical industry in the development of technologies that provide trustworthy treatments using light.

1.4 The Kuramoto Model of SCN Synchronisation

The SCN neurons exhibit oscillatory behaviour, characterised by rhythmic molecular processes (Herzog, 2007). The classification of SCN neurons as oscillators was initially proposed by Colin Pittendrigh, one of the fathers of chronobiology, like Aschoff (Evans and Silver, 2015). Clock cells within the SCN exhibit nearly sinusoidal oscillations that persist without external forces, making them amenable to modelling as weakly nonlinear oscillators with a stable limit cycle, since the behaviour of the system settles into a repeating and bounded pattern.

In 1975, Kuramoto first introduced a model capable of describing the process of synchronisation in a large system of coupled self-sustaining oscillators. This model allows the introduction of an external force parameter, that can drive the synchronisation of the network (Strogatz, 2000). In summary, the Kuramoto model explains that if the oscillators are characterised only by their phase, then synchronisation in the network is driven by the phase differences of each pair of oscillators. For example, if one oscillator is slightly advanced in phase relative to another, it will slow down and the other will accelerate to reduce the phase difference between them - it is a joint effort for synchronisation (Strogatz, 2000, 2015).

By now, the reader might be correctly guessing: the Kuramoto model takes into account all peculiarities of the SCN neuronal network, being able to describe it and even include the effect of the external light field, whose signals are sent from the retina and received by the core neurons. This model also takes into account the heterogeneity of the network, i.e., the number of groups of oscillators. In this case, one can model the core and shell regions of the SCN and their differences in intra- and intercouplings. These regional differences in the SCN are extremely important for the emergence of circadian rhythms, driving extensive research into how the SCN operates (Evans and Silver, 2015; Evans et al., 2015; Silver, 2018).

In summary, the Kuramoto model is the basis for the model used in this work, the core-shell model, which represents the SCN under the effects of jet lag and light therapy, for eastward and westward travel. This way, it is possible to address existing gaps in our current understanding of the mechanism of jet lag and light therapy on the SCN, the differences between eastward and westward travelling, the role of the core-shell organisation and the optimal parameters of light therapy for the shortest recovery from jet lag. The Kuramoto model has been previously validated by some works in the field of chronobiology to explain certain phenomena (Gu et al., 2016; Lu et al., 2016; Rohling et al., 2011). The present work is based on a study by Goltsev et al., 2022, which aimed to establish the boundaries between entrainment and free-running activity, as well as to demonstrate the potential for dissociation (the emergence of a second rhythm in the SCN) and the SCN's anticipation of future events. They also showed that their results under constant light conditions were consistent with Aschoff's first rule. Since light therapy can be thought of as a period of constant light, this

rule will be extremely important in this work to understand the effects of light therapy on the SCN.

1.5 Objectives and Structure of the Dissertation

The main objectives of this work are to **1**) understand the jet lag recovery process of the SCN and **2**) understand the effectiveness of light therapy in facilitating the adaptation of the SCN to a new time zone.

The specific objectives for the first part of the work are the following:

1) Model recovery after rapid travelling within the core-shell model of the SCN;
2) Obtain the core and shell recovery times from jet lag for the phase shifts from 12 h westward to 12 h eastward in 1 h intervals and compare with experimental results and
3) Understand the differences in recovery between eastward and westward travelling.

The specific objectives for the second part of the work are the following:

1) Model light therapy with the core-shell model;
2) Study the influence of light intensity, therapy duration and multi-session therapy and
3) Find optimal parameters of light therapy to minimise jet lag recovery time for the phase shifts of 6 h eastward/westward and 8 h eastward/westward.

This dissertation is organised into six chapters. The first and present one is a general introduction, stating some background on the theme, the motivation for this work and its objectives. Chapter 2 presents some theoretical foundations on circadian rhythms, the role of the SCN in the regulation of said rhythms, jet lag and already-existing light therapy strategies. Chapter 3 reviews existing models of the circadian system, the SCN and jet lag and presents the Kuramoto model, used in this work. Chapter 4 describes the methodology used by explaining the core-shell model, how the simulations were made and how to interpret the results. In this chapter, jet lag results are also presented and discussed. Chapter 5 introduces the methodology for including light therapy in the simulations and describes some results on its influence on the SCN and their discussion. The final chapter, Chapter 6, presents a general discussion of the results, a general conclusion for this work, some limitations and future directions for improvement.

CHAPTER 2

Regulation of the Biological Clock

2.1 Circadian Rhythmicity

Most of our biological processes are periodic and this characteristic greatly contributes to their optimal efficiency. This periodicity is known as the circadian rhythm and plays a crucial role in the survival of most living beings on our planet, namely multicellular organisms and cyanobacteria. It is close to 24 h and corresponds to the periodicity of the Earth's rotation on its axis. This is in the origin of the term "circadian": it comes from the Latin "circa dies", meaning "about a day" (Evans and Silver, 2015; Karatsoreos and Silver, 2017; Silver, 2018).

The biological processes which require this periodicity encompass everything from sleep regulation to the cellular machinery, as well as hormone secretion, metabolism, and the immune response. The circadian system coordinates the rhythm of these processes (Evans and Silver, 2015). This rhythm is endogenous, meaning it is produced by the body, and is self-sustaining, meaning it persists even when external timing cues are not perceived, such as when the light is absent or constant. Under these conditions, the circadian system is disrupted but has an intrinsic frequency. Thus, it is still capable of maintaining a period not equal to, but slightly longer than 24 h. In this case, it is said to be "free-running" (Evans and Silver, 2015; Hastings et al., 2019; Silver, 2018).

Several aspects of our modern life can be disruptive of the circadian rhythms, such as irregular sleep patterns, shift work or jet lag. In these cases, external (and even internal) cues can have a resetting influence on the circadian timing of the body, being capable of synchronising the rhythms to a 24 h pattern. Curiously, because the periodicity of humans' circadian rhythms is not exactly 24 h, they need to be corrected every day (Evans and Silver, 2015). This correction process that enables resynchronisation of the rhythms to external cues is called "re-entrainment". The external cues that are capable of entraining the circadian rhythms are called "*zeitgebers*", which means, in German, "timegivers". Some external cues are light, temperature and humidity changes, and even the timing of social interactions. Nevertheless, the most influential *zeitgeber* is light for most living beings with circadian rhythmicity (Hastings et al., 2019; Karatsoreos and Silver, 2017).

However, not only changes in the external lighting conditions disrupt the circadian system - psychiatric disorders, obesity and metabolic syndromes can be also disruptive. Curiously, the vice-versa also occurs: these causes of disturbance might be symptoms of permanent circadian disruption. When the circadian disturbance is temporary, it can also cause dysfunction in the body, like sleep disturbance and gastric dysfunctions or even changes in the emotional and cognitive functions, characterised by difficulty concentrating or remembering and learning

(Karatsoreos and Silver, 2017). The pace of adaptation of an individual is set by the pace of adaptation of their body tissues. Each tissue has a different recovery rate - for example, it has been shown that the thymus and lungs take only 3 days to adapt to a phase advance of 6 h, while the spleen and esophagus take 5 days to entrain. The extended duration required for the spleen to entrain has been associated with the possibility of the immune system becoming susceptible to phase-shift-related morbidity (Davidson et al., 2009).

2.2 Suprachiasmatic Nucleus: the Master Biological Clock

Since the brain is the centre of information integration and control, it is not surprising that the circadian rhythms are, to some extent, controlled by the brain. Therefore, after the discovery that the body has a timekeeping system, the search began for the brain structure responsible for its control. In the 1970s, it was discovered that this brain structure was a small nucleus of the hypothalamus in mammals, the SCN (Evans and Silver, 2015).

2.2.1 The SCN as a Network of Oscillators

The human SCN is a network of about $100,000$ neurons which are often referred to as "oscillators" since they show cyclic changes in their physiological processes (Herzog, 2007). This description was first proposed by Colin Pittendrigh, one of the fathers of chronobiology. Later, in the 60s, Arthur Winfree, proposed that the biological clock could be mathematically modelled by a limit-cycle oscillator (Evans and Silver, 2015). This type of oscillator represents the behaviour of a system that has settled into a repeating pattern without the need for any exterior force (Strogatz, 2015). The cyclic changes of SCN neurons have an intrinsic frequency, close to 24 h, which varies from neuron to neuron. This has been observed experimentally when SCN neurons are disconnected from the network. However, within the SCN network, each neuron forms between 300 and 1,000 connections with other neurons, meaning they are densely interconnected (Varadarajan et al., 2018). Thus, the network can be considered fully connected (Goltsev et al., 2022). These connections are made through electrochemical signals: the stronger the firing signals, the stronger the coupling between the oscillators. Because of these connections, the SCN has an average period of circadian rhythm, effectively functioning as a synchronised network of oscillators (Evans and Silver, 2015). This synchronisation process can be observed in many other real-world examples, like the synchronisation of power grids and the flashing lights of fireflies in Southern Asia (Strogatz, 2015). Fortunately, physics and mathematics can explain this phenomenon and models have been developed to simulate this process.

The SCN shows plasticity in the connections between neurons. When external conditions change, the network can undergo rearrangements in its spatiotemporal organisation. These rearrangements correspond to the network's adaptation to the external conditions. For example, when people travel across several time zones, they experience jet lag symptoms, which occur due to the time that the entire network takes to adapt to the new conditions (Karatsoreos and Silver, 2017).

The self-sustaining circadian rhythms occur in the cells of the SCN, but it was discovered that they also occur in most of the body's cells, known as "peripheral clocks", which form the peripheral tissues. Although these cells are able to generate rhythms, they are not able to generate sustained rhythms: without an external force, the rhythms weaken over time as the cells go out of phase with each other. Therefore, the circadian signals formed in the SCN network of oscillators are sent to peripheral tissues. If this did not happen, most of these cells would not be able to synchronise with nearby cells (Evans and Silver, 2015). The SCN is then referred to as the master biological clock: it sets the frequency and phase of peripheral intracellular rhythms and enables synchrony within the network. The structure of

the circadian system is, thus, considered to be hierarchical: the mammalian master circadian clock, the SCN, controls the rhythms generated by peripheral clocks (Evans et al., 2015; Silver, 2018). This description fits well with experimental evidence, for example, when isolated from the SCN, circadian oscillations generated by the peripheral cells began to attenuate within a week, whereas the isolated SCN showed persistent oscillations in firing activity for over a year (Herzog, 2007; Karatsoreos and Silver, 2017; Silver, 2018). Despite this, some studies have shown that there are more structures that show persistent circadian rhythms independent of the SCN, such as the retina and olfactory bulb (Herzog, 2007; Karatsoreos and Silver, 2017), and also that light may directly influence peripheral clocks despite the SCN (Husse et al., 2015). However, the central role of the SCN in the timekeeping function of the body cannot be denied, hence it is important to understand its properties and how its function arises.

2.2.2 Anatomy of the SCN

The SCN is located in the hypothalamus, above the optic chiasm. Figure 2.1 shows the relative location of the SCN in the brain. It is a bilateral structure, meaning that it has two lobes, one on each side of the third ventricle. SCN neurons make most of the connections with other SCN neurons, but can also connect with other surrounding neuronal structures. Each lobe can be further divided into two groups of neurons, the core or ventrolateral region and the shell or dorsomedial region, that surrounds the core. These two regions have different input and output connections and neurochemical properties, i.e., the core and shell neurons produce different neurotransmitters/neuropeptides (Figure 2.2). These differences establish different functional properties for the core and shell (Evans and Silver, 2015; Silver, 2018).

The circadian system of the SCN has three components: the input pathways that send information about internal and external changes to the SCN from various sources, the SCN itself and the output pathways that send circadian signals to other tissues.

There is one main input pathway that leads information to the SCN, having a denser innervation with the core region than with the shell: the retinohypothalamic tract (RHT). The SCN has several input pathways, conveying non-photic information, like locomotor activity and arousal changes, but the RHT is particularly involved in the transmission of information about the external LD cycle from the retina to the SCN (Figure 2.2). The core neurons that are sensitive to light are also influenced by circadian information provided by other parts of the body, like gonadal hormones. In addition, feeding-related and metabolic signals can also influence circadian rhythms (Karatsoreos and Silver, 2017). Since photic input is the most influential in SCN neurons (Silver, 2018), the process of receiving and transmitting light information will be discussed in detail in Section 2.2.4.

In terms of output pathways, the SCN sends signals to spatially close structures in the hypothalamus and thalamus, but their projections have differences, for example in density and/or pattern (Evans and Silver, 2015). It has been experimentally proven that the SCN region which primarily sends timing cues to other brain regions is the shell (Evans et al., 2015). Some of those regions project signals to peripheral clocks. Furthermore, the same study found that the shell also directly sets the phase of peripheral clocks. The SCN can control some peripheral tissues indirectly by influencing hormone production, body temperature, and/or locomotor activity rhythms (Evans and Silver, 2015).

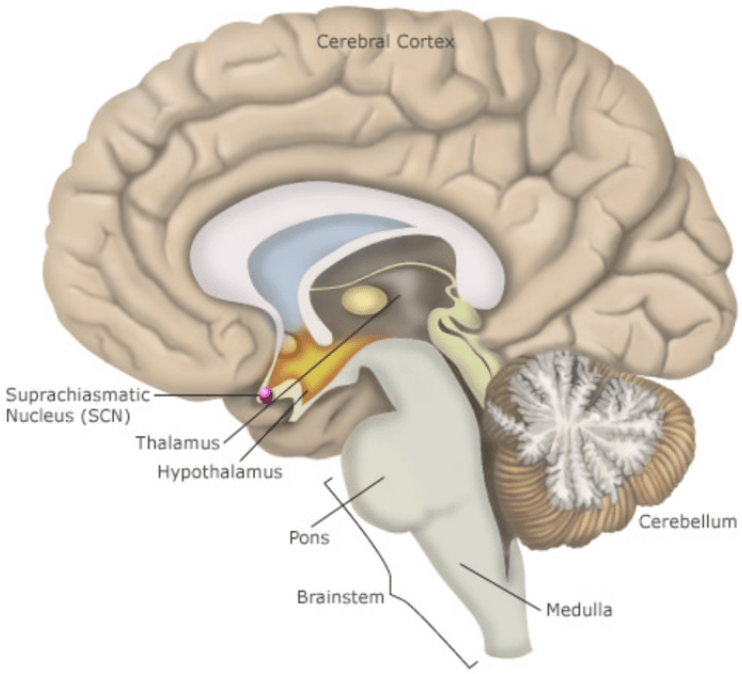

Figure 2.1: Relative location of the SCN in the brain. Adapted from Juda, 2010.

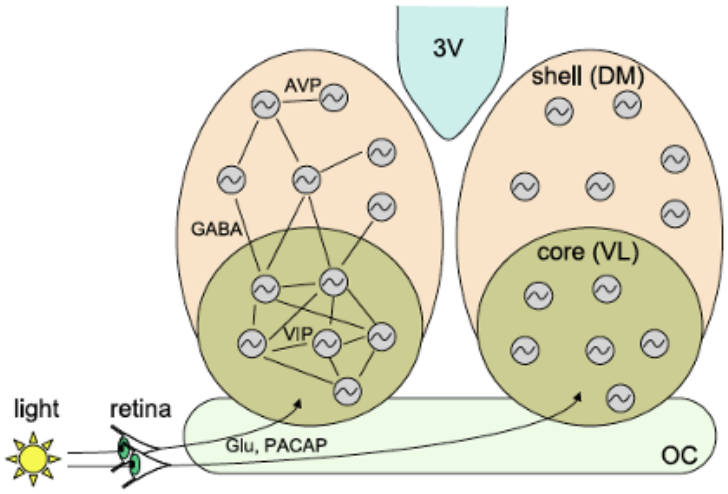

Figure 2.2: The SCN is located above the optic chiasm (OC) and has two lobes separated by the third ventricle (3V). Each one is divided into the core (ventrolateral region or VL) and the shell (dorsomedial region or DM). Core neurons produce more abundantly VIP and GABA and the shell, AVP and GABA. The core region receives light cues from the retina through the RHT. This transmission process is influenced by glutamate (Glu) and pituitary adenylate cyclase-activating polypeptide (PACAP). Adapted from Hafner et al., 2012.

2.2.3 Molecular Mechanism of Circadian Rhythms Generation

The mechanism of generation of circadian rhythms starts with the generation of molecular rhythms within each SCN neuron through transcriptional-translational feedback loops. This means that, within each neuron, there are gene transcription and translation loops that produce important proteins for the regulation of the loops. These genes are called clock genes. As mentioned before, the self-sustaining circadian rhythms at the cellular level occur in the SCN cells as well as in other brain structures, such as thalamic nuclei, amygdala and cerebellum (Evans and Silver, 2015) and in organs and tissues, such as the heart, adipose tissue, liver, skeletal muscle, adrenal and thyroid glands (Figure 2.3) (Evans and Silver, 2015; Herzog, 2007; Karatsoreos and Silver, 2017).

Figure 2.4 shows simple models of the molecular genetic loop that occurs in the SCN core and shell neurons. It is a negative feedback loop, meaning it is based on patterns of activation and self-repression (2.4, a)). Essentially, the binding of circadian locomotor output cycles kaput (CLOCK) with brain and muscle ARNT-like 1 (BMAL1) proteins activates the transcription of the period (Per) gene and, eventually, the expression of PER proteins. These proteins, then, bind with cryptochrome (CRY) proteins, in mammals, and inhibit the action of the CLOCK/BMAL1 pair. This inhibition stops the transcription of the Per genes and, consequently, the formation of the PER/CRY pair. The whole process starts again as soon as the concentration levels of PER and CRY drop enough through degradation so that the CLOCK/BMAL1 complex can, again, promote the transcription of Per genes (2.4, b)) (Ashton et al., 2022; Hussein et al., 2019; Ramkisoensing and Meijer, 2015).

To communicate signals, for example, regarding this genetic loop, to other neurons, each neuron produces neurotransmitters and/or neuropeptides (or "coupling factors"). These modulate the signal passed in the neuronal network. Therefore, depending on the type of coupling factor produced, the core and shell neurons have different functions. The core abundantly produces vasoactive intestinal peptide (VIP), while the shell produces arginine vasopressin (AVP) in large quantities. It is also possible to find core and shell neurons which produce the same type of neurotransmitters and neuropeptides. For example, almost all SCN neurons produce gamma-aminobutyric acid (GABA) (Hastings et al., 2019; Hussein et al., 2019; Silver, 2018).

Regarding the role of each one of the mentioned neuropeptides, VIP is produced rhythmically by specific core neurons, inducing Per expression in both core and shell neurons.

VIP sustains circadian rhythms, especially in darkness (Silver, 2018), and shapes the

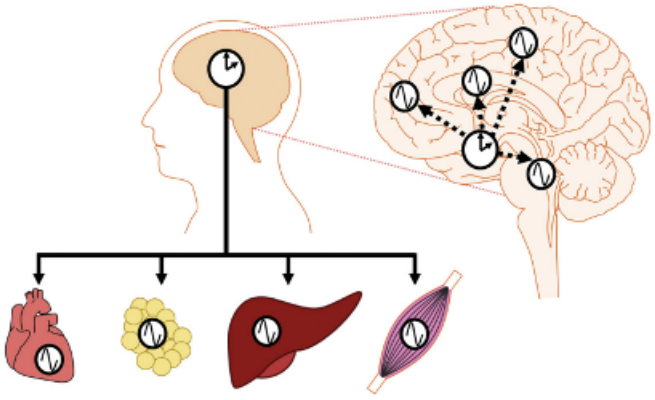

Figure 2.3: The SCN controls circadian rhythms in the brain and peripheral organs (e.g., heart, adipose tissue, liver and skeletal muscle). The cells in the organs are also clock cells, having their own gene expression cycles. Adapted from Karatsoreos and Silver, 2017.

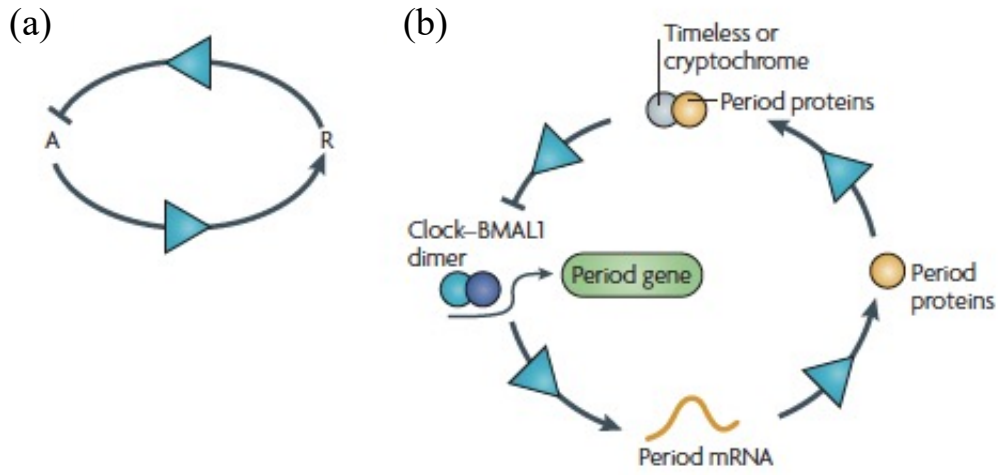

Figure 2.4: Simple models of the genetic loop in the SCN neurons responsible for the generation of circadian rhythms. a) Model of this loop showing it is based on periodic activation (A) and self-repression (R). b) Molecular compounds involved in the genetic loop. The timeless proteins are produced by flies and are equivalent to the cryptochrome proteins produced by mammals. Adapted from Herzog, 2007.

network's spatiotemporal structure (Li and Androulakis, 2021; Ono et al., 2021). On the other hand, GABA disrupts the synchronisation of SCN neurons. This effect is countered by VIP under symmetric LD cycles. However, if the neurons are out-of-phase following prolonged light exposure, GABA works with VIP to promote synchrony (Evans et al., 2013; Silver, 2018). Finally, AVP influences the SCN reentrainment pace since mice lacking AVP receptors show jet lag resistance (Evans and Silver, 2015). AVP can also induce behavioural rhythms, like the food and water intake prior to sleep in mice, and regulate glucocorticoid cycles, thus, influencing circadian rhythms on peripheral clock cells (Li and Androulakis, 2021; Ono et al., 2021; Silver, 2018).

This neurochemical architecture remains broadly consistent across mammals, indicating its stability and essential nature within the network (Evans and Silver, 2015).

2.2.4 Photic Entrainment

The adjustment of an individual to variations in light levels during the day, i.e., the LD cycle, is called photic entrainment. Since light is the most influential external factor on the rhythm of SCN neurons (Evans and Silver, 2015; Silver, 2018), this section will shed light on this process.

The retina, critical for circadian photoreception, contains specialised cells in light detection, the rods and cones. However, mice lacking these cells maintain regular circadian rhythms. At the turn of the 21^{st} century, a new type of cell was discovered, the intrinsically photosensitive retinal ganglion cell (ipRGC), which is able to fire action potentials when the rods and cones cannot sense light. This is due to the expression of photopigments, chemicals that undergo a chemical change when they absorb light, in the ipRGCs, called melanopsins.

The light information received by ipRGCs arrives at the SCN core neurons through the RHT cells. These cells release neurotransmitters and neuropeptides at synapses, which cause action potentials to be created and transmitted across the neurons. Inside the cells, through an internal cascade, Per gene expression is induced, restarting the transcriptional-translational loop that gives rise to circadian rhythms. The purpose of the induction of Per expression is to shift the phase of the SCN neurons' genetic loop so that it aligns with the LD cycle,

entraining the neurons (Ashton et al., 2022; Evans and Silver, 2015).

If light exposure occurs at a time when the expression of PER protein is decreasing, around dusk, this means that this expression will increase again, prolonging the repression of the CLOCK/BMAL1 pair and delaying the restart of the cycle. Thus, there will be a phase delay in the clock and processes that occurred earlier in the day will be reset. The opposite can also happen, if light exposure occurs at a time when the expression of PER protein is increasing, around dawn, it means that this expression will increase before it is time, promoting the repression of the CLOCK/BMAL1 pair and the restart of the cycle (Ashton et al., 2022; Evans and Silver, 2015).

Thus, light plays an important role on the resetting of the circadian system since it directly influences the genetic loop that gives rise to oscillations. These effects of light on the circadian rhythm are important to understand, for example, what to do in practice to help reduce the recovery time from jet lag, which is the main subject of this work.

2.3 Aschoff's Rules

The circadian free-running period varies from species to species, from individual to individual and even from cell to cell. In nocturnal organisms, this circadian period is lower than the period of the external light field, which is about 24 h. In diurnal organisms, on the other hand, this period is longer than 24 h. Particularly in humans, it is approximately equal to 24.2 h. This has several molecular and behavioural consequences under constant conditions (constant darkness is referred to as dark-dark (DD) and constant light as light-light (LL)). The circadian behaviour of diurnal and nocturnal animals was first described in the middle of the 20^{th} century by Jürgen Aschoff. This circadian biologist then developed the Aschoff's rules of chronobiology based on several studies of the free-running periods of many animal species. The Encyclopedia of Neuroscience (Beaulé, 2008) states the three Aschoff's rules as the following:

- **Aschoff's first rule** - in LL, the free-running period (T_{LL}) shortens for diurnal animals and lengthens for nocturnal animals when compared to DD conditions. The brighter the light, the more amplified are these effects. In summary, $T_{LL} < T_{DD}$ for diurnal animals and $T_{LL} > T_{DD}$ for nocturnal animals.
- **Aschoff's second rule** - in LL, the activity duration (α_{LL}) of diurnal animals increases when compared to the rest duration (μ_{LL}) and decreases for nocturnal animals. Again, the brighter the light, the more enhanced are these effects. In summary, $\alpha_{LL} > \mu_{LL}$ for diurnal animals and $\alpha_{LL} < \mu_{LL}$ for nocturnal animals.
- **Aschoff's third rule** - as stated above, for nocturnal animals, generally it is observed that $T < 24$ h, and for diurnal animals, generally $T > 24$ h.

The present work will draw some conclusions regarding the effects of constant light on the core and shell neuronal networks under jet lag. Among the Aschoff's three rules, the first is therefore fundamental to understanding the results of this work. It would also be interesting to make observations that take into account the genetic machinery behind this rule, but unfortunately, the physiological effects of constant light are not yet understood and there are only a few studies on the subject, such as Muñoz et al., 2005; Prabhat et al., 2020.

2.4 Jet Lag

Travelling across several time zones causes a disruption in the body's internal clock, which can lead to various symptoms, such as fatigue, sleeping and digestion problems or even cognitive dysfunction. These symptoms form a condition known as jet lag and they are a common challenge for travellers. For frequent travellers, such as business people, airline

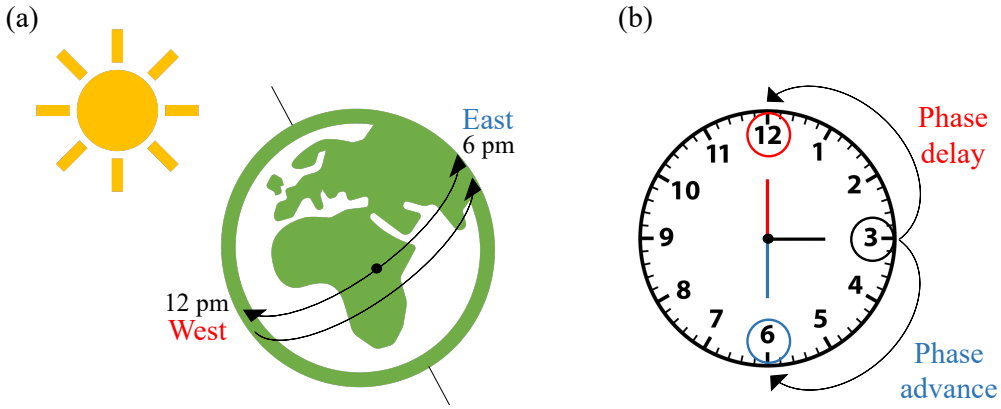

Figure 2.5: a) The counterclockwise rotation of the Earth results in an advanced timing in the east compared to the west. For instance, it could be 6 p.m. in an eastern region and 12 p.m. in a western region. b) Assuming it is 3 p.m. at the departure place, and the traveller wants to fly 3 time zones to the west, at the arrival place it would be 12 p.m.. To adapt to the new time zone, the biological clock would undergo a 3 h phase delay. On the other hand, assuming it is 3 p.m. at the departure place and the traveller wants to fly back 3 time zones to the east, at the arrival place it would be 6 p.m.. To adapt to the new time zone, the biological clock would undergo a 3 h phase advance.

employees, diplomats, performers, athletes or even astronauts, jet lag can cause long-term health problems. However, these circadian disruption symptoms can also be experienced by people who work irregular hours, such as shift workers (Karatsoreos and Silver, 2017; Roach and Sargent, 2019.

Upon arrival at the destination, the timekeeping system will be out of phase with the phase of the new LD cycle and will need to adapt. It is quite intuitive that travelling west and east should have opposite adaptation mechanisms - because the Earth rotates counterclockwise, the east is ahead of the west in the LD cycle (Figure 2.5, a)), so its time is earlier. To understand these differences, consider a diplomat who is currently living in Armenia, but needs to travel to continental Portugal, which corresponds to a westward travel since Portugal is 3 h behind Armenia. Therefore, before travelling, the system is considered to be in a stable state, which means that the diplomat is entrained to the conditions of their departure point, Armenia. After the travel, the diplomat's circadian clock is 3 h advanced in relation to the Portugal time because their system is still on Armenia time (see Figure 2.5, b), assuming 3 p.m. in Armenia and 12 p.m. in Portugal) - this is, the system is in an unstable state. In order to entrain to the timing conditions in Portugal, the diplomat's circadian system needs to delay its phase. Regarding eastward travels, for example, consider that the diplomat, who has already recovered from jet lag in continental Portugal, travels again to Armenia, which is 3 h advanced (see Figure 2.5, b), assuming 3 p.m in Portugal and 6 p.m. in Armenia). The system is then again in an unstable state and will regain its stability by phase advancing, i.e., by increasing its phase.

Travelling westward or eastward has significant differences in the body's adaptation to the new time zone/phase of the LD cycle. It is common for travellers to experience an easier and faster recovery from westward trips than from eastward trips. One of the possible reasons for this observation is that the endogenous free-running period of a typical human is about 24.2 h. For a westward trip, since the destination timing is delayed in relation to the traveller's circadian timing, a day at the destination will be "longer" than 24 h in the point of view of

the traveller because they will be getting more hours of the day compared to their departure time zone. Taking into account that the traveller's circadian period is already longer than a normal day of 24 h, it would be easier to adjust from a westward trip, where the day is "longer". For an eastward travel, the opposite occurs: the timing is advanced, therefore the day is "shorter" and the traveller's circadian phase will have to advance as much as the phase shift between the departure and destination time zone plus the additional phase delay that the circadian system has in relation to a day of about 24 h (Diekman and Bose, 2018; Eastman and Burgess, 2009).

2.4.1 Treating Jet Lag

To ease the symptoms of jet lag, the traveller can attempt to adjust as much as possible their sleep-wake schedule with the upcoming LD cycle before the travel. But, sometimes, this is not feasible or it would take a long adaptation time. Some treatments have already been developed, for example, ingesting melatonin (Arendt, 2018; Morgenthaler et al., 2007; Roach and Sargent, 2019), exercising at certain times of the day (Bin et al., 2019; Roach and Sargent, 2019) or even eating a highly caloric meal for breakfast, such as chocolate (Escobar et al., 2020). Because light is the most powerful *zeitgeber* to reset the circadian system, it is not surprising that light can also be a form of jet lag therapy. However, the appropriate time to apply these treatments is key to getting the optimal effect - if applied at certain times, the treatments can even worsen the effects of jet lag (Arendt, 2018; Bin et al., 2019; Eastman and Burgess, 2009; Forbes-Robertson et al., 2012; Roach and Sargent, 2019).

Combining certain therapies may also be more beneficial than using one alone. For example, the combination of melatonin and light has been studied to treat jet lag (Choy and Salbu, 2011).

2.4.2 Light Therapy of Jet Lag

Exposure to natural light at the destination is the ideal form of jet lag therapy. But, to accelerate the recovery, or for those who cannot be exposed to natural light at their destination, light therapy (LT) may be the answer. This therapy is based on exposure to artificial light at specific times of the day, for a certain period of time, before, during or after the travel (Choy and Salbu, 2011; Morgenthaler et al., 2007; Roach and Sargent, 2019).

To study the effect of perturbations on circadian rhythms, experimentalists often construct a phase-response curve (PRC). These curves show the dependence of the amount of phase shift caused by a perturbation on the phase of the neuronal system at the time of the perturbation (Dewan et al., 2011; Guevara Erra et al., 2017; Khalsa et al., 2003; St Hilaire et al., 2012). The timing of when LT should be delivered has been studied by constructing a PRC. PRC studies have proven that exposure to white bright light in the early evening delays the internal clock, while bright white light in the early morning advances the internal clock. These findings are rather intuitive: when an individual is exposed to bright light in the early evening just before bedtime, their circadian system interprets it as daytime, which means that it is not yet time to sleep. So, the system will undergo a phase delay. Conversely, if bright light is encountered in the early morning before waking, the circadian system interprets it as daytime, which means that the individual should have been already awake. So, the system will undergo a phase advance. Approximately, the time at which light exposure transitions from producing phase delays to phase advances occurs at the timing of the minimum core body temperature (CBTmin) (Dewan et al., 2011; Roach and Sargent, 2019). Behind this intuition, there is a molecular mechanism, explained in Section 2.2.4.

LT methods are being studied in chronobiology laboratories (Boivin and James, 2002; Comtet et al., 2019; Eastman and Burgess, 2009) and have already been commercialised around the world in various forms, for example, as light boxes, which are panels that emit

light, visors or lamps. Philips and Ortorex are examples of companies that commercialise light boxes and lamps, providing the EnergyLight (Philips, 2023) and Therapy Lamp (ORTOREX, n.d.) (see Figure 2.6 a) and c)), respectively. Lucimed is a company that focuses on the production of light glasses, the Luminette (Lucimed, 2023), which emits bright light to the eyes (Figure 2.6, b)). The purposes of these objects are to ameliorate the symptoms of SAD, characterised by depressive feelings at certain seasons of the year, and jet lag, help regulate the sleep schedules or even help the user gain more energy, in place of ingesting substances like caffeine. EnergyLight and Luminette have some models which use blue light instead of white light. In fact, blue light has been studied to be more efficient than white light in shifting the circadian clock, as phototransduction by melanopsin has a peak sensitivity in the blue spectrum (Comtet et al., 2019). Therefore, a study (Comtet et al., 2019) aimed to understand the differences in effects between using EnergyLight white light box and Luminette blue-light glasses. More discomfort was reported when using blue light glasses than light boxes, but the tolerance level for both is generally high.

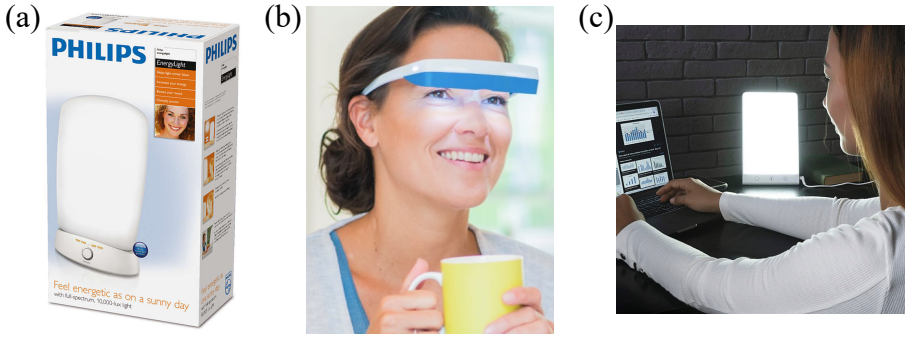

Figure 2.6: Products used for LT: a) EnergyLight from Phillips, b) Luminette 3 from Lucimed and c) Therapy Lamp from Ortorex. Adapted from Philips, 2023, Lucimed, 2023 and ORTOREX, n.d., respectively.

Besides these light sources for LT, there are other ways in which LT can be commercialised. Garmin is a company that makes smartwatches with personalised tips for light exposure to help jet lag depending on the time shift (Garmin, 2023). Also, there are some applications that can identify the optimal LT, such as Jet Lag Rooster (Sleepopolis Team, 2023), Timeshifter (Timeshifter, 2023) or Arcascope (Ng, 2023).

Studies have shown that a higher light intensity and duration are beneficial for entrainment compared with a lower light intensity and duration (Roach and Sargent, 2019). Despite that, higher light intensity ($\approx$ 170 lux) is associated with poor metabolic homeostasis in mice whose rhythms are continuously disrupted (Fan et al., 2022). The authors hypothesised that a higher light intensity results in pupillary constriction (pupillary light reflex), which has been proven to hinder circadian robustness (Fan et al., 2022). Bright light, such as when staring directly at the sun, is also known to damage the retina and the surrounding tissues (Dunaief, 2021). These findings suggest that consistent exposure to high-intensity light could lead to a poorer quality of life.

The most common brightness values, timing and duration used to study the effect of light in the circadian system in laboratories are shown in Section 5, in Table 5.1 and the ones used in commercialised light therapies are shown in the same section, in Table 5.2.

CHAPTER 3

Models of the Biological Clock

Mathematical modelling is essential for the analysis of complex physiological systems like the circadian system, helping to comprehend its characteristics across different scales and hierarchical levels through quantitative approaches. It can also aid in the designing of experiments and allow targeted in silico manipulations that overcome limitations of cost, time, and feasibility in experiments. Essentially, there are three ways to build models of biological systems, namely, the SCN neuronal system. These approaches can also be combined to construct a model (Asgari-Targhi and Klerman, 2019). More specifically:

- **Physiological modelling** - Its main purpose is to model the physiology of the system. It is common to use differential equations of concentrations of neurotransmitters/neuropeptides, genetic compounds and other molecular quantities. This type of modelling often requires a large number of equations and parameters (Asgari-Targhi and Klerman, 2019; Goltsev et al., 2022), therefore, it also requires considerable computational power. The advantage is that the results have a direct physiological meaning and it is easier to analyse the conclusions. Examples of models of the SCN physiology are Becker-Weimann et al., 2004; Goodwin, 1965; Li and Androulakis, 2021.
- **Dynamical modelling** - Mathematical principles are used to describe the dynamical characteristics of the system and are typically formulated using differential equations. Generally, this type of modelling is simpler than physiology modelling since the models have fewer variables and equations. However, they lack direct biological meaning and are sometimes complex to analyse (Goltsev et al., 2022). Most models of the SCN or the circadian system represent the system as self-sustained oscillatory since this is a feature of circadian rhythmicity (Asgari-Targhi and Klerman, 2019).
- **Statistical modelling** - It uses statistical methods, like curve-fitting, to make predictions of the model's parameters and variables. Some apply a sinusoidal curve to simulate circadian rhythms (Asgari-Targhi and Klerman, 2019). An example of a statistical model of the circadian clock is Brown and Luithardt, 1999. In this paper, the authors used differential equations and model-fitting with harmonic regression to simulate circadian rhythms.

3.1 Dynamical Models of the SCN

Dynamical models can be either deterministic or stochastic. Deterministic models are often described by ordinary or partial differential equations and do not consider statistical noise, in contrast to stochastic models.

In this work, the focus is on deterministic models. They can represent the system at organism-level or multicellular-level. Organism-level models represent the circadian clock as an oscillator. They aim to reproduce experimental observations of circadian rhythms, namely, the ability to be entrained by an external force. Recently, more complex models were developed, with two or more coupled oscillators. They can model more complex phenomena like the reentrainment after a perturbation or the phase splitting of the SCN under constant conditions in rodents (Asgari-Targhi and Klerman, 2019; Lara-Aparicio et al., 2006).

More specifically, dynamical models of the SCN can shed light on the neuronal mechanism of adaptation to a new time zone and explain some experimental observations on jet lag. They also contribute to developing ways of reducing the recovery time from jet lag.

For example, Diekman and Bose, 2018 simulated the SCN with the Forger–Jewett–Kronauer model, which is based on the Van der Pol oscillator (Forger et al., 1999). This type of oscillator is generally used to simulate the circadian clock and the SCN since it generates self-sustaining oscillations characterised by a stable limit cycle (Van Der Pol, 1926). The authors, then, obtained values for the recovery time after travelling between any two points on Earth, at any time. They also showed that the endogenous frequency of the traveller's circadian rhythm, as well as the length of the day, determines the severity of the symptoms of eastward and westward travel. Li and Androulakis, 2021 developed a model of the neuronal interactions between the core, shell and the hypothalamic–pituitary–adrenal axis and discovered that an individual's weak light sensitivity is related to a reduction of circadian flexibility. Then, they concluded that LT is a promising method for tackling disorders associated with shift work and jet lag. Lastly, Serkh and Forger, 2014 developed a methodology to mathematically determine light exposure and avoidance schedules that minimised jet lag recovery time using the Forger–Jewett–Kronauer model. Based on the available information, this is the only article aimed at finding the optimal parameters of LT using a mathematical model.

3.1.1 The Kuramoto Model for SCN Modelling

Several one-dimensional models, i.e., models in which the amplitude of oscillators is considered to be constant being characterised only by their phase, have been developed. A notable example is the Kuramoto model (explained in the next section), which has found applications in the study of circadian rhythms by accurately representing the SCN neuronal system. However, a potential limitation of this model is its neglect of the amplitude of oscillations, which is a crucial characteristic to understanding some circadian processes (Asgari-Targhi and Klerman, 2019; Jewett et al., 1994). For example, Jewett et al., 1994 showed that fast phase resetting of the SCN can occur due to circadian amplitude suppression. Such an observation cannot be adequately explained by a phase-only model such as the Kuramoto model.

Despite this limitation, several works have shown the effectiveness of this model in describing various phenomena in the chronobiology field, more specifically the phase-splitting of the SCN (Rohling and Meylahn, 2020) and even the adaptation of the circadian clock to different photoperiods (Gu et al., 2016). Moreover, Lu et al., 2016 used the Kuramoto model to investigate the asymmetry in jet lag symptoms when travelling eastward versus westward. The authors also aimed to understand the dependence of the recovery time on certain parameters of the circadian clock and the external light. In a more recent study, Goltsev et al., 2022 implemented the Kuramoto model as a description of the core and shell regions of the SCN. Their study aimed to compare model results with experimental observations under different LD, DD, and LL conditions. They focused on establishing the boundaries between entrainment and free-running activity, as well as demonstrating the potential for dissociation (the emergence of a second rhythm in the SCN) and the anticipation of future events by the SCN. Their results under LL conditions are also consistent with the Aschoff's first rule. It is

worth noting that the work of Goltsev et al., 2022 established the groundwork for the current project.

3.2 Review of the Kuramoto Model

In this work, the Kuramoto model was used to simulate the SCN dynamics. It was first developed to describe the synchronisation of a large system of coupled oscillators (Kuramoto, 1975). Synchronisation occurs when a large number of oscillators with different natural frequencies, connected by a coupling constant, lock on to a particular frequency (usually the averaged group frequency) after the disturbance of the system. One might notice that they have already come across this synchronisation phenomenon. It occurs in various forms in biology, for example, the synchronisation effect on networks of pacemaker cells in the heart, the synchronised flashing of fireflies, the metabolic synchrony observed in yeast cell suspensions, the synchronised clapping of a large audience after a show and finally, the synchronisation effect in the pacemaker cells of the SCN that leads to the emergence of circadian rhythms in the whole body (Strogatz, 2000).

In the Kuramoto model, each oscillator, or neuron, in the case of this work, is characterised by its phase, assuming a constant amplitude of oscillations. The oscillators are, therefore, called phase oscillators and can be represented as dots moving around the unit circle in the complex plane with a given angular velocity. The angle of the oscillator on the circle corresponds to its phase θ (Figure 3.1) (Strogatz, 2000).

Equation 3.1 characterises the dynamics of phase oscillators on a fully connected network, with equal weights and sinusoidal coupling. In this equation, θ_i is the phase of the oscillator i, ω_i is the natural frequency of the oscillator i, i.e., the angular frequency at which the oscillator rotates when uncoupled from the network, K is the coupling strength ($K \geq 0$) and N is the number of oscillators in the system (Acebrón et al., 2005; Strogatz, 2000).

$$\frac{d\theta_i}{dt} = \omega_i + \frac{K}{N}\sum_{j=1}^{N}\sin\left(\theta_j - \theta_i\right), i = 1, ..., N \tag{3.1}$$

Considering a simulation of the dynamics of neurons characterised by their phase, at each time step, the rate of phase variation, or angular frequency, of the neuron i would be influenced by its natural frequency ω_i (the first term of Equation 3.1), as well as by the interaction with the other oscillators (the second term of Equation 3.1). This interaction is defined by the phase difference between every neuron on the network and neuron i. This means that, for

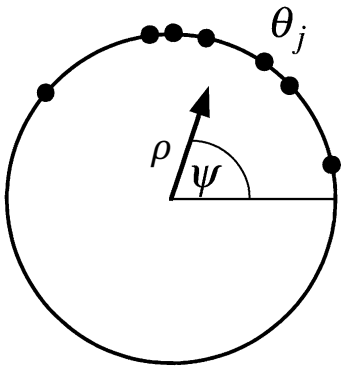

Figure 3.1: Phase oscillators on the unit circle. θ_j represents the phase of the j-th oscillator. The order parameter $\rho e^{i\psi}$ is represented by the arrow, with ρ corresponding to the length of the arrow and ψ to its angle. Adapted from Strogatz, 2000.

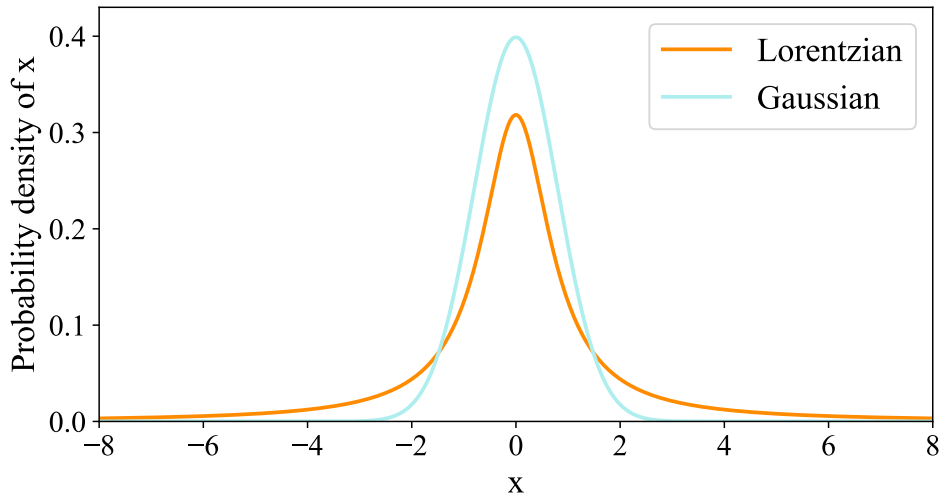

Figure 3.2: Comparison of the standard Lorentzian and Gaussian probability density functions for a real number x.

example, if every neuron in the network was phase advanced in relation to neuron i and the coupling is positive, neuron i would accelerate in order to reduce its phase difference with the rest of the network. The closer the phases of two oscillators are $((\theta_j - \theta_i) \to 0)$ or the further they are apart $((\theta_j - \theta_i) \to \pi)$, the less influence the coupling has on the phase shift of oscillator i since $\sin(\theta_j - \theta_i) \to 0$.

Simulations with the Kuramoto model require the assumption of a probability density $g(\omega)$ for the natural frequencies of the neurons. In developing his model, Kuramoto considered this distribution to be unimodal (a distribution with only one mode) and symmetric around its mean frequency since it corresponds to the simplest case of the model. Therefore, $g(\omega)$ can be a Gaussian density (Equation 3.2, where σ is the standard deviation and ω_0 is the mean frequency) or a Lorentzian/Cauchy density, referred to as Lorentzian, from now on (Equation 3.3, where Δ is the half-width at half-maximum and ω_0 is the mean frequency). Figure 3.2 presents a comparison of the standard Gaussian and Lorentzian densities. To simplify the problem even further, one can reassign $\omega_i \to \omega_i - \omega_0$, meaning that $\theta_i \to \theta_i + \omega_0 t$. In this way, $g(\omega) = g(-\omega)$ (Acebrón et al., 2005; Goltsev et al., 2022; Strogatz, 2000).

$$g(\omega) = \frac{1}{\sigma\sqrt{2\pi}} e^{-\frac{1}{2}(\frac{\omega-\omega_0}{\sigma})^2} \tag{3.2}$$

$$g(\omega) = \frac{1}{\pi} \frac{\Delta}{(\omega - \omega_0)^2 + \Delta^2} \tag{3.3}$$

To measure the synchronisation in the system of oscillators, Kuramoto introduced a novel order parameter (check the box on the right), with Equation 3.4. The amplitude ρ of this complex quantity, also called the synchronisation index, represents the phase alignment of the oscillators. Therefore, if $\rho = 0$, it means that the phases of the SCN neurons would be randomly distributed in the unit circle and the system would be completely asynchronous. On the other hand, if $\rho = 1$, it means that the phases of the SCN neurons would be equal to the average phase of the system ψ and the neurons would be completely synchronised (Strogatz, 2000; Yoon et al., 2021). In Figure 3.1, there is a geometric representation of the complex order parameter,

But, what is an order parameter?
It is a measure of the degree of order in a system, indicating its state (Strogatz, 2015)

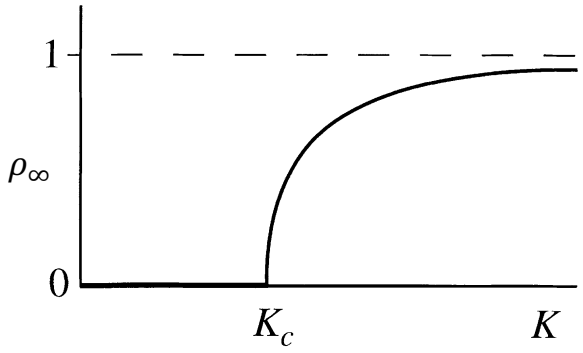

Figure 3.3: Dependence of the synchronisation index ρ at the steady-state on the coupling K. Before the critical coupling K_c, oscillators are completely desynchronised. After K_c, the synchronisation of the system starts to increase, while some of the oscillators spontaneously synchronise. Adapted from Strogatz, 2000.

where the length of the arrow is equal to the synchronisation index and the angle is equal to the average phase of the system.

$$z = \rho e^{i\psi} \equiv \frac{1}{N} \sum_{j=1}^{N} e^{i\theta_j} \tag{3.4}$$

At $t \to \infty$, this is, at the steady-state, the neuronal system can be in different synchronisation conditions, depending on the coupling between neurons K. Figure 3.3 shows this dependence, which is a second-order phase transition (check the box on the right), meaning that a partial synchronisation state develops continuously from an asynchronous state. Therefore, if K is smaller than a critical coupling K_c, then the neurons are in an asynchronous state and $\rho = 0$. However, when K is higher than K_c, there is a macroscopic group of neurons that start to synchronise, eventually locking to a common frequency, ω_0, thus, $\rho \neq 0$. If ω are sampled from a Lorentzian distribution, then $K_c = \frac{2}{\pi g(0)}$, which is equal to 2Δ, taking into account Equation 3.3, where Δ is the half-width at half-maximum of the distribution (Acebrón et al., 2005; Strogatz, 2000). Figure 3.4 shows the distribution of ten phase oscillators in the unit circle at the steady-state for different coupling values. In a), $K = 0$ and the oscillators are randomly scattered in the circle; in b), $K = K_c$ and the phase difference between oscillators is reduced; and in c), $K = 5$ and synchronisation was achieved.

But, what is a phase transition?
It is a significant change of a system's state when a change of a parameter of the system occurs, like temperature or, in this case, coupling (Strogatz, 2015)

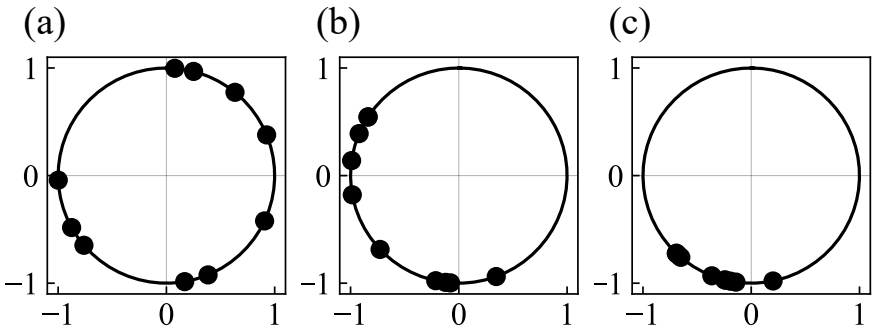

Figure 3.4: Synchronisation of phase oscillators on the unit circle for different coupling values K - (a) $K = 0$, (b) $K = K_c$, (c) $K = 5$. To obtain these images, simulations were done with Python, for ten oscillators and 10,000 time steps. These are the results for the last time step.

3.2.1 Heterogeneous Field in the Periodically Forced Kuramoto model

However, in order to accurately model the SCN, Equation 3.1 is not sufficient. It is necessary to introduce the influence of an external field and to model the SCN as two groups of oscillators, core and shell (although it possesses two identical lobes, in this case, the SCN can be simplified and represented as a single lobe) (Goltsev et al., 2022).

Let's consider a periodic external field with intensity F, period T_F, angular frequency $\omega_F = 2\pi/T_F$ and local field phase $\omega_F t + \phi$. Therefore, the influence of this external field on oscillator i is $F \sin(\omega_F t + \phi - \theta_i)$. This term can be added to the equation of the simple Kuramoto model (Equation 3.1), resulting in what is referred to as the Periodically Forced Kuramoto model (Antonsen et al., 2008; Sakaguchi, 1988).

Introducing the two groups of neurons, core and shell, in Equation 3.1 can be seen as considering a heterogeneous external field that impacts different oscillators with two different intensities and phases. In this way, two distinct groups of oscillators are formed, and within each one, the oscillators are affected by the same intensity and phase of the external field. For the general case of M oscillator groups, each one having N_m neurons, where m is the group index, the equation for the phase dynamics of the m^{th} group is Equation 3.5 and for the complex order parameter is Equation 3.6 (Goltsev et al., 2022; Yoon et al., 2021).

$$\frac{d\theta_i^{(m)}}{dt} = \omega_i^{(m)} + \frac{1}{N_n} \sum_n \sum_{j \in G_n} K_{nm} \sin(\theta_j^{(n)} - \theta_i^{(m)}) + F^{(m)} \sin(\omega_F t + \phi^{(m)} - \theta_i^{(m)}) \tag{3.5}$$

$$z_m = \rho_m e^{i\psi_m} \equiv \frac{1}{N_m} \sum_{j \in G_m} e^{i\theta_j^{(m)}} \tag{3.6}$$

In the Kuramoto model, when the probability density of the natural frequencies (ω) of the oscillators is unimodal, increasing the coupling K above a critical coupling K_c will cause a continuous transition in the oscillator system from an incoherent state to a state with increasing synchronisation, as seen in the previous section - this type of phase transition is referred to as a second-order phase transition (Martens et al., 2009; Strogatz, 2000), like the transition from a paramagnetic state to a ferromagnetic state, described by the Ising model. On the other hand, let's consider a bimodal probability density of ω. This situation can occur when, in a system of oscillators, there are two groups with unimodal distributions, like core and shell. In this case, the transition from an incoherent to an increasing synchronisation

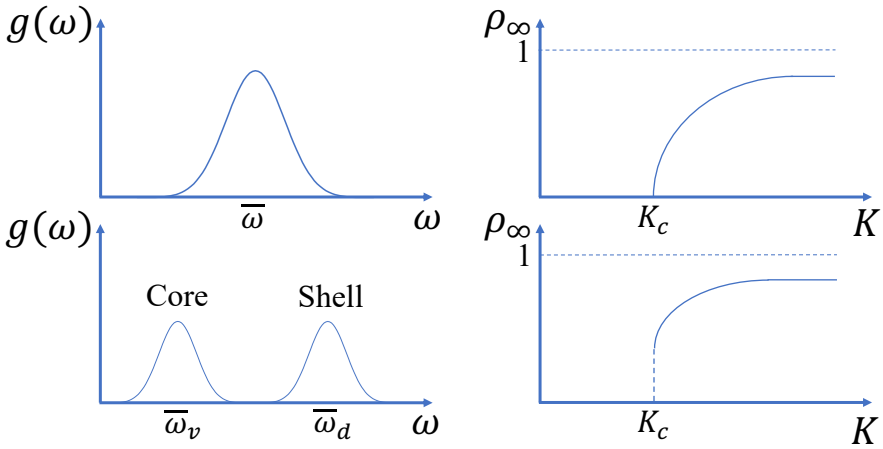

Figure 3.5: For an unimodal probability density of the natural frequencies (ω) of the oscillators (upper left plot), at coupling K equal to the critical coupling K_c, the system undergoes a second-order phase transition (upper right plot). A bimodal probability density can occur for a system of oscillators with two groups, such as core and shell, in which ω can have unimodal probability densities (lower left plot). In this case, they are considered to be symmetric, and therefore, the peak corresponds to both the mode and the mean of ω. For the core, this is $\overline{\omega}_v$ and for the shell, this is $\overline{\omega}_d$. Thus, for a bimodal density, at $K = K_c$, the system undergoes a first-order phase transition (lower right plot).

state is discontinuous, which is often called explosive synchronisation. This type of phase transition is referred to as a first-order phase transition, like the transition from liquid to gas and vice-versa. In the case of a bimodal distribution, this first-order phase transition is associated with hysteresis: the K_c for a situation with increasing K is different from the K_c for a situation with decreasing K (Hu et al., 2014; Martens et al., 2009; Pietras et al., 2018). Figure 3.5 graphically illustrates an unimodal density (upper left) which induces a second-order phase transition on the system, represented by a continuous increase of the synchronisation index at the steady-state with the increase of K beyond K_c (upper right). It also illustrates a bimodal density, with the core and shell peaks (lower left), which induces a first-order phase transition on the system, represented by a discontinuous increase of the synchronisation index at the steady-state with the increase of K past K_c (lower right). For simplicity, the hysteresis has not been represented in this plot.

CHAPTER 4

Modelling Jet Lag with the Core-Shell Model

This chapter introduces the core-shell model employed in this study, its selected parameters and the methodology behind the simulations. Subsequently, the process of modelling jet lag will be explained. Lastly, the differences between jet lag from eastward and westward travels will be studied in the light of the core-shell model and results will be compared with published experimental observations.

4.1 The Core-Shell Model

The spatial organisation of the SCN is an evolutionary adaptation that allows for the emergence of circadian rhythms. Therefore, the implemented model is based on the division into the core/shell regions and the neuronal interactions between and within them. This dynamical model, thus, focuses on the functional aspects rather than the molecular mechanisms underlying neuronal communications. For these reasons, throughout this work, it is referred to as the core-shell model.

The SCN core and shell are composed of neurons that are self-sustaining endogenous oscillators, meaning they maintain oscillations in the absence of interactions between them or an external force. The behaviour of this type of oscillator is described by the Kuramoto model, introduced in Section 3.2. Therefore, this model is a good explanation of the behaviour of the SCN and is the basis of the core-shell model.

In this model, the parameters that characterise the state of the core and shell are the synchronisation index, $\rho_{v(d)}$, and the group phase, $\psi_{v(d)}$ of the order parameter in Equation 4.1 (the letter "v" stands for the ventral part of the SCN, or core, and the letter "d" stands for the dorsal part of the SCN, or shell). As explained in Section 3.2, the amplitude or synchronisation index $\rho_{v(d)}$ can take values between 0 and 1: if it is 0, it means that the oscillators are not synchronised; if it is 1, the oscillators are fully synchronised. Because this parameter measures the synchronisation between neurons, it represents how efficient the transfer of circadian information is. On the other hand, the group phase $\psi_{v(d)}$ is the mean value of the phase of the oscillators.

$$z_{v(d)}(t) = \rho_{v(d)} e^{i\psi_{v(d)}}. \tag{4.1}$$

It is known that the core receives external light from the retina and passes this information on to the shell (Evans and Silver, 2015). This is an important feature that is reproduced in

the core-shell model. The external light input received by the core is modelled as a periodic external force $F\sin(\omega_F t + \phi_0)$, where F is the light intensity, ϕ_0 is the phase of the field, set to 0, for simplicity, and ω_F is the angular frequency of the field, set to $2\pi/24\ h^{-1}$ since the period is 24 h. This is a positive frequency resulting from the fact that the Earth rotates from west to east, i.e., viewed from the North Pole, it rotates counterclockwise, or in a positive direction (Goltsev et al., 2022). The information about this light cue is received by the core, as mentioned earlier. Then, the core neurons transmit this information to each other. In the core-shell model, the coupling constant K_{vv} is the parameter that characterises the strength of the intra-communication between the core neurons. Then, core neurons transmit the information to the shell neurons with a strength of inter-communication given by K_{vd}. Similar to the core, the shell neurons communicate with each other with a strength given by the coupling constant K_{dd}. They also communicate back with the core, which is characterised by K_{dv}. In summary, Figure 4.1 represents the core-shell model and the constants associated with the external cue, core and shell. An attentive look notices that the arrow that corresponds to the communication from the core to the shell is thicker than the inverse arrow. This means that the strength of communication from core to shell is greater than in the opposite direction, which will be explained in detail in the next section.

Since there is an external periodic force acting on two heterogenous groups of oscillators, the core-shell model is a form of the heterogenous periodic Kuramoto model, as seen in Section 3.2.1. There are two ways of simulating the system: the microscopic and the macroscopic way. In the first scenario, Equation 3.5 is used to determine the phase of each neuron at a given time. In this way, it is possible to model the behaviour of the system taking into account the behaviour of its smaller parts, the neurons. In the second scenario, the behaviour of the whole system is characterised by two macroscopic quantities, the amplitude and phase of the complex order parameter, as mentioned earlier in this section. To reduce the computational complexity of the simulations, the second approach was employed in this work. Therefore, from Equation 3.5, using a method proposed by Ott and Antonsen, 2008, one can derive the coupled ordinary differential equations that characterise the temporal evolution of $\rho_{v(d)}$ (Equation 4.2, for the core, and Equation 4.4, for the shell) and $\psi_{v(d)}$ (Equation 4.3, for the core and Equation 4.5, for the shell). In these equations, $\Delta_{v(d)}$ is the half-width at half-maximum of the natural frequency distribution in the core (shell) oscillators and $\overline{\omega}_{v(d)}$ is the mean of the natural frequencies of the core (shell) oscillators. These equations describe the characteristics of the core and shell as two groups of neurons, i.e. as two macroscopic systems. These equations correspond to a state in a rotational frame running at the periodic field frequency, ω_F. This way, the stable steady-state solutions of these equations directly correspond to the situation where the core and shell are entrained to/synchronised with the external field, which will be better explained later. In the original frame, the order parameter of these steady-state solutions is an oscillating function given by Equation 4.6 (Goltsev et al., 2022).

$$\frac{d\rho_v}{dt} = -\rho_v\Delta_v + \frac{1}{2}\rho_v K_{vv}(1-\rho_v^2) + \frac{1}{2}F(1-\rho_v^2)\cos\psi_v + \frac{1}{2}\rho_d K_{dv}(1-\rho_v^2)\cos(\psi_d - \psi_v), \tag{4.2}$$

$$\frac{d\psi_v}{dt} = \overline{\omega}_v - \omega_F - \frac{1}{2}F\frac{(1+\rho_v^2)}{\rho_v}\sin\psi_v + \frac{1}{2}\rho_d K_{dv}\frac{(1+\rho_v^2)}{\rho_v}\sin(\psi_d - \psi_v), \tag{4.3}$$

$$\frac{d\rho_d}{dt} = -\rho_d\Delta_d + \frac{1}{2}\rho_d K_{dd}(1-\rho_d^2) + \frac{1}{2}\rho_v K_{vd}(1-\rho_d^2)\cos(\psi_v - \psi_d), \tag{4.4}$$

$$\frac{d\psi_d}{dt} = \overline{\omega}_d - \omega_F + \frac{1}{2}\rho_v K_{vd}\frac{(1+\rho_d^2)}{\rho_d}\sin(\psi_v - \psi_d), \tag{4.5}$$

$$z_{v(d)}(t) = \rho_{v(d)}e^{i\omega_F t + i\phi_0 + i\psi_{v(d)}}. \tag{4.6}$$

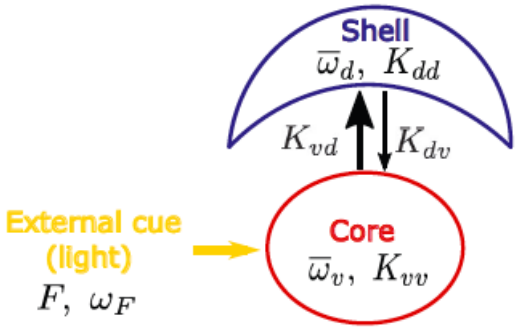

Figure 4.1: Representation of the core-shell model. An external cue (light) characterised by the parameters F and ω_F acts on the core neurons. The core (shell) is characterised by the mean free-running frequency $\overline{\omega}_{v(d)}$ and intracoupling constant $K_{vv(dd)}$. The strength of the interaction between core and shell is K_{vd} and the contrary is K_{dv}. Adapted from Goltsev et al., 2022.

4.2 Selection of Parameters

For convenience, all the parameters of the core-shell model were rescaled in order to be dimensionless. More specifically, both sides of the Equations 4.2–4.5 were divided by the half width at half maximum of the natural frequency distribution in the core, Δ_v. In this way, the time variable t was multiplied by Δ_v ($t\Delta_v \to t$) and all coupling constants were divided by Δ_v ($K_{nm}/\Delta_v \to K_{nm}$).

The parameters $\overline{\omega}_{v(d)}$ and $\Delta_{v(d)}$ were based on experiments from Taylor et al., 2017. This paper aimed to understand what intra and intercellular changes occurred during the process of resynchronisation. For that matter, the authors experimented with mice and kept them under a 12:12 h LD cycle (12 h of light and 12 h of darkness). After that, they reproduced the findings with a mathematical model. According to the experimental free-running periods of the SCN, in their model, they sampled the core free-running periods from a Gaussian distribution with mean (τ_v) 25.1 h and with a standard deviation (σ_v) of 1.3 h and for the shell, they sampled from a Gaussian distribution with mean (τ_d) 23.9 h and a standard deviation (σ_d) of 1.9 h. Then, the mean free-running frequency is given by $\overline{\omega}_{v(d)} = 2\pi/\tau_{v(d)}$. To make the simplification from Equation 3.5 to Equations 4.2–4.5, it was assumed that the natural frequencies of the core and shell neurons followed a Lorentzian distribution. Although Taylor et al., 2017 used the Gaussian distribution, the parameters found would be analogous to the parameters of a Lorentzian distribution due to the similarities between these two distributions: they are both symmetric and unimodal. Therefore, $\overline{\omega}_{v(d)}$ was considered to be the same as the one found by Taylor et al., 2017, leaving us with the task of determining $\Delta_{v(d)}$. According to the definition of standard deviation, and knowing that $\tau_{v(d)} \gg \sigma_{v(d)}$, the standard deviation of the free-running frequencies is $SD_{v(d)} \approx 2\pi\sigma_{v(d)}/\tau^2_{v(d)}$. Since $\Delta_{v(d)}$ (from the Lorentzian distribution) and $SD_{v(d)}$ (from the Gaussian distribution) represent the spread of free-running frequencies, it is assumed that $\Delta_{v(d)} = SD_{v(d)}$.

Regarding the coupling constants, there are no direct measurements, although they can be inferred from experimental data if the coupling is considered an approximation to neuron communication. There is also the need to restrict the parameters' range of possible values. For example, when the system has very large couplings it is insensible to the external cue. On the other hand, if the external cue strength is considerable, then the system cannot be influenced by the coupling, contradicting the possibility of neuronal plasticity.

Studies on mice have shown that, when isolated from the core, the shell becomes desynchronised and not the core (S. Yamaguchi et al., 2003), meaning the core's intracoupling is

strong enough to sustain regional synchronisation. Besides this, Moore, 1996 showed that dendritic arbours in the core are larger and broader than in the shell. This suggests that K_{vv} should be higher than the critical value of $2\Delta_v$ and higher than K_{dd}. The values of the intracouplings are found for the case under constant darkness, for simplicity. This way, the core and shell are free-running and the intercouplings can be reduced to 0 ($K_{vd} = K_{dv} = 0$ and $F = 0$). From Equation 4.2 and Equation 4.4:

$$K_{vv(dd)} = \frac{2\Delta_{v(d)}}{1 - \rho_{v(d)}^2} \tag{4.7}$$

where $\rho_{v(d)} \neq 1$ and $K_{vv(dd)} \neq 0$. To establish $\rho_{v(d)}$, assuming positive intracouplings, let's consider the case where $\rho_v > \rho_d$. If this occurs, then $K_{vv}/K_{dd} > \Delta_v/\Delta_d$. This is true, since $K_{vv} > K_{dd}$ and $\Delta_d > \Delta_v$. Therefore, it is true that $\rho_v > \rho_d$. Since there are no experimental results from which to assume $\rho_{v(d)}$, it was considered $\rho_v = 2\rho_d$. Taylor et al., 2017 theoretically found that the synchronisation index for the entrained SCN was 0.9. For the core, it was considered a smaller value, $\rho_v = 0.8$, which makes $\rho_d = 0.4$. Then, from Equation 4.7, $K_{vv} = 5.6$ and $K_{dd} = 4.0$.

Let us focus on the intercouplings. There are experimental data which shows that the VIP neurons in the core make more connections to AVP neurons in the shell than otherwise (Varadarajan et al., 2018) and there has been evidence that the core entrains the shell under symmetric LD conditions (Taylor et al., 2017). This indicates that the intercoupling between core and shell is higher than the contrary ($K_{vd} > K_{dv}$). However, the action of several neurotransmitters might influence the intercoupling. GABA is a neurotransmitter produced in core and shell neurons and it is known for destabilising synchronisation (Evans and Silver, 2015), counteracting the effects of VIP, produced by core neurons. However, since the core entrains the shell under symmetric LD cycles, it is assumed that the role of VIP in establishing synchronisation is more significant than the role of GABA. Therefore, it is assumed that $K_{vd} > 0$. If GABA had more influence than VIP, then $K_{vd} < 0$, since it would hinder synchronisation.

The values of the parameters K_{vd}, K_{dv}, τ_d and F were adjusted according to experimental data about the difference between the peak activity time of the core $t_v^{(p)}$ and the shell's $t_d^{(p)}$. This difference $t_v^{(p)} - t_d^{(p)}$ was calculated to be 2.4 ± 0.9 h (Taylor et al., 2017). The referred values were then chosen by inspection in order to verify $t_v^{(p)} - t_d^{(p)} = 2.3$ h. Thus, $\tau_d = 23.3$ h, $K_{vd} = 1.1$, $K_{dv} = 0.5$ and $F = 1.5$, in dimensionless units. The present study of the values of the parameters of the core-shell model was described by Goltsev et al., 2022.

To computationally solve the differential equations of the core-shell model, the *solve_ivp* function from the package *Scipy* for the Python programming language was utilised and the mathematical method used for solving the equations was the Radau method, which is the implicit Runge-Kutta method of Radau IIA family of order 5 (The SciPy community, 2023). This method was selected for its ability to consistently generate stable solutions in this particular case.

In the simulations of this chapter, it was used $10,000$ time steps, from $t_0 = 0$ to $t_{max} = 100$. As mentioned at the beginning of the section, these values are already multiplied by Δ_v for simplification of units. Explicitely, $t(h) \times \Delta_v(h^{-1}) \to t$ (adimensional).

Table 4.1: List of parameters in Equation 4.2–4.5 for the core-shell model: $\tau_{v(d)}$, the mean free-running period of the core (shell); $\sigma_{v(d)}$, the standard deviation of free-running periods; $K_{vv(dd)}$, the intracoupling in the core (shell); K_{vd} and K_{dv}, the core-shell intercouplings; F, the strength of the periodic cue; $\overline{\omega}_{v(d)} = 2\pi/\tau_{v(d)}$, the mean free-running frequency of core (shell) oscillators; $\Delta_{v(d)}$, the Lorentzian spread of free-running frequencies in the core (shell).

Dimensional parameters				Dimensionless parameters								
τ_v	τ_d	σ_v	σ_d	K_{vv}	K_{dd}	K_{vd}	K_{dv}	F	$\overline{\omega}_v$	$\overline{\omega}_d$	Δ_v	Δ_d
25.1 h	23.3 h	1.3 h	1.9 h	5.6	4.0	1.1	0.5	1.5	19.3	20.8	1.0	1.7

4.3 The Dynamical Phase Flow Portrait

The dynamical phase flow portraits of the core-shell model contain information about the temporal evolution of the core and shell dynamics (Figure 4.2). These portraits are complex planes, in which the evolution of the SCN is characterised by trajectories. The coordinates of the points constituting these trajectories are the solutions of the nonlinear dynamical equations for the core and shell 4.2–4.5 at each instant. Therefore, each point is characterised by polar coordinates, this is, the amplitude of the order parameter ($\rho_{v(d)}$) and the phase of the order parameter ($\psi_{v(d)}$). The analysis of this portrait is fundamental to understanding how the SCN neuronal system evolves when it is faced with a phase shift. For example, it can explain the recovery from jet lag when people travel across several time zones. This methodology has been proposed by some works, such as Diekman and Bose, 2018; Gundel and Spencer, 1999; Lu et al., 2016, regarding different models.

By solving Equation 4.2–4.5 using the function *findroot* of the package *mpmath*, it is possible to find three fixed points (check the box on the right): one stable point (filled circles on Figure 4.2), one unstable point (empty circles in Figure 4.2) and one saddle point (crosses in Figure 4.2), whose coordinates are stated in Table 4.2). The stable fixed point attracts all the trajectories, the unstable point repels them and the saddle might attract or repel, as one can see by the grey flows in Figure 4.2. Because there are four parameters to be solved ($\rho_v, \psi_v, \rho_d, \psi_d$), the phase portrait should be in four-dimensional space. However, it is easier to understand the trajectories in the phase portrait if they are projected onto the two-dimensional subspaces (ρ_v, ψ_v) and (ρ_d, ψ_d), which are in regard to the core and shell, respectively. Therefore, in Figure 4.2 a) and Figure 4.2 b), the phase portrait can be observed with respect to the core and shell, respectively. Looking at Figure 4.2, one can see that these three steady-state solutions are different between core and shell, which characterises some differences between the response of the core and shell to perturbations. It is important to note that the phase portraits in Figure 4.2 are in a rotational frame running at the periodic field frequency, $2\pi/24\ h^{-1}$. Also, for simplicity, the phase of the periodic field is set to 0.

But, what is a fixed point?

It is a point on the phase portrait with fixed coordinates (Strogatz, 2015). It corresponds to an equilibrium solution at $t \to \infty$, in this case, of Equations 4.2–4.5, under the conditions $\rho_{v(d)}/dt = \psi_{v(d)}/dt = 0$

A more attentive look would also notice that the fixed stable point of the core lies on the lower half of the phase portrait, while that of the shell lies on the upper half. In other words, at equilibrium, the phase of the shell is advanced relative to the phase of the field and the phase of the core is delayed relative to the phase of the field. This translates into the phenomenon

Table 4.2: Approximate polar coordinates (ρ and ψ) of the fixed points on the dynamical phase flow portraits of the core ("v"), on Figure 4.2 a), and shell ("d"), on Figure 4.2 b).

-	**Stable node**	**Unstable node**	**Saddle node**
ρ_v	0.854171	0.445944	0.699221
ψ_v	-0.487264	-2.847832	-2.702607
ρ_d	0.601986	0.470325	0.570425
ψ_d	0.119943	-1.586229	-1.956326

of "anticipation", in which the shell, the SCN structure that primarily communicates with peripheral tissues (Davidson et al., 2009; Evans et al., 2015), provides them with phase cues in anticipation of certain events that depend on the time of day. Behaviours that are consequences of this phenomenon are, for example, the instinctive search for water before sleep and the food-seeking prior to meal times (Goltsev et al., 2022). By making the calculations for an external light period of 24 h, the shell is advanced in relation to the core by about 2.5 h, which corresponds to a phase difference of, approximately, 35 degrees. In relation to the field phase, the shell is advanced, approximately, by 30 minutes (phase difference of about 7 degrees), while the core is delayed, approximately, by 2 h (phase difference of about 28 degrees).

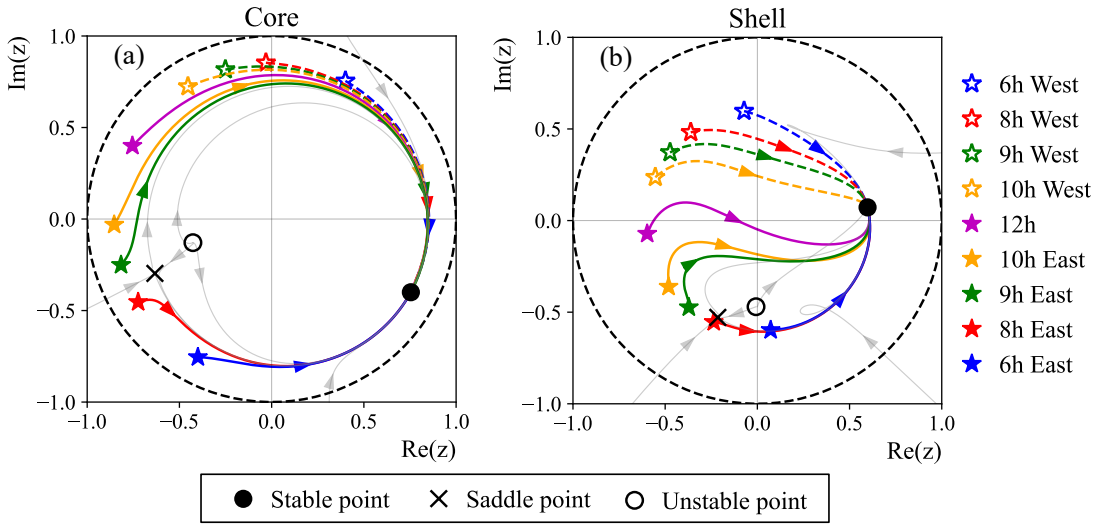

Figure 4.2: Projections of the dynamical phase flow portrait of the core and shell order parameters onto the subspaces (ρ_v, ψ_v) (a) and (ρ_d, ψ_d) (b) (polar coordinates), respectively. There are three fixed points: a stable point (filled circle), an unstable point (empty circle) and a saddle point (cross). The recovery process trajectories after eastward travelling are represented by a continuous line and the filled stars represent the initial point. For westward travelling, the trajectories are represented by a dashed line and the initial points are the empty stars. In grey, there are some additional flows. All of the trajectories are numerical solutions of Equations 4.2)–4.5.

4.4 Jet Lag, the Recovery Process and Initial Conditions

Jet lag occurs due to the reentrainment process of the body clocks to the new time zone. Therefore, considering the travel to be instantaneous, upon arrival to the destination, our timekeeping system will be out of phase: if travelling eastward, the system will be phase delayed in relation to the new LD cycle and it will recover by phase advancing and if travelling westward, the opposite will occur.

This recovery process from jet lag after eastward and westward travels can be modelled with the core-shell model. The phase portraits in Figure 4.2 show some trajectories (the colourful lines) that correspond to the recovery process of the core and shell after undergoing phase shifts of 6 h, 8 h, 9 h, 10 h and 12 h, both as phase advances (eastward travel) and phase delays (westward travel). The trajectories are the numerical solutions of Equations 4.2–4.5 at each time step after the rapid phase shift, occurring at t_0.

A very important detail to note is that the stable fixed point has frequency 0 because it is not moving in that frame. However, since the frame is moving at the external field's frequency, this point corresponds to the state in which both the core and shell neurons are in an equilibrium state, running at the field's frequency. Thus, the core and shell are entrained to the field.

Having this in mind, the final point of these trajectories is always the stable point: it corresponds to entrainment to the LD cycle of the arrival site, this is, the steady-state in the arrival site. At t_0, the initial points of the trajectories (stars on Figure 4.2), the traveller is already at the arrival site but is still entrained to the departure phase conditions. This means that the initial point corresponds to the steady-state at the departure site. Then, after the rapid phase shifts, the system tries to get back to stability, represented by the stable point, in the direction indicated by the arrows in each trajectory of Figure 4.2.

More specifically, considering that the core and shell's systems are entrained to the departure site, i.e. the dynamics are at the stable points, before the travel, this rapid travelling effect is modelled by a change of the phase of the stable points. Thus, at t_0, right after the instantaneous travel, the core and shell have the parameters $\rho_{v(d)(t_0)} = \rho^*_{v(d)}$ and $\psi_{v(d)}(t_0) = \psi^*_{v(d)} \pm 2n\pi/24$, where n the number of time zones crossed. The initial point is, then, $(\rho^*_v, \psi^*_v \pm 2n\pi/24, \rho^*_d, \psi^*_d \pm 2n\pi/24)$, where $\rho^*_{v(d)}$ and $\psi^*_{v(d)}$ are the synchronisation index and group phase of the core (shell) at the stable point. The sign of the phase shift is $+$ if it is a westward travel because the system is advanced with respect to the new LD cycle phase and tries to return to the stable point by phase delay. This is why the initial points corresponding to westward travels are on the upper half of the phase portrait. In opposition, the sign of the shift is $-$ if it is an eastward travel since the system is delayed in relation to the new LD cycle and will try to get back to stability by phase advance. Therefore, the initial points corresponding to eastward travels are on the lower half of the phase portrait.

But a question still remains: how to determine that the system has recovered from jet lag? Following the work of Lu et al., 2016, the recovery time is assumed to be equal to the time it takes for the condition

$$|z_{v(d)}(t) - z^*_{v(d)}| \leq 0.2 \tag{4.8}$$

to be satisfied, where $z^*_{v(d)}$ is the order parameter at the stable point. Under this condition, it was assumed that the order parameter reaches close enough to the stable state. The recovery time in days was then calculated as $(t/\Delta_v)/24$. It is possible to use more strict conditions, such as a threshold of 0.1. Figure 4.3 shows monotonically decreasing curves that represent the temporal evolution of the quantity $|z_{v(d)}(t) - z^*_{v(d)}|$. Note that choosing a lower threshold will quantitatively produce longer recovery times, but the qualitative results in terms of jet lag

recovery time remain the same. It is suggested that, in the future, this value can be adjusted so that the study yields the closest possible results to experimental values.

Lastly, it is important to note that, in a real scenario, it is the recovery time of the whole system that matters in questions of jet lag, and not just the recovery times of the SCN core and shell. However, the core-shell model has not yet been implemented to model peripheral clocks, such as the liver or thyroid, whose recovery times could better indicate the recovery time of the whole system. Since the shell is the SCN structure that primarily communicates with the peripheral clocks (Evans et al., 2015; Nagano et al., 2003), the recovery of the system is limited by the rate of re-entrainment of the shell (Evans and Silver, 2015). For this reason, in this work, the recovery time of the shell can be approximated to the recovery time of the whole system for the sake of generality.

It is now clear that the trajectories on the phase portraits correspond to the recovery process from jet lag. The position and nature of the fixed points can shape those trajectories, and, therefore, influence the recovery time for eastward and westward travels differently, depending on the phase shift, as will be noted in the next section.

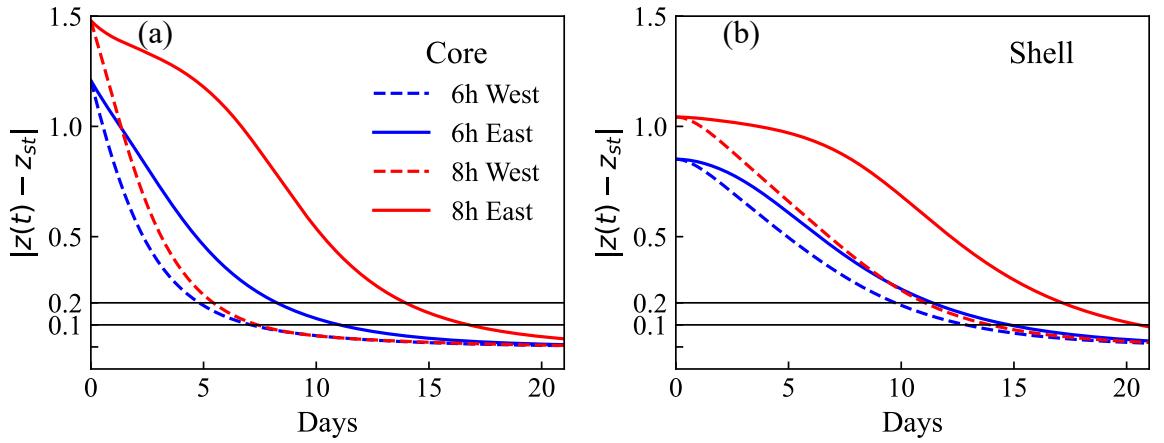

Figure 4.3: Recovery curves for the core (a) and shell (b) regarding a 6/8 h eastward travel and 6/8 h westward travel. The y-axis refers to the distance between the order parameter and the stable point, while the x-axis refers to the time in days.

4.5 Differences between Eastward and Westward Travelling

A shift in the LD cycle causes the core and shell to become desynchronised and the process of resynchronisation underlies the symptoms of jet lag. The recovery might take days and cause several health-related issues. Therefore, in order to find a jet lag therapy, it is necessary to shed light on the mechanism of jet lag. This was done by simulating the recovery process after travelling to all possible time zones. The results were then analysed by observing the phase portrait of the core and shell order parameters (Figure 4.2).

Figure 4.4 shows the core (orange bars) and shell (blue bars) recovery time in days for travelling to every possible time zone from a given departure point. The recovery times correspond to the time it took for the condition 4.8 to be verified during the simulations.

By analysing Figure 4.4, it is possible to draw four main conclusions:

(a) There is a good agreement between the results from biological experiments and the results of the model, which validates them.

(b) There is a sharp maximum in recovery time after travelling 8 h eastward, but not for westward travels;

(c) Travelling eastward yields longer recovery times than travelling westward - there is an east-west asymmetry in recovery times;
(d) The recovery time of the core is shorter than the recovery time of the shell[1].

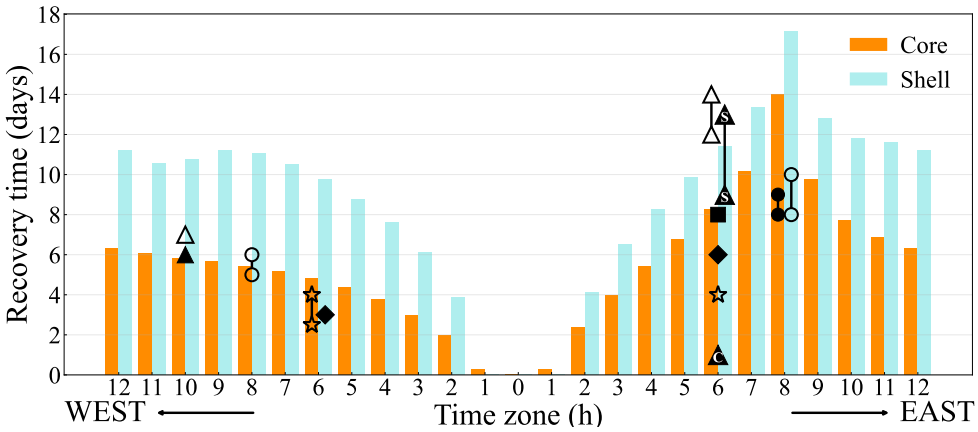

Figure 4.4: Recovery time of the core (orange bars) and shell (blue bars) versus the number of time zones crossed by travelling west and east. Experimental data for the recovery time of the SCN are represented by symbols. Empty and filled symbols correspond to the recovery time of locomotor rhythms and molecular rhythms, respectively. Triangles represent data from Nagano et al., 2003, circles from Y. Yamaguchi et al., 2013, stars from Richardson et al., 2020, diamonds from W. Nakamura, 2005 and the square from Davidson et al., 2009. These results are explicitly shown on Table 4.3. The triangles with the letters "C" and "S" correspond to the core and shell recovery times, respectively.

Examining the dynamical phase portraits in Figure 4.2, it is possible to observe that the recovery time depends on the initial point of the trajectory. In Section 4.3, it was mentioned that there are three steady-state solutions, which can be seen in the phase portraits: a saddle, a stable and an unstable point. These solutions influence the shape of the trajectory. As seen before, the trajectories tend to the stable node, but the saddle node can exert an important force on these trajectories. Let's address conclusion b). Observing the trajectories of the order parameter after travelling up to 8 time zones to the east, it is possible to verify that the trajectories start in the third quadrant and evolve to the stable point in the fourth quadrant through the lower half-plane. Thus, this evolution happens in the counterclockwise direction, that is, by phase advance. However, for more than 8 time zones to the east, the trajectories also start in the third quadrant and evolve to the fourth quadrant by entering the upper half-plane. Therefore, the evolution happens in the clockwise direction, that is, by phase delay. This distinction is caused by the presence of the saddle node. Both initial points for the 8 h eastward shift and the 9 h eastward shift are localised near the saddle node, on either side of it. Due to the contrary effects of repulsion and attraction, the nearer to this point, the longer the order parameter takes to flow to the stable point. This slowing down of the relaxation process due to the presence of the saddle node occurs in many real biological systems (Strogatz, 2015). It is now clear why the recovery after an 8 h eastward travel takes the longest time: the initial point is the closest to the saddle node and the order parameter takes the longest to reach the stable point. Although the initial point for a 9 h eastward shift is also close to the saddle node and the phase shift to reach stability is larger, the saddle node has a bigger influence on the recovery time from 8 h eastward shifts.

[1]Except for travelling 1 time zone to the east and west, where the shell recovery time is 0. This is due to the threshold of 0.2 chosen in Equation 4.8 - in this case, the quantity $|z_d(t) - z_d^*|$ is always below 0.2. A lower threshold should be considered.

Now, regarding conclusion c), it can be seen that, since both the saddle and the stable point are in the lower half plane, the initial points corresponding to eastward shifts are closer to the saddle node than the initial points corresponding to westward shifts. This means that, for the same shift, the eastward shift will take longer to recover than the westward shift. This is a general conclusion that many travellers arrive to after crossing several time zones: there is an east-west asymmetry in recovery times. Figure 4.3, which represents how close the order parameter is to the stable point as a function of time, also shows this observation in regard to 6 h and 8 h eastward and westward shifts. For any threshold value, the results remain the same - westward travels take longer to recover than their eastward counterparts.

Importantly, this saddle node influence occurs because the initial points, whose amplitude is equal to the stable point, have an amplitude similar to that of the saddle node. The role of the unstable node is less obvious as its amplitude is lower than that of the starting points. This means that they are further away from it than from the saddle node.

Now, let us look at the differences between the core and shell. First, as stated in conclusion d), the recovery times of the core are longer than those of the shell. Second, in Figure 4.2, the first noticeable difference is in the trajectories of the core and shell order parameters. In other words, the synchronisation index $\rho(t)$ and group phases $\psi(t)$ have different temporal behaviours. This occurs because the steady-state points have different coordinates, which can dramatically change the dynamics.

Furthermore, looking at Figure 4.2, the core trajectories show less variations in amplitude ($\rho_v(t)$) compared to the trajectories of the shell ($\rho_d(t)$). This means that, during the resynchronisation process, the core neurons approximately maintain synchronisation, compared to the shell neurons. In a deeper analysis, for the core and shell and for each time zone from -12 h to 12 h, the amplitude variations relative to the steady amplitude are calculated: $|\rho_{v(d)} - \rho^*_{v(d)}|$, and the largest amplitude variation is obtained ($\Delta\rho_{v(d)}$). Then, the average value of $\Delta\rho_{v(d)}$ is determined, i.e., $(\sum_n \Delta\rho_{v(d),n})/N$, where n corresponds to each time zone and N is equal to 23, the total number of considered time zones. Also, the time in the recovery process at which $\Delta\rho_{v(d)}$ occurs for every time zone ($t(\Delta\rho_{v(d),n})$) is obtained. Then, the average value of $t(\Delta\rho_{v(d)})$ is calculated in the same way as the average value of $\Delta\rho_{v(d)}$.

For the core, the average $\Delta\rho_v$ is ≈ 0.04 and the average $t(\Delta\rho_v)$ is ≈ 1.43 days after the start of the recovery process. The average core recovery time is 5.57 days. This means that, on average, $\Delta\rho_v$ occurs early in the recovery process. Moreover, the largest $\Delta\rho_v$ of all time zones occurs for a 9 h eastward shift for which $\Delta\rho_v \approx 0.156$, after 4.27 days since the start of the recovery process. For the shell, the average $\Delta\rho_d$ is ≈ 0.16 and the average $t(\Delta\rho_v)$ is ≈ 6.49 days after the start of the recovery process. The average shell recovery time is 9.05 days. This means that, on average, $\Delta\rho_d$ occurs later in the recovery process than for the core. Moreover, the largest $\Delta\rho_d$ of all time zones occurs for a 12 h shift for which $\Delta\rho_v \approx 0.56$, after 7.14 days since the start of the recovery process. It is also curious that the shell synchronisation index for a 12 h shift gets very close to 0, which, in biological terms, indicates that the shell neurons become almost completely desynchronised before reentraining. For other time zones, it also approaches 0, but not as much as for a 12 h shift. Comparing these observations, it is clear that the shell undergoes a greater weakening of synchronisation and later in the resynchronisation process than the core. Figure 4.5, which will be presented in the next section, illustrates these conclusions graphically for a 6 h eastward and a 10 h westward shift. Overall, because the shell has longer recovery times and a greater weakening of synchronisation, it can be concluded that the shell is more sensitive to jet lag than the core, which could have implications for peripheral clocks that depend on shell neurons for reentrainment signals (Evans and Silver, 2015; Silver, 2018).

Another difference between the core and shell recovery times is that, in Figure 4.4, despite

the 8 h eastward maximum which occurs for both core and shell, the shell shows a broad maximum for westward travels, while the core recovery times always increase with the phase shift.

In summary, the core-shell model was able to demonstrate that there are notable differences between recovery from eastward or westward phase shifts: core and shell neurons take longer to reentrain to the new LD cycle after eastward shifts, especially after an 8 h shift, but, despite that, core neurons reentrain faster than shell neurons. The presence of a saddle node in the dynamical phase portraits of the core and shell order parameters provides a solid mathematical explanation of these biological differences.

4.5.1 Comparison between the Theory and the Experiment

The previous section described some results of the resynchronisation process obtained with the core-shell model. In this section, more specific results on the temporal behaviour of synchronisation and group phase of the SCN will be shown. To verify their validity, these results and the conclusions drawn in the previous section will be then compared with the results of biological experiments. These were obtained in mice and rats after rapid phase shifts of the LD cycle (Davidson et al., 2009; Nagano et al., 2003; W. Nakamura, 2005).

Firstly, as mentioned in conclusion a) in the previous section, the results of the biological experiments are close to the results of the model (see Figure 4.4). The experiments were obtained after assessing molecular rhythms (filled symbols) and locomotor rhythms (empty symbols) of mice and rats. Table 4.3 presents these results, explicitly stating the paper, the animal tested (mice or rats), the method of measurement (whether the assessment of the circadian rhythms was made by analysing molecular or locomotor rhythms), the time shifts tested and the respective recovery times measured. Regarding the method of measurement, locomotor rhythms were obtained by observing spontaneous locomotor activity recorded by an infrared sensor and/or by determining wheel-running activity. On the other hand, molecular rhythms refer to the rhythms of generation and destruction of messenger RNA involved in the genetic loop that generates circadian rhythms (see Section 2.2.3). Only Nagano et al., 2003 clearly reported a difference between the core and shell recovery times - the other papers investigating molecular rhythms in the SCN reported the recovery time as the time taken for all SCN to regain the regional relative phase differences. There is a lack of studies which directly approach the core and shell recovery times. For the same time shift studied, the measured recovery times fluctuate due to the different methods of measurement, animal tested, sample size, or other differences in the experiments. The analysis in this section is based on the fact that there is a phase correlation between cellular genetic oscillations and group phases of the core and shell.

Studies of human melatonin's circadian rhythm have shown that, after an 8 h phase advance or more, reentrainment can be completed by a phase delay rather than a phase advance (Eastman and Burgess, 2009). These observations on humans are analogous to the presented conclusions that, on the core and shell phase portraits (Figure 4.2), the direction of entrainment is opposite to the phase shift, when this phase shift is a 9 h advance or more. One of those studies (Takahashi et al., 1999) even revealed that, after an 8 h advance, one of the subjects did not phase shift for 5 days in the new time zone. This observation was probably the result of a biological conflict between phase delay and advance, which prevented any phase shift. This conflict has been already demonstrated by Mitchell et al., 1997. According to the presented phase portraits in Figure 4.2, this conflict may be due to the saddle node and the results are in accordance with conclusion b).

Moreover, W. Nakamura, 2005 discovered that there is a desynchrony of Per1-luciferase expression between the core and shell after a rapid phase shift of the LD cycle. When they compared the desynchrony between a 6 h phase advance and phase delay of the LD cycle,

they found that the desynchrony was more pronounced and prolonged in the case of a phase advance, which corresponds to travelling eastward. This is in accordance with conclusion c). Nagano et al., 2003 had similar results, but for the RNA cycles of the Per1, Per2 and Cry genes for a 6 h phase advance and a 10 h phase delay. Some of the results obtained by Nagano et al., 2003 were compared with the results of the core-shell model shown in Figure 4.5. Figure 4.5 a) shows the temporal evolution of $\rho_{v(d)}$, while b) shows the temporal evolution of $\psi_{v(d)}$, both for a 6 h phase advance and a 10 h phase delay. These results show that, after the first day of reentrainment to a 10 h westward shift, $\psi_v(0) - \psi_v(1d) \approx 2.5$ h and $\psi_d(0) - \psi_d(1d) \approx 0.2$ h. For the 6 h eastward shift, after the first day of reentrainment $|\psi_v(0) - \psi_v(1d)| \approx 0.8$ h and $|\psi_d(0) - \psi_d(1d)| \approx 0.1$ h. These observations show that, for the 10 h westward shift, there is a larger phase difference after the first day than for the 6 h eastward shift, for both core and shell, which is evidence for the east-west asymmetry in recovery times. These numerical results are in agreement with observations in Nagano et al., 2003. Nagano et al., 2003 also states that 3 days after a rapid 10 h westward shift, there is a phase difference of 12 h in Per1 expressions between core and shell. According to the numerical results in Figure 4.5, a maximum phase difference of 8.5 h between the core and shell regions occurred after 4.8 days of reentrainment, which is close to the result obtained by Nagano et al., 2003.

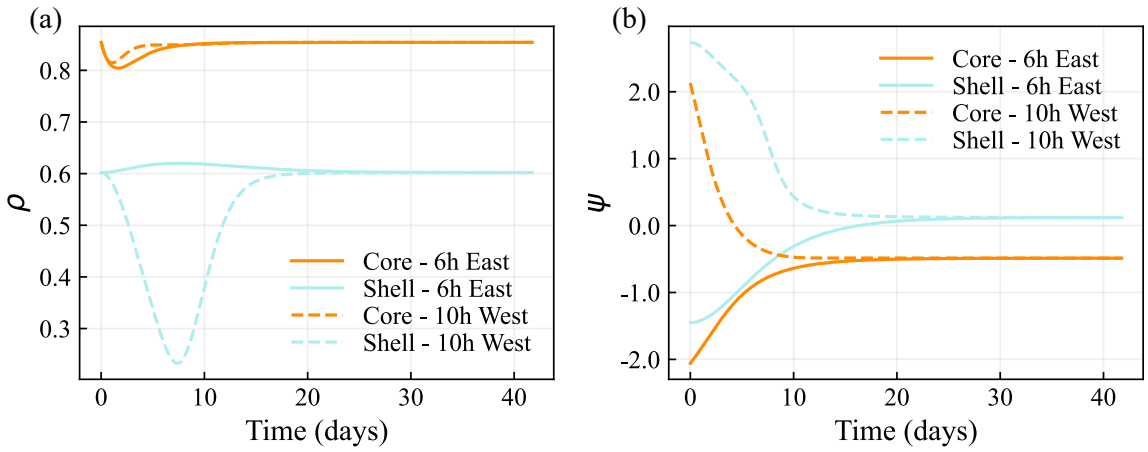

Figure 4.5: (a) Time dependence in days of the synchronisation indices ($\rho_{v(d)}$) of the core (orange lines) and shell (blue lines) after instantaneous travelling across 10 time zones to the west (dashed lines) and across 6 time zones to the east (full lines). (b) Time dependence in days of the group phases (in radians) ($\psi_{v(d)}$) of the core and shell.

The next observation to consider is conclusion d) in the previous section, which states that the recovery times of the core are shorter than those of the shell, for both eastward and westward travel. This observation can be verified in Figure 4.5, since ρ_v and ψ_v stabilizes earlier than ρ_d and ψ_d, respectively. In the core-shell model, the coupling between core oscillators is higher than the coupling between shell oscillators (see Section 4.2). The direct input of optic cue information as well as the stronger intracoupling may explain why the core entrains faster than the shell to the new LD cycle (W. Nakamura, 2005). Nagano et al., 2003, W. Nakamura, 2005 and Davidson et al., 2009 have used biological experiments to show that different regions of the SCN adapt to the new phase of the LD cycle at different rates, with the core region being the fastest to adapt.

Table 4.3: Experimental procedures described by different papers for testing recovery times to different time shifts. The "Measuring method" column corresponds to the type of rhythms analysed to obtain measures of the recovery time. These experimental results are also represented in Figure 4.4.

Paper	**Animal tested**	**Measuring method**	**Time shifts tested**	**Measured recovery times**
Richardson et al., 2020	Male mice	Locomotor rhythms (wheel-running)	6h delay	$\approx$ 2.5 to 4 days
			6h advance	$\approx$ 4 days
Y. Yamaguchi et al., 2013	Mice	Locomotor rhythms (spontaneous activity and wheel-running)	8h delay	5 to 6 days
			8h advance	8 to 10 days
		Molecular (Per1, Per2, Bmal1 transcription) rhythms in the SCN and the peripheral timing system	8h advance	8 to 9 days
Davidson et al., 2009	Mice	Molecular (Per2 transcription) rhythms in the SCN and the peripheral timing system	6h advance	8 days, for both the SCN and other tissues
W. Nakamura, 2005	Male rats	SCN molecular (Per1 transcription) rhythms	6h delay	3 days
			6h advance	6 days
Nagano et al., 2003	Male rats	SCN molecular (Per1 transcription) rhythms	10h delay	6 days
			6h advance	Core - 1 day, Shell - 9 to 13 days

CHAPTER 5

Search for an Optimal Light Therapy

A simple light pulse is a non-pharmacological alternative to reduce jet lag (Arendt, 2018; Bin et al., 2019; Morgenthaler et al., 2007). This has been experimentally proven in mice and humans (Boivin and James, 2002; Richardson et al., 2020; St Hilaire et al., 2012; Zeitzer et al., 2000) and is already being commercialised as light boxes or even glasses which emit light. But, to what extent have humans figured out the optimal way to use light in our favour? Commercialised LT is based on a few biological experiments (Comtet et al., 2019). These types of studies are time-consuming and have several limitations. Moreover, the number of studies which focused on explicitly studying light as a jet lag therapy is still reduced (Boivin and James, 2002; Comtet et al., 2019; Eastman and Burgess, 2009). To date, the exact mechanism of LT has not been fully understood. As mentioned in Chapter 3, some mathematical models have already been used to study the biological mechanism of jet lag with very good results. Therefore, using the core-shell model to understand exactly what LT does to our organism from a dynamic point of view can help to determine the optimal parameters to reduce jet lag and encourage new experimental procedures.

In order to understand what parameters of light have been used in experimental studies, Table 5.1 summarises four works in this area. Each work tested the effect of light on the human circadian rhythm and the phase shift that the light can cause. The second column of Table 5.1 indicates the duration, intensity and timing of the light used to produce the phase shifts (the third column). Table 5.2 presents some protocols suggested by commercialised LT solutions. Looking at the light intensities utilised in the protocols of Table 5.1, the tested values range is $\approx$ 2,000 - 10,000 lux, where lux = lumen/m^2. To understand how bright can this light be, take as a reference the following values: 1 lux typically corresponds to moonlight with a full moon, 250 - 500 lux can be seen in offices, laboratories or classrooms, 1,000 lux corresponds to an overcast day and operating theatres and 10,000 - 25,000 lux correspond to full daylight on a clear day (Green Business Light, 2020). Regarding light duration, Table 5.1 shows that the range of studied values is 0.5 - 6.7 h. Finally, the timing of the treatment varies according to the type of phase shift: in the case of phase advance, the light was applied early in the morning, in circadian time; in the case of phase delay, the light was applied late at night, in circadian time (intuition on this point is presented in Section 2.4.2).

With this in mind, this section explains the implementation of LT in the core-shell model. It then describes the parameters used in the simulations and the LT protocols tested. Finally, the effectiveness of LT will be ascertained. This will require an analysis of the influence of

different LT parameters on jet lag recovery time, with the ultimate aim of identifying optimal parameters for minimising it.

Table 5.1: Examples of protocols of light exposure used in biological experiments and the corresponding produced time shifts. Note that DLMO is the moment when melatonin production starts in dim light conditions (Khalsa et al., 2003).

Paper	**Experimental protocol (light duration, intensity and timing)**	**Produced time shifts**
Comtet et al., 2019	30 minutes white light with an intensity of 10,000 lux in the early morning	Not assessed
St Hilaire et al., 2012	1h white light with an intensity of 8,000 lux in the late night	$\approx$ 1.5h delay
	1h white light pulse with an intensity of 8,000 lux in the early morning	$\approx$ 1h advance
Dewan et al., 2011	1, 2, or 3h white light with intensities of 2,000, 4,000, or 8,000 lux (all combinations were tested) 3h before CBTmin.	The largest phase shifts were produced by the 3h exposures ($\approx$ 1h-2h delay)
Khalsa et al., 2003	6.7h white light with intensities $\approx 5,000 - 9,000$ lux at $\approx$ DLMO	$\approx$ 4h delay
	6.7h white light pulse with intensities $\approx 5,000 - 9,000$ lux at $\approx$ 8h after DLMO	$\approx$ 2h advance

Table 5.2: Suggested protocols of LT products' usage by Philips, 2023, ORTOREX, n.d. and Lucimed, 2023.

Company	**Light therapy product**	**Suggested protocols**
Philips	EnergyLight (light panel)	Choice of light intensity up to 10,000 lux, from 15 minutes to 2h
Ortorex	Therapy Lamp (light panel)	Choice of light intensity up to 12,000 lux, in intervals of 10 to 30 minutes
Lucimed	Luminette (light-emitting glasses)	There are three settings: 500 lux for 45 minutes, 1,000 lux for 30 minutes and 1,500 lux for 20 minutes

5.1 Modelling of Light Therapy

In the context of this work, LT corresponds to a period of light with a constant intensity. Thus, to model LT in the core-shell model, the parameter in Equation 3.5 correspondent to the influence of the LD cycle on the core, $F^{(m)} \sin(\omega_F t + \phi^{(m)} - \theta_i^{(m)})$, is replaced by a

constant parameter B, where the magnitude $|B|$ characterises the light intensity. The equation is now as follows:

$$\frac{d\theta_i^{(m)}}{dt} = \omega_i^{(m)} + \frac{1}{N_n}\sum_n \sum_{j\in G_n} K_{nm}\sin(\theta_j^{(n)} - \theta_i^{(m)}) + B \tag{5.1}$$

The dimensionless value $B = 1$ corresponds to 18.75 lux (this conversion was derived from experimental observations, as stated in Goltsev et al., 2022). The substitution of the LD cycle term for the parameter B in Equation 3.5 is equivalent to stating that B renormalises the endogenous free-running frequencies of the core oscillators (Goltsev et al., 2022). In contrast, shell neurons are not directly affected by this constant B since they do not directly receive optic cues. Therefore, in other words:

$$\omega_i^v \Rightarrow \omega_i^v + B \tag{5.2}$$

The periodic external force term on the macroscopic equations 4.2, 4.3 is also replaced and the mean endogenous free-running frequencies of core oscillators are renormalised: $\overline{\omega}_v \Rightarrow \overline{\omega}_v + B$.

The sign of B determines the chronotype of the animals, i.e., if they are diurnal or nocturnal. Note that, if B is positive, the mean free-running frequencies of core oscillators are increased by B. In contrast, if B is negative, those mean free-running frequencies are reduced by $|B|$. These observations are in agreement with the Aschoff's first rule, which states that constant light shortens the free-running period for diurnal animals and lengthens the free-running period for nocturnal animals (see Section 2.3). Therefore, for diurnal animals B is considered positive and for nocturnal animals, B is considered negative (Goltsev et al., 2022).

The new macroscopic equations are now rewritten as Equations 5.3-5.6.

$$\frac{d\rho_v}{dt} = -\rho_v\Delta_v + \frac{1}{2}\rho_v K_{vv}(1-\rho_v^2) + \frac{1}{2}\rho_d K_{dv}(1-\rho_v^2)\cos(\psi_d - \psi_v), \tag{5.3}$$

$$\frac{d\psi_v}{dt} = \overline{\omega}_v - \omega_F + B + \frac{1}{2}\rho_d K_{dv}\frac{(1+\rho_v^2)}{\rho_v}\sin(\psi_d - \psi_v), \tag{5.4}$$

$$\frac{d\rho_d}{dt} = -\rho_d\Delta_d + \frac{1}{2}\rho_d K_{dd}(1-\rho_d^2) + \frac{1}{2}\rho_v K_{vd}(1-\rho_d^2)\cos(\psi_v - \psi_d), \tag{5.5}$$

$$\frac{d\psi_d}{dt} = \overline{\omega}_d - \omega_F + \frac{1}{2}\rho_v K_{vd}\frac{(1+\rho_d^2)}{\rho_d}\sin(\psi_v - \psi_d), \tag{5.6}$$

In the simulations, it is assumed that LT starts as soon as the organism arrives at the destination time zone, at t_0. The core-shell model assumes that the LD cycle is given by $F\sin(\omega_F t + \phi)$. Therefore, t_0 is the instant when the light section of the LD cycle begins, which means that t_0 approximately corresponds to 6 a.m.. Thus, for modelling purposes, it can be assumed that the LT starts at 6 a.m., the arrival time in the destination time zone.

The initial conditions of the simulations, at t_0, correspond to those in the entrained state and the phases $\psi_{v(d)}(t_0)$ are shifted by the number of time zones crossed (n), $\psi_{v(d)}(t_0)\pm 2\pi n/24$, as mentioned in Section 4.4. Then, the following steps were taken in order to complete the simulations, which now include LT:

1. At the moment of arrival at the destination time zone, 6 a.m., the individual takes the LT for a duration D. During the therapy, the Equations 5.3-5.6, which correspond to the period of constant light with intensity B, are solved.

2. The final condition of the LT is the initial point for the next step. Then, at $t = D$, LT ends and the Equations 4.2-4.5, which correspond to the normal LD cycle, are solved until the solutions satisfy the condition 4.8.

That is, the simulations are constituted by a first part of LT followed by the normal recovery process. The amount of time to verify the condition 4.8 is defined as the recovery time in the given time zone.

The purpose of this study is to understand how LT affects jet lag recovery time and to find the optimal LT protocol for recovery after specifically chosen time shifts, using the core-shell model. The time shifts are chosen as 6 h to the east (or a 6 h advance), 6 h to the west (or a 6 h delay), 8 h to the east (or an 8 h advance) and 8 h to the west (or an 8 h delay) since these are the time shifts with more experimental results on recovery time found in the literature (Table 4.3). For the same amount of time shifts, both the westward and eastward shifts are compared. The choice of the 8 h advance is also due to the fact that, according to the present model, this time shift yields the longest recovery time. Therefore, it would make sense to prioritise its minimisation. In this study, it is assumed that minimising the recovery time of the shell would be closely related to minimising the recovery time of the whole body. This assumption is made based on the understanding that the shell coordinates the circadian rhythms of most tissues, setting the pace of reentrainment, as evidenced by Evans and Silver, 2015; Evans et al., 2015; Nagano et al., 2003.

Then, the sequence of steps to achieve the objectives is presented: 1) the influence of light intensity is studied, proving that LT is effective in reducing the SCN recovery time. 2) The influence of LT duration is also investigated. 3) By varying light intensity and LT duration, the pair of values of intensity and duration that minimise the recovery time of the shell is obtained. 4) Using the optimal intensity and duration found, this LT duration is divided into shorter time intervals or sessions, with each session occurring once per day. The recovery time found for this multi-session LT is then compared with the single-session LT. 5) Finally, the optimal light intensity, duration, timing and number of LT sessions for the four considered time shifts are presented.

The simulations were performed with the parameters in Table 4.1 and computational methods described in Section 4.2. The specific parameters of LT used in this work will be presented throughout the next sections. The appropriate conversion to dimensionless units was also performed.

5.2 Mechanism of Light Therapy

Let us first try to understand the mechanism of a light pulse in the core-shell model. In Section 5.1, it was shown that constant light increases the frequency of neurons, according to the Aschoff's first rule. In order to visually understand this rule, Figure 5.1 qualitatively shows the recovery process using LT by showing the dynamics of $z_{v(d)}$. To understand the effect of a light pulse on the core and shell dynamics, let us focus first on the phase portraits of Figure 5.1 a) and b), regarding the core and shell, respectively. In the simulations, it was used a light intensity of 2,000 lux (in adimensional terms, $B \approx 107$) and a light pulse duration of 1 h.

In Figure 5.1 a), it is possible to observe that LT increases the phase of z_v since it moves counterclockwise. There is a noticeable difference in Figure 5.1 a) between the 8 h west and 8 h east trajectories. For the westward travel, the normal recovery process occurs by decreasing the phase of the order parameter. However, constant light increases the phase and the trajectory takes the opposite direction to the normal recovery trajectory. Since this trajectory is clockwise, LT increases the phase difference between the stable point and the z_v. Thus, LT may not accelerate resynchronisation in this case. For the eastward travel, the

trajectory of the normal recovery process is in a counterclockwise direction, by increasing the phase of z_v. In this case, constant light increases the phase of z_v (its trajectory has a counterclockwise direction) and quickly moves z_v away from the saddle point, where the dynamics are the slowest. This reduces the phase difference between the stable point and the z_v.

Note that in Figure 5.1 b), the end point of LT (square symbol) overlaps the start point of LT (star symbol). Comparing the trajectories in Figure 5.1 b) after LT with the trajectories without LT in Figure 4.2, there are minor changes, more visible for an 8 h delay. This means that, during LT, the light has little effect on the dynamics of the shell, probably since this region does not receive any direct optic cues.

Now, let us focus on Figure 5.1 c) and d), which correspond to a LT of 4,000 lux for 1 h and Figure 5.1 e) and f), which correspond to a LT of 2,000 lux for 2 h. Note that Figure 5.1 c) and d) were obtained for a double intensity of Figure 5.1 a) and b), while maintaining the duration of 1 h and e) and f) were obtained for a double duration of a) and b), while maintaining the intensity of 2,000 lux. The purpose of showing these phase portraits is to compare the effect of changing the light intensity with the effect of changing the light duration in equal proportions. In fact, there are no direct differences between Figure 5.1 c) and e), which correspond to the dynamics of the core and between Figure 5.1 d) and f), which correspond to the dynamics of the shell. This means that the effects of doubling the intensity appear the same as doubling the duration of LT. To understand this observation from a theoretical point of view, let us analyse the equation governing the core group phase (Equation 5.4). In Equation 5.4, one can replace the infinitesimal changes for macroscopic changes in phase ($\Delta\theta$), which occur in a macroscopic interval of time (Δt). If both sides of the equation are multiplied by Δt, then a change in the core group phase $\Delta\psi_v$ after Δt is given by:

$$\Delta\psi_v = A\Delta t + B\Delta t \tag{5.7}$$

From Equation 5.4, $A\Delta t$ corresponds to the phase shift produced by the influence of the core's mean frequency and interactions among oscillators and $B\Delta t$ is the phase shift produced by the influence of the constant light during LT. Assuming LT is being applied, Δt corresponds to the LT duration, D. There are two main conclusions to be drawn from this equation. First, as stated above, the increase in the phase of z_v shown in the phase plots during LT is not only due to the constant light. However, the A term on Equation 5.7 is not very significant. When $D \ll 24$ h, $\Delta\psi_v \approx B \times D$. This is because, in the A term of Equation 5.7, the maximum value of the non-constant terms (i.e. the sinusoidal term, ρ_v and ρ_d) is 1. Therefore, the maximum achievable value for the A term is approximately 0.49. Comparing this value with the usual light intensities B used in LT (see Table 5.1) and those examined in this chapter, which are in the order of hundreds (equivalent to thousands of lux), it is clear that the A term is at least three orders of magnitude smaller than the B term. Consequently, its contribution to the overall phase shift is not significant. Second, the LT duration D and light intensity B are inversely proportional. Therefore, it is expected that doubling the intensity would yield similar results to doubling the duration, as seen in Figure 5.1.

By analysing Figure 5.1 c)/e) (dynamics of the core), for the 8 h westward travel, it is possible to observe that the light pulse is so intense/is so long that moves z_v in the counterclockwise direction, past the saddle point. Because z_v is now below this point, the recovery after LT is done in the opposite direction to the normal recovery - in this case, by phase advancing instead of phase delaying. For an 8 h eastward travel, a similar situation occurs: LT pushes z_v past the stable point and then the recovery after LT is made by phase delaying instead of phase advancing. For Figure 5.1 d)/f) (dynamics of the shell) and for an 8 h westward travel, the direction of entrainment after LT is opposite to the normal direction of

entrainment, while for an 8 h eastward travel, these directions are the same. Nevertheless, these conclusions show that, in certain cases, LT may cause an individual's system to be entrained in the opposite direction to normal.

It is important to note that for sufficient intensity or duration of constant light, the phase shift caused by LT can be of multiples of 2π. When this occurs, LT has absolutely no effect on the core and shell recovery from jet lag since the system begins its recovery from the initial conditions before LT.

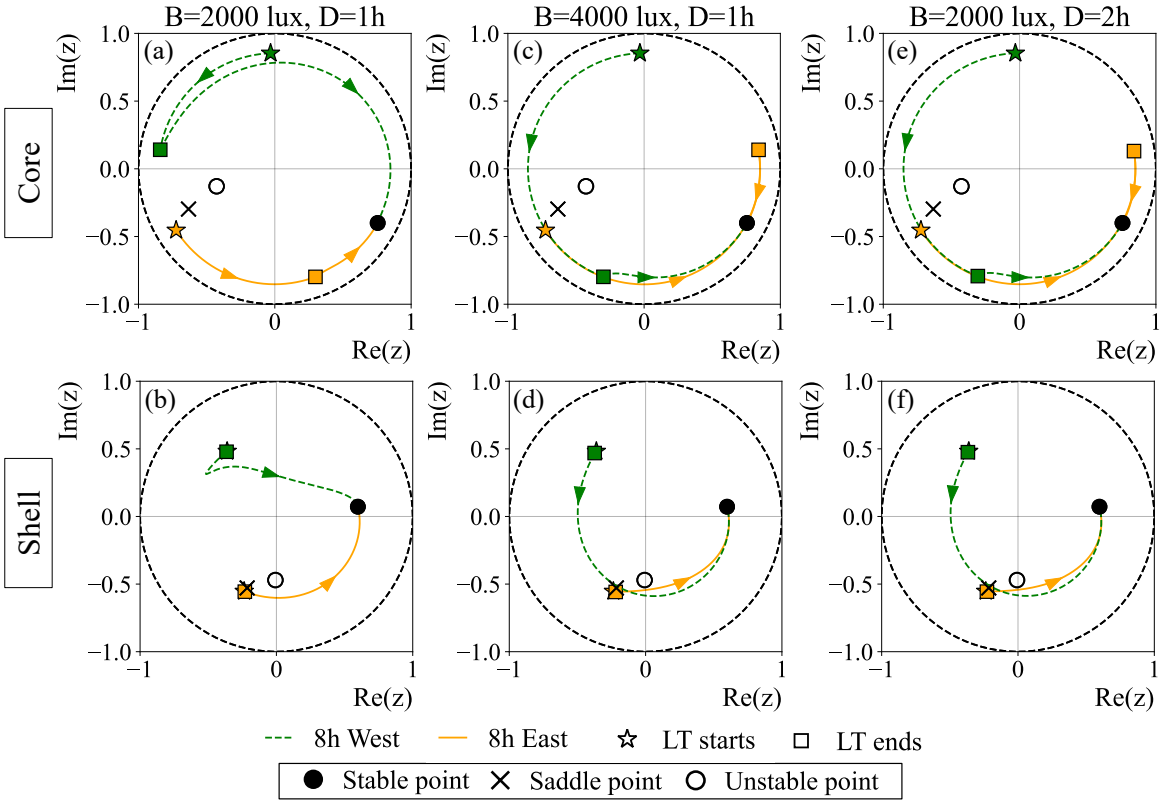

Figure 5.1: Trajectories of the recovery dynamics of the core (first row, a), c) and e)) and the shell (second row, b), d) and f)). For each column, the light intensity B and LT duration D used in the simulations are given at the top of the column. The recovery process after travelling 8 h to the west is shown by a green dashed line and after travelling 8 h to the east is shown by a yellow solid line. The beginning of LT is represented by a star filled with the colour corresponding to the phase shift. The end of LT and start of the normal recovery process is marked by a square also filled with the colour corresponding to the phase shift. The positions of the saddle node, the unstable point, and the stable point are marked by the cross, the empty circle, and the filled circle, respectively.

5.3 Influence of Light Therapy Intensity and Duration on Recovery Time

Light Intensity. Figures 5.2 and 5.3 were constructed to further investigate the influence of light intensity on the recovery time for the 6/8 h east/west time shifts. The light intensities chosen range from -1,000 to 20,000 lux and the duration is 1 h. Although it has no physical meaning, a light intensity of -1,000 lux is chosen to emphasise the continuation of the curves into the negative range.

Looking at the horizontal lines corresponding to the recovery time of the core and shell without LT, the main conclusion from the plots is that LT effectively reduces the recovery time for some light intensity values, both for the east and the west.

All plots in Figures 5.2 and 5.3 show a waveform of recovery times along the selected range of light intensities. If this range was continuous, the minima and maxima would have a periodicity of about 9,087 lux, according to Equation 5.7. This nonlinear behaviour can be explained by the mechanism of LT. First, let us focus on the recovery times of the core in all the plots. Looking at the phase portraits in Figure 5.1, light induces large phase shifts of approximately $B \times D$ on z_v, creating a counterclockwise trajectory. Therefore, when travelling eastward, increasing LT intensities shift the order parameter closer and closer to the stable point (see the yellow line in Figure 5.1, a)), until the recovery time reaches a minimum. However, a sufficiently high light intensity shifts the order parameter beyond the stable point and the higher the intensity, the further it is from the stable point (see the yellow lines in Figure 5.1, c) and e)), until the recovery time reaches a maximum. In contrast, when travelling westward, increasing LT intensities brings the order parameter farther away from the stable node, until the recovery time reaches a maximum (see the green line in Figure 5.1, a)). A sufficiently high intensity forces the dynamics to pass the saddle node and be close to the stable point, until the recovery time reaches a minimum (see the green lines in Figure 5.1, c) and e)). This behaviour of the recovery time can be clearly seen in Figure 5.2 and 5.3. The periodicity observed in these figures is due to the fact that the phase shift produced by the LT ($\approx B \times D$) might reach multiple values of 2π, yielding approximately the same recovery times for different values of light intensity. The recovery times of the shell also show a periodic dependence on the light intensity, with minima occurring at higher intensity values than the core. This periodicity may occur due to the influence of the core on the shell, which is itself periodic. This is, the values of ψ_v vary periodically, which further influences the values of ρ_d and ψ_d according to Equation 5.5 and Equation 5.6.

Let us look at the specific values of light intensity that reduce the recovery time. For a 6 h time shift to the east, from 1,000 lux to 7,000 lux, from 10,000 lux to 16,000 lux, and at 19,000 lux and 20,000 lux, the recovery times of both core and shell are shorter than the recovery times without LT. In addition, for a 6 h time shift to the west, these light intensities are 6,000 lux to 9,000 lux and 15,000 lux to 18,000 lux. For an 8 h time shift to the east, they are 1,000 lux to 8,000 lux and 10,000 lux to 20,000 lux. Finally, for an 8 h time shift to the west, they are 6,000 lux to 9,000 lux and 15,000 lux to 18,000 lux. Note that there are more light intensities that reduce recovery times for eastward shifts than for westward shifts. Also, the light intensities that reduce the recovery time for westward shifts are higher. This is because, for westward shifts, higher light intensities push the z_v past the saddle node, bringing it closer to the stable point. For eastward shifts, lower light intensities can have the same effect.

In addition, it is possible to verify that for the 6 h and 8 h westward and the 8 h eastward shifts, the recovery times of the shell are longer than those of the core for every light intensity considered, as expected (see Section 4.5 for more details). However, for the 6 h eastward time shift, there are some values of light intensity for which the core has longer recovery times than the shell. The biological origin of this behaviour is still unclear, but in Section 6.1 it will be further analysed.

Finally, it can be noted that the recovery times for the 8 h eastward and westward time shifts are longer than for the 6 h eastward and westward time shifts, respectively, which follows the results for the recovery times without LT (see Figure 4.4).

LT Duration. Next, the dependence of the recovery time on LT duration is investigated. For this purpose, Figures A.1, A.2, 5.4 and 5.5 were constructed, corresponding to time shifts of 6 h east, 6 h west, 8 h east and 8 h west respectively. Each figure shows four plots of recovery time as a function of LT duration, corresponding to different light intensities (2,000, 5,000, 7,000 and 10,000 lux), in order to also observe the dependence on light intensity. In this

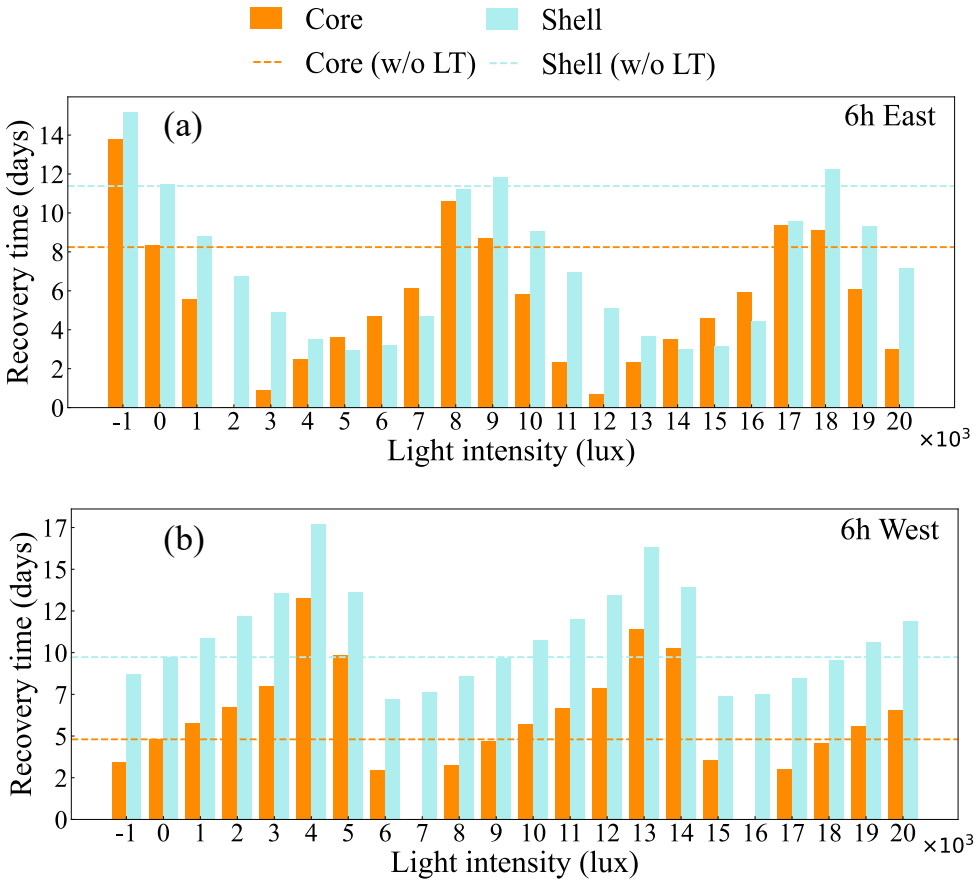

Figure 5.2: Recovery times of the core (orange bars) and shell (blue bars) as a function of the light intensity B after a a) 6 h eastward time shift and a b) 6 h westward time shift. For all the plots, $B = [-1,000; 20,000]$ (lux), $\Delta B = 1,000$ (lux). LT was applied at arrival time ($T = 0$) and $D = 1$ h. In the absence of LT, the recovery times are shown by dashed lines.

section, only Figures 5.4 and 5.5 (for an 8 h time shift to the east and west, respectively) are shown, as the others give similar conclusions. The main difference between the figures for 8 h and 6 h is that the recovery times are generally longer for the former, for both the eastward and westward shifts.

For these figures, a range of LT durations from 15 minutes to 3 h are assumed. It is possible to notice that, for the time shifts to the east, only 15 minutes of LT can significantly reduce the recovery time of both core and shell. In fact, for an 8 h eastward time shift, every combination of duration and light intensity considered in Figure 5.4 reduces the recovery time of the core and shell.

The behaviour of the recovery time of the core and shell as a function of the LT duration is nonlinear. It is also highly dependent on the light intensity used. For both core and shell, the recovery time appears to oscillate in the range of the LT durations. The principle is the same as discussed in the previous section: for $D \ll 24$ h, $\Delta\psi_v \approx B \times D$. Therefore, for sufficiently long durations, the order parameter undergoes a phase shift of about 2π, eventually yielding approximately the same recovery times for different durations with a certain periodicity.

This oscillatory characteristic of the recovery time with LT duration/intensity implies that increasing the duration or intensity is not always beneficial to reduce the recovery time. It must be taken into account that the generated phase shift of the z_v may end up in a region of slow dynamics, such as near the saddle node, or in a region further away from the stable point

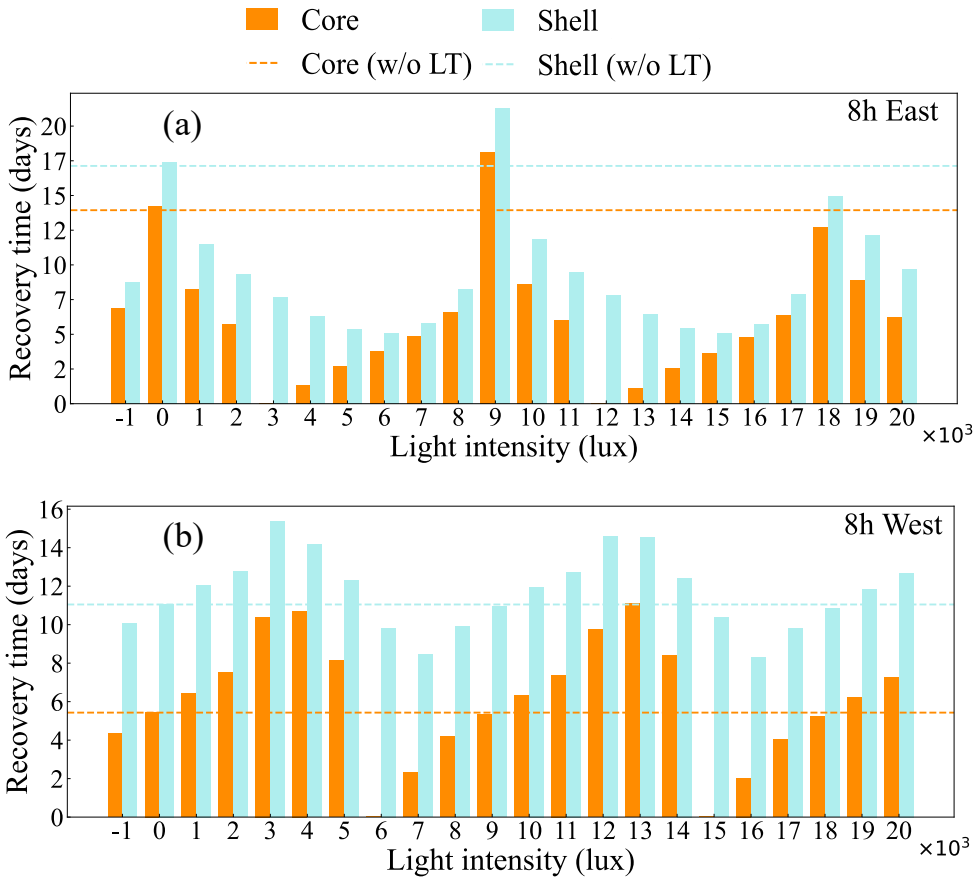

Figure 5.3: Recovery times of the core (orange bars) and shell (blue bars) as a function of the light intensity under an a) 8 h eastward time shift and an b) 8 h westward time shift. The parameters used are the same as Figure 5.2. In the absence of LT, the recovery times are shown by dashed lines.

compared to without LT. Therefore, the presented figures can help to choose the pairs of intensity/duration which actually reduce the recovery times. In the next section, 3D figures of the dependence of the recovery times of the core and shell on LT duration and light intensity are presented, as well as the optimal parameters for minimising the recovery time of the shell for each time shift considered in this work.

A curious observation is that, for all four figures of the recovery time versus LT duration, the number of recovery time oscillations for both the core and shell appears to increase with increasing light intensity values. This is because increasing the intensity B increases the phase shift of the order parameter for a given duration D and the number of 2π phase shifts for a higher B is greater for the given range of durations. Therefore, the frequency of the recovery time oscillations along the range of durations is higher for higher B.

Another insight to take from the plots with increasing B is that, for a given oscillation of recovery time, its values move further to the left of the plot. This means that the higher the B, the shorter the D required to achieve a given recovery time. More specifically, if an individual wishes to have a shorter duration of LT in order to obtain the minimum recovery time possible, increasing B is key. The other way around is also valid: if one desires to use less B during LT, one must increase the duration of the light exposure to obtain the minimum recovery time.

On another note, comparing the figures for an 8 h time shift to the east (Figure 5.4) and

west (Figure 5.5), it is possible to see that there are fewer pairs of B and D which lower the recovery time for the westward time shift than for the eastward time shift. Observing the plots corresponding to an 8 h westward time shift, any D value for $B = 2,000$ lux (except $D = 3$ h) does not accelerate the resynchronisation of the core and shell. Higher intensities are needed.

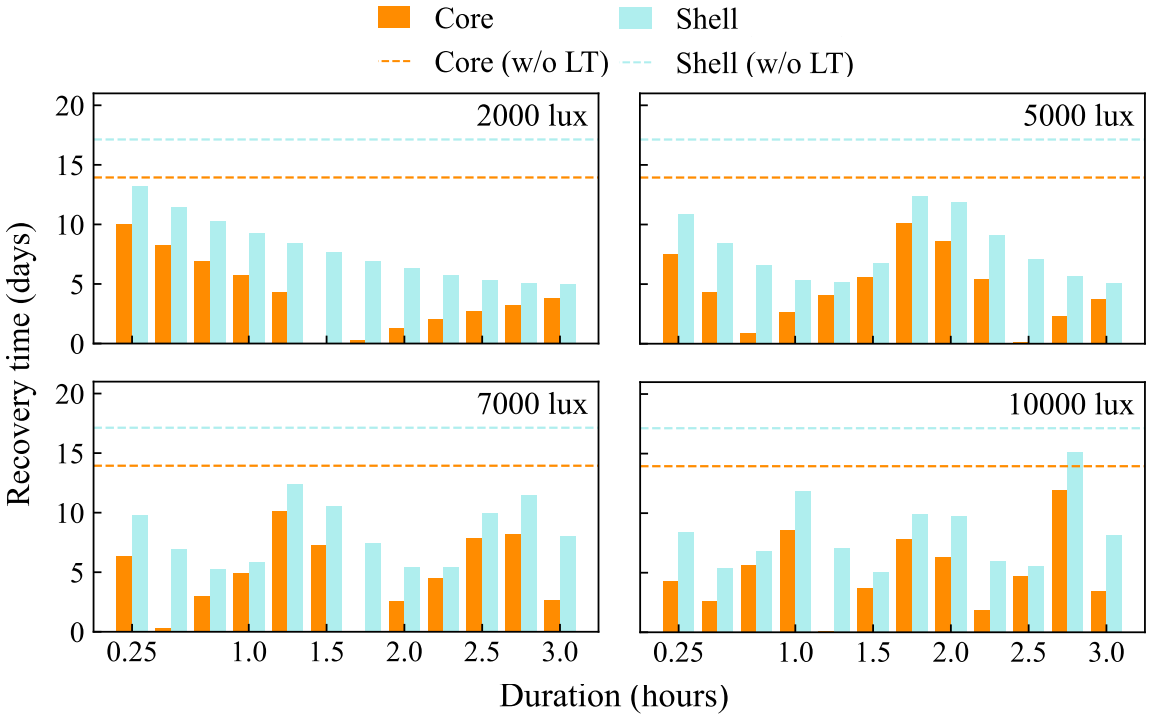

Figure 5.4: Recovery times of the core (orange bars) and shell (blue bars) as a function of the LT duration for an 8 h eastward time shift and light intensities of a) 2,000 lux, b) 5,000 lux, c) 7,000 lux and d) 10,000 lux. LT was applied at arrival time ($T = 0$) and $D = [15/60; 3]$ h, $\Delta D = 15/60$ h. In the absence of LT, the recovery times are shown by dashed lines.

Optimal Parameters of Light Intensity and LT Duration. To minimise the recovery time from jet lag by employing LT, it is essential to use the optimal light intensity and duration. In this study, as mentioned in Section 5.1, the recovery time of the shell is minimised, since it is closely related to minimising the recovery time of the whole body.

Therefore, the recovery times of the core and shell after the four considered time shifts are obtained for a wide range of light intensities ($B = [2,000; 10,000]$ (lux), $\Delta B = 50$ (lux) - 161 values of B) and LT durations ($D = [15/60; 3]$ h, $\Delta D = 1/60$ h - 166 values of D). The ranges of B and D values were chosen purposefully, as they cover the typical range of parameters often investigated in LT studies (see Table 5.1 and Table 5.2). This study is based on a large number of values to obtain precise optimal B and D parameters and a good resolution in the 3D plots of the dependence of recovery time with B and D (Figure A.3, Figure A.4, Figure 5.7 and Figure A.5).

In these plots, it is possible to observe the nonlinear dependence of the recovery time on light intensity and LT duration, explored in the previous sections. The recovery time appears to oscillate over the 2D plane of B and D. Observing the peaks and valleys, B and D appear to have an inverse proportionality: to achieve similar recovery times, it requires a pair of higher light intensity and shorter duration or a lower light intensity and a longer duration. It

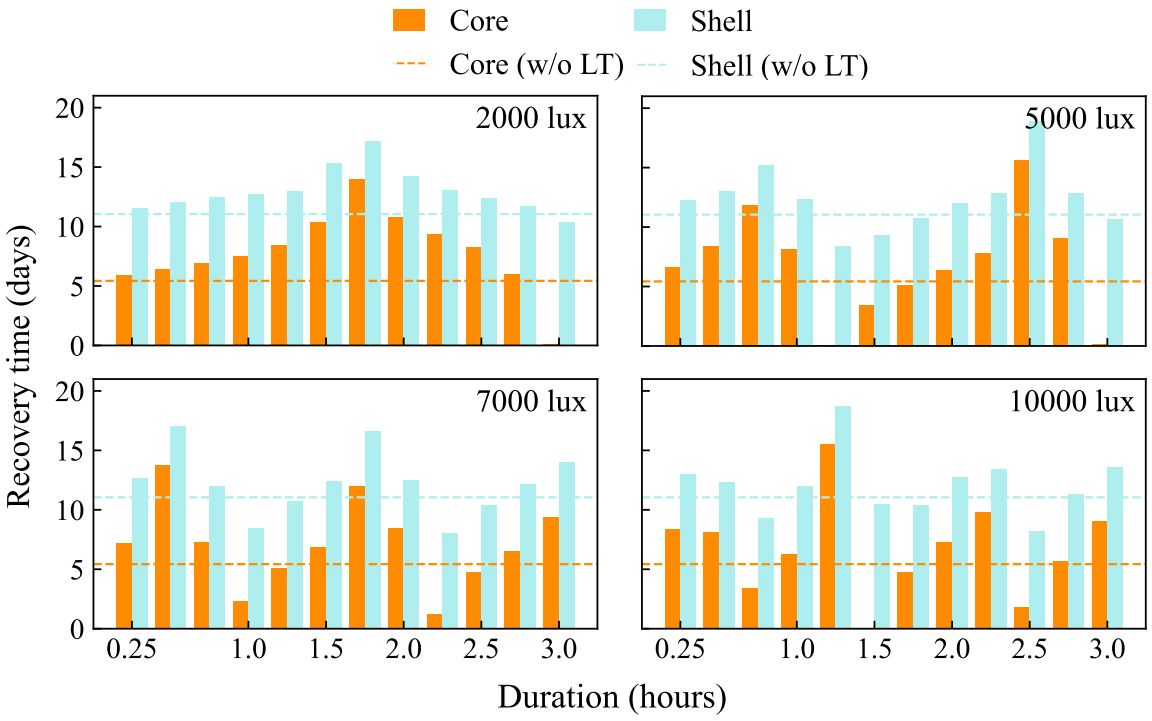

Figure 5.5: Recovery times of the core (orange bars) and shell (blue bars) as a function of the LT duration for an 8 h westward time shift and light intensities of a) 2,000 lux, b) 5,000 lux, c) 7,000 lux and d) 10,000 lux. The parameters used are the same as Figure 5.4. In the absence of LT, the recovery times are shown by dashed lines.

is a trade-off between the light intensity and therapy duration to maintain consistent recovery times.

Note there are several peaks of recovery time over the maximum of the oscillations, which has to do with the resolution of the image, this is, each peak corresponds to a pair of values B and D and in the continuum limit of considered B and D values, there would be only one maximum instead of several peaks. Another insight to take from the plots is that the 3D plots for the core and shell are qualitatively similar, demonstrating oscillations across the 2D plane of B and D.

The valleys of these 3D plots represent the minimum recovery time possible for the set of intensities and durations. It is therefore important to analyse them in more detail in order to be able to select the optimal intensity and duration parameters. There are three to four valleys in the 3D plots and, for the same B, one or more values of D give a minimal recovery time and vice-versa. For further analysis, the valley that corresponded to lower LT durations is chosen. Figure 5.6 shows the projection of the valley onto the 2D plane of D versus B for the four time shifts. To be clear, the plots in this figure were made by finding the D which minimised the recovery time for a given B, also called "Duration*" in the plots[1].

[1]In Figure 5.6, along the curves, the recovery time varies weakly. For a 6 h time shift to the east, the maximum value of the core recovery time on the considered valley was ≈ 0.04 and the minimum ≈ 0.01 (mean ≈ 0.017) and for the shell, the maximum was ≈ 2.94 and the minimum ≈ 2.91 (mean ≈ 2.93); for a 6 h time shift to the west, for the core, the maximum was ≈ 3.32 and the minimum ≈ 0.03 (mean ≈ 0.10) and for the shell, the maximum was ≈ 7.49 and the minimum ≈ 7.09 (mean ≈ 7.13); for an 8 h time shift to the east, for the core, the maximum was ≈ 0.06 and the minimum ≈ 0.01 (mean ≈ 0.02) and for the shell, the maximum was ≈ 5.08 and the minimum ≈ 5.00 (mean ≈ 5.06); lastly, for an 8 h time shift to the west, for the core, the maximum was ≈ 0.12 and the minimum was ≈ 0.02 (mean ≈ 0.05) and for the shell, the maximum was ≈ 10.4 and the minimum ≈ 7.96 (mean ≈ 8.02).

Table 5.3: Coefficients of the fitted curve with Equation 5.8 for a 6/8 h time shift to the east/west. In Equation 5.8, a and B are dimensionless and D and $\Delta\psi_v$ are in hours.

-	**6h East**	**6h West**	**8h East**	**8h West**
a (Core)	8.10742033	4.59372747	2.12068263	0.290993003
b (Core)	112.30177773	356.36667753	153.61427707	309.567731
a (Shell)	-0.42444116	-0.231045216	-1.52046485	2.57637754
b (Shell)	278.8606456	332.578272	309.97281099	352.26974925

It is possible to derive the general equation for the curves in Figure 5.6, a), which corresponds to the core. From Equation 5.7, it follows that:

$$D = \frac{\Delta\psi_v}{A+B} \Leftrightarrow D = \frac{b}{a+B} \Leftrightarrow \frac{1}{D} = \frac{a}{b} + \frac{B}{b} \tag{5.8}$$

Therefore, a regression analysis was performed on the core and shell's curves of Figure 5.6. In this figure, it is possible to observe the regression curves in grey. These have the general equation in Equation 5.8 and the correspondent fitted coefficients a and b were found with the function *curve_fit* from the Python package *Scipy*. The values of the coefficients a and b for the four considered time shifts are stated in Table 5.3. Also, a, which corresponds to the effect of the mean natural frequency of the core, the external light and the interaction between and within the core and shell on the group phase shift of the core, was considered constant during LT, since it does not have large variations. For the shell, this general equation would be more complicated, since the ψ_d does not directly depend on B - it depends on ψ_v, whose variation in time directly depends on B. Despite that, Equation 5.8 was employed to fit the curves of the shell, resulting in a highly accurate approximation to the data. To assess the quality of the fitting, R-squared (R2) scores were calculated for each fitted curve for the core and shell. The lowest R2 value obtained was approximately 0.994 and corresponded to the core's curve for a 6 h time shift to the east. All other curves had R2 values greater than 0.994. The proximity of these scores to 1 suggests that the curves align exceedingly well with the data.

As seen in the 3D plots and Figure 5.6, the relationship between D and B is inversely proportional for both core and shell as in Equation 5.8.

It is also possible to note that increasing the light intensity has a greater effect on reducing the duration when the initial intensity is low. As the intensity increases, the reduction in duration becomes less significant for each additional increase in intensity. Therefore, the system is more sensitive to changes in duration at lower light intensities.

We now compare the curves for eastward time shifts with the curves for westward time shifts in relation to the core. There is a clear difference between them: in order to minimise the recovery time after a westward travel, compared to the equivalent eastward travel, one has to use a longer duration of LT. For the shell, this difference is not so obvious, but the conclusion is the same. This observation reiterates the fact that LT is less effective for westward travels than for the equivalent eastward travels. Also, for the core, the reduction in duration with increasing intensity is lower for the eastward travels than for the westward ones. For the shell, this difference is not significant.

The objective is to find the optimal parameters that minimise the recovery time of the shell. Therefore, for each point on the plot of Figure 5.6 b), the recovery time is obtained and

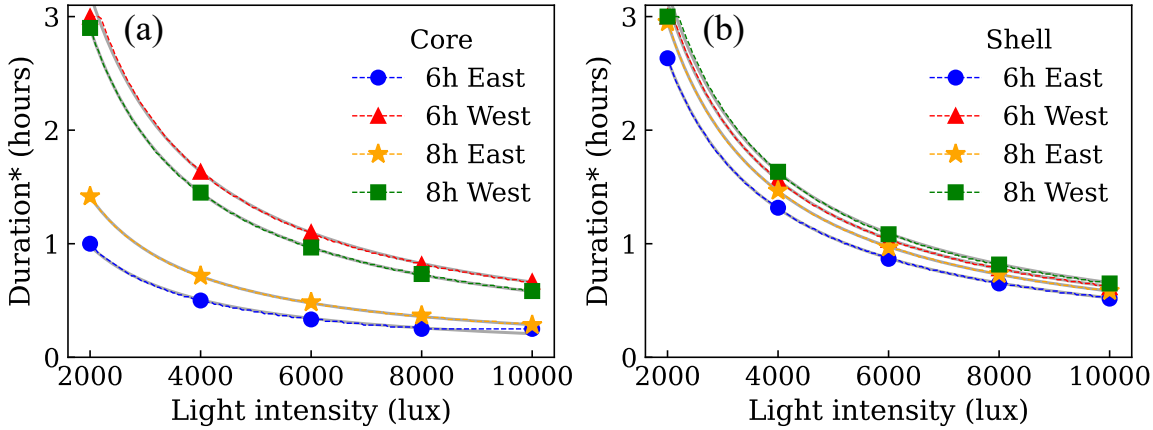

Figure 5.6: Given a time shift, for each light intensity B there is a duration which minimises the recovery time (in this plot, it is called "Duration*"). These plots show the dependence of this duration on B for the time shifts of 6/8 h to the east/west, where a) corresponds to the core and b) to the shell. The simulations were perfomed for $B = [2,000; 10,000]$ (lux), $\Delta B = 50$ (lux) and $D = [15/60; 3]$ h, $\Delta D = 1/60$ h. LT was applied at arrival time ($T = 0$). The grey lines correspond to the fitted curves of the data according to Equation 5.8 and their coefficients are given in Table 5.3.

Table 5.4: Optimal parameters of LT duration and light intensity for a 6/8 h time shift to the east/west.

-	**6h East**	**6h West**	**8h East**	**8h West**
B	2,000 lux	9,800 lux	2,000 lux	10,000 lux
D	2h40	38 min	2h57	39 min

the pair of duration-intensity values that minimise it is found. Table 5.4 shows the selected optimal values for the four studied time shifts.

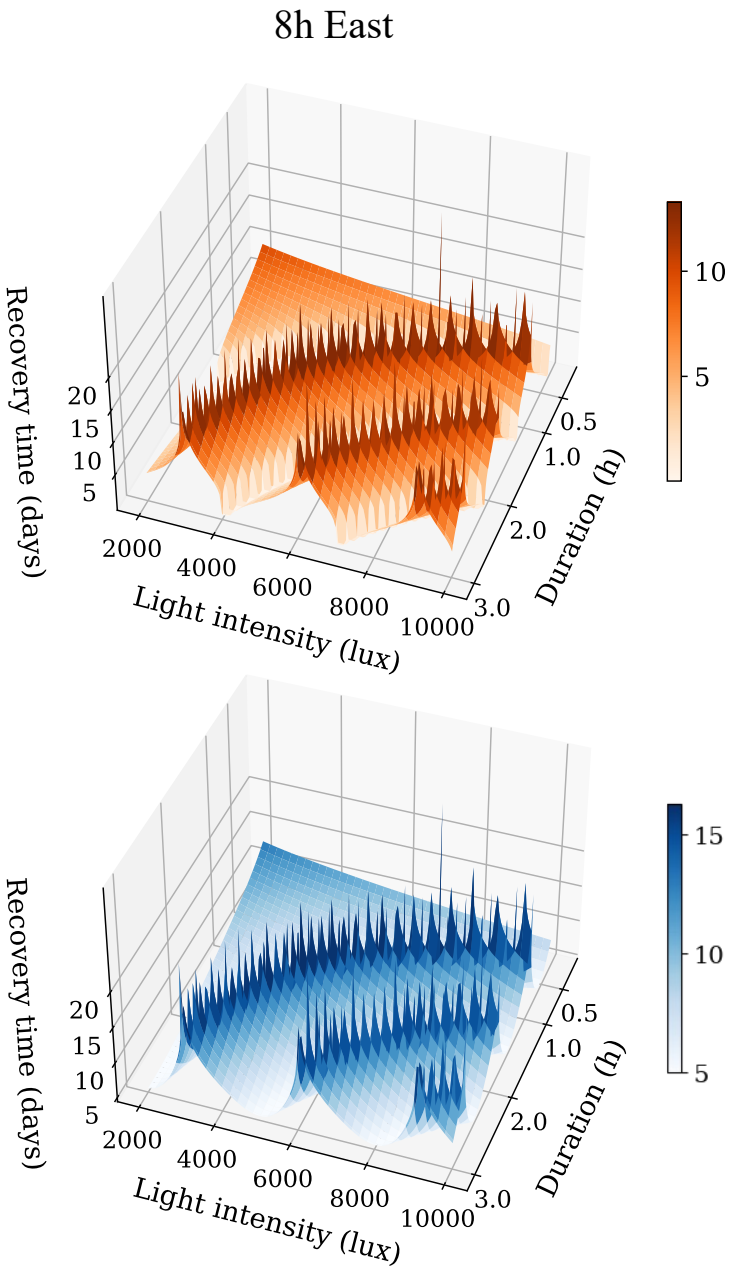

Figure 5.7: 3D plots of the recovery time for an 8 h time shift to the east versus the LT light intensity and LT duration. The upper orange plot corresponds to the core and the lower blue one to the shell. The simulations were perfomed for $B = [2,000; 10,000]$ (lux), $\Delta B = 50$ (lux) and $D = [15/60; 3]$ h, $\Delta D = 1/60$ h. LT was applied at arrival time ($T = 0$). There is a side colourbar which indicates the correspondence of colour to a recovery time value.

5.4 Influence of Multi-Session Light Therapy on Recovery Time

LT can be time-consuming and burdensome, making it impractical for many individuals. For example, in the study focusing on optimal durations for 6 h and 8 h time shifts to the east, it was found that individuals would require approximately 3 h of LT in a single session to achieve minimal recovery time, which is a long time. Therefore, the option of splitting the single session into more sessions is a way of making the treatment more versatile for the user.

In this section, the effectiveness of dividing the LT into sessions is verified. It is assumed that there was a LT session at the same time each day (at the arrival time, 6 a.m.). The optimal parameters in Table 5.4 are employed and the optimal duration D^* is divided by the number of sessions m so that each session has the same duration D^*/m. The number of sessions is selected considering the number of days it takes for the shell to recover with a single session. For example, for an 8 h time shift to the east, the shell takes ≈ 5 days to entrain counting as soon as the individual arrives. Therefore, the maximum number of sessions assumed is 5, counting the day of arrival, because if it was more than 5, it is certain that the shell would take more than 5 days to entrain, which would not be beneficial compared to a single session. Taking this into account, the number of sessions assumed for a 6 h time shift to the east is 3, for a 6 h time shift to the west it is 8, for an 8 h time shift to the east it is 5 and for an 8 h time shift to the west, it is 8.

Considering the optimal parameters of intensity and total duration as B^* and D^*, respectively, the following steps were taken in order to complete the simulations for the multi-session LT:

1. At the moment of arrival at the destination time zone, an individual takes the first LT session during D^*/m h for a given constant light intensity B^*. During the therapy, the Equations 5.3–5.6, in which the initial point corresponds to the departure zone, are solved.
2. The final condition of the first LT session is the initial point for the next step. Therefore, the Equations 4.2–4.5 are solved to obtain the evolution of the SCN on the $(24 - D^*/m)$ h after the first LT session.
3. On the second day at the destination time zone, step 1 and step 2 are repeated. The final point in step 2 is the initial point of the second LT session of duration D^*/m h and the Equations 5.3–5.6 are solved. After the second LT session, the Equations 4.2–4.5 are solved to obtain the evolution of the SCN during the next $(24 - D^*/m)$ h.
4. On the next days at the destination time zone until the end of the m LT sessions, the previous steps are repeated.
5. After the last LT session, the Equations 4.2–4.5 are solved until the condition of Equation 4.8 is satisfied.

Figures 5.8 and 5.9 show the recovery time of the core and shell for different amounts of LT sessions. The first figure refers to a 6 h time shift to the east and west and the second one to an 8 h time shift to the east and west. The recovery times without LT are represented as columns with stripes for comparison.

For the eastward travels, regardless of the number of sessions, LT reduces the recovery time of both core and shell. Also, as the number of sessions increases, the recovery time of the shell remains approximately constant, while that of the core increases slightly. Thus, multi-session LT does not strongly affect the resynchronisation process of the shell while the core is more sensitive to the number of LT sessions. A curious observation is that in Figure 5.8 a) and Figure 5.9 a), which regard a 6 h and 8 h time shift to the east, respectively, it is possible to notice that some values of the recovery time of the core are longer than those of the shell, as also seen in Section 5.3.

For the westward travels, multi-session LT appears to be less effective than for the eastward travels. For a 6 h westward travel, a single session reduces the recovery time, but up to three sessions, the recovery time of the core and shell increases and exceeds the recovery time without LT. After three sessions, the recovery time becomes approximately constant. For an 8 h westward travel, the core recovery time is lower than the recovery time without LT for up to three sessions, while the shell recovery time is lower than the recovery time without LT for only one session. The core and shell recovery times also increase up to five sessions and then remain approximately constant. This long resynchronisation process of the shell would result in a long recovery time of the peripheral tissues and, thus, of the individual (Evans and Silver, 2015; Evans et al., 2015; Nagano et al., 2003). Therefore, although the optimal duration of a single session is not long compared to the optimal duration of a single session for eastward travels, it would not be a good idea to increase the number of sessions for westward travels.

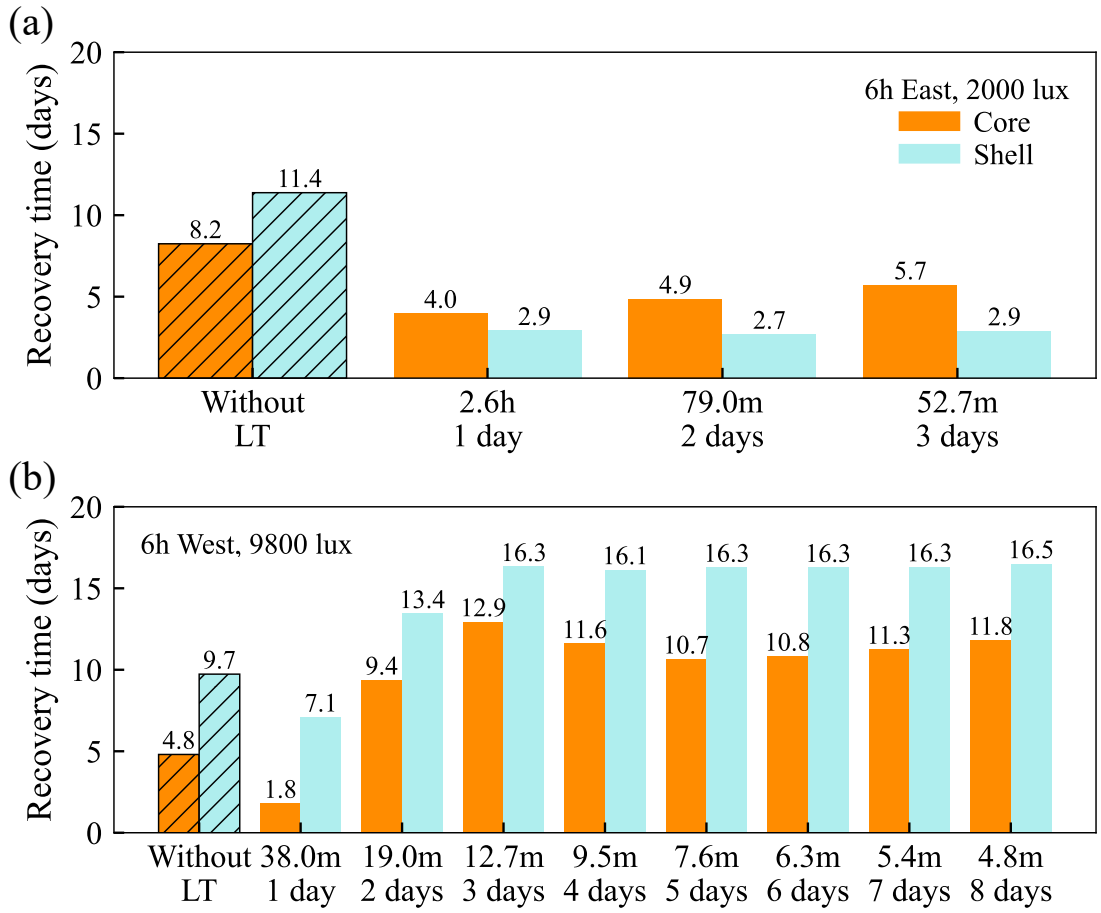

Figure 5.8: Recovery time of the core (orange bars) and shell (blue bars) as a function of the number of LT sessions for a 6 h time shift to the east (a) and west (b). The sessions took place at 6 a.m., at arrival time. The recovery times without LT are represented by bars with black stripes. The labels on the x-axis refer to the duration of one session (first line) and to the number of sessions (second line). For example, if it says "1.0 h, 3 days", there were three sessions, each one on one separate day, counting the arrival day, with a duration of 1 h.

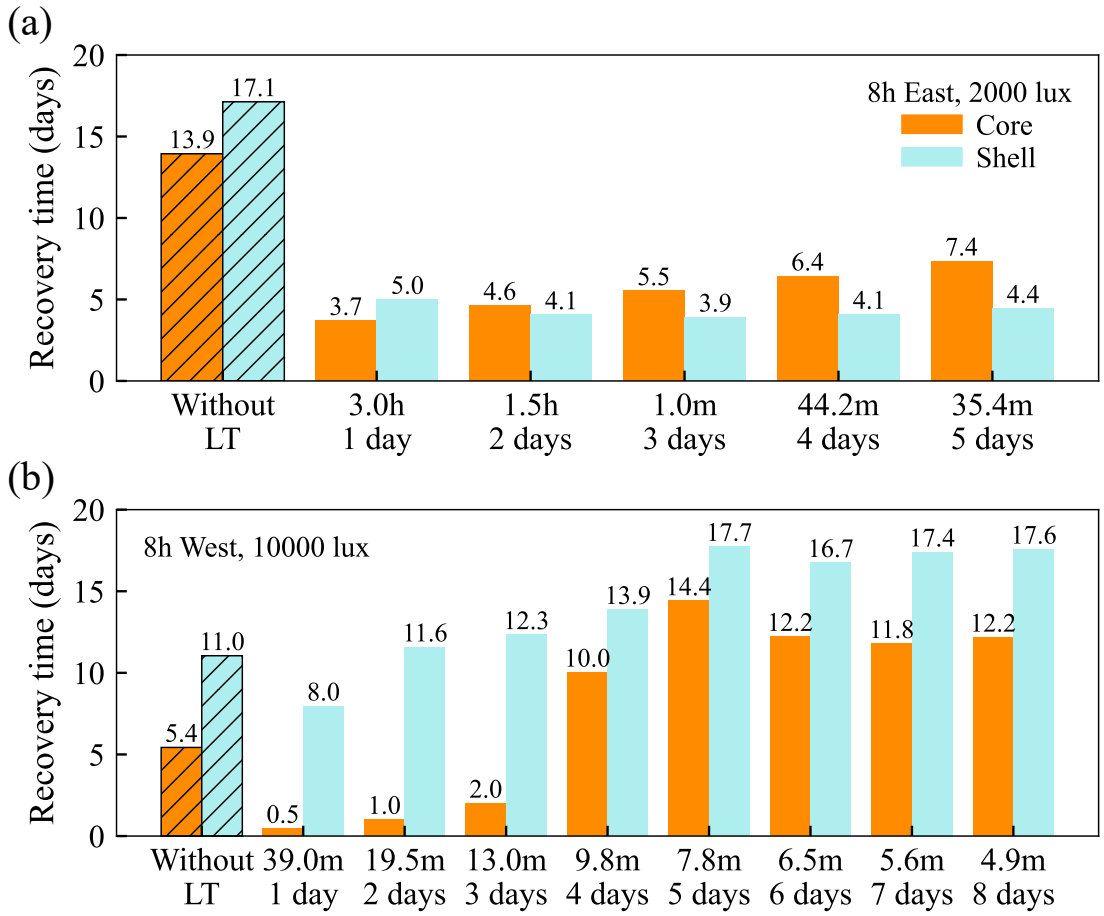

Figure 5.9: Recovery time in days of the core (orange bars) and shell (blue bars) as a function of the number of LT sessions for an 8 h time shift to the east (a) and west (b). The sessions took place at 6 a.m., at arrival time. The recovery times without LT are represented by bars with black stripes.

5.5 Optimal Light Therapy Parameters

In conclusion, assuming that an individual is planning to choose the optimal LT protocol including the optimal light intensity, total therapy duration and number of LT sessions, then they should follow Table 5.5. Note that the optimal LT yields a more significant reduction in recovery time for the eastward travels than for the westward ones. For the eastward travels, this reduction is in the range of 70-80% and for the westward is in the range of 20-30%.

One could compare these results with those obtained by Serkh and Forger, 2014, which used the Forger–Jewett–Kronauer model (see Section3) to model LT protocols. However, they considered a 16:8 LD cycle (16 h of light and 8 h of darkness), whereas in this study a 12:12 LD cycle was used. Since they presented more detailed results for an 8 h time shift, these will be compared to this work. The timing of the therapy slightly changed each day, but for phase delays, it was before the CBTmin and for phase advances, it was after CBTmin. For an 8 h time shift to the west, they predicted that the optimal protocol was the one using 10,000 lux and approximately 8 h light periods over 4 days, giving a recovery time of about 2 days. For an 8 h time shift to the east, the optimal protocol was the one using 10,000 lux and approximately 6 h light periods over 3 days, giving a recovery time of about 3 to 4 days. For this last time shift, the recovery time is similar to the 3.9 days obtained in this work. For the

Table 5.5: Optimal parameters of LT obtained with the core-shell model. Note that these results were obtained assuming that LT would be applied at arrival time, 6 a.m.. The last two rows present a comparison between the recovery time of the shell without LT and with the optimal LT.

-	**6h East**	**6h West**	**8h East**	**8h West**
Light intensity	2,000 lux	9,800 lux	2,000 lux	10,000 lux
Total duration	2h40	38 min	2h57	39 min
Number of LT sessions	3[2]	1	3	1
Shell recovery time without LT/ with optimal LT	11.4/2.9 days	9.7/7.1 days	17.1/3.9 days	11.0/8.0 days
Reduction in recovery time	74.6%	26.8%	77.2%	27.3%

former time shift, the result was better than the one obtained in this study, 8 days. However, the suggested periods of light exposure by Serkh and Forger, 2014 are very long compared to the ones suggested in this work, which would be a downside of using their optimal protocols.

[2]In Figure 5.8, a), the shell recovery time for three sessions is 2.9 days, the same as for one session. However, if not rounded, for three sessions it is about 2.8975 days, while for one session it is about 2.9144 days, which is a difference of approximately 24 minutes. Although this difference is not very significant, it is true that for three sessions the shell recovery time is minimised.

CHAPTER 6

Discussion and Conclusions

6.1 General Discussion

In this study, the SCN of the brain was modelled by the core-shell model, based on the Kuramoto model. This enabled the modelling of jet lag after travelling eastward and westward, or equivalently, after a rapid phase shift in the LD cycle, and its influence on the resynchronisation of the core and shell regions of the SCN. It was also possible to model light therapy and determine its efficacy in reducing the recovery time from jet lag after travelling eastward and westward.

The core-shell model is based on the Kuramoto model, which describes the synchronisation process of a large system of coupled oscillators (Strogatz, 2000). The core-shell model mimics the connections between and within the core and shell to provide a good approximation of the SCN neuronal network. The advantage of this model is its simplicity since it uses only 9 parameters and is based on just 4 differential equations. It has been used to establish the boundaries between entrainment and free-running activity, as well as to demonstrate the potential for dissociation (the emergence of a second rhythm in the SCN) and the SCN's anticipation of future events (Goltsev et al., 2022). The parameters of the model are calibrated by use of experimental data from the SCN of mice.

In order to understand some results, it was necessary to analyse the evolution of the core and shell dynamics in the phase space after the shift in the LD cycle, which corresponds to the crossing of time zones. This space is a complex plane in which the evolution of the SCN is characterised by a trajectory, that represents the resynchronisation process. The trajectories of the core and shell are characterised by the amplitude, the level of synchronisation and phase, the mean group phase of the neurons, on the complex plane. The coordinates of each point are the solutions of the nonlinear dynamical equations 4.2–4.5 or 5.3–5.6, in the case of light therapy. The initial point of the trajectories corresponds to the arrival place, being the system still entrained to the LD cycle of the departure zone. In the phase space, there are three fixed points, which influence the dynamics, a stable fixed point, attracting the trajectories, an unstable fixed point, repelling the trajectories and a saddle point, attracting or repelling the trajectories. Thus, trajectories end at the stable point, reflecting an entrained state at the arrival zone. The influence of the saddle node is quite dramatic in the resynchronisation process after jet lag and light therapy. Near it, the dynamics slow down and the system takes a long time to leave this region, increasing the jet lag's recovery time of the core and shell.

The first part of this work focused on understanding the jet lag recovery process from eastward and westward travels. Its main conclusions are summarised in the next points.

- **East-west asymmetry.** Experimental evidence has confirmed that travelling eastward yields longer adaptation times than travelling westward, creating an east-west asymmetry (Diekman and Bose, 2018; Eastman and Burgess, 2009; Rohling et al., 2011). In this work, the recovery times were obtained from a 12h phase delay to a 12h phase advance in steps of 1h, which confirmed this asymmetry. It is based on the fact that the Earth rotates from west to east, viewed from the North Pole, meaning that travelling to the east requires a phase-advancing adaptation of the circadian system while travelling to the west requires a phase-delaying adaptation. Therefore, in the phase space, adaptation after eastward travels follows a counterclockwise trajectory that reaches the stable node, while the adaptation after westward travels follows a clockwise trajectory. The initial points of the eastward travels' trajectories are closer to the saddle node than for the equivalent westward travels. Thus, the SCN takes longer to recover from eastward travels. This proximity also explains the observed maximum recovery time for the core and shell when travelling 8 time zones eastward.
- **The core recovers faster than the shell.** It was suggested that the initial fast resynchronisation of the core results from the fact that it receives a strong input from the retina and that it is more densely coupled than the shell. This observation corroborates with experimental studies (Davidson et al., 2009; Nagano et al., 2003; W. Nakamura, 2005). Despite that, there were some values of light therapy parameters for which the core showed longer recovery times than the shell. This remark occurred for a 6 h and 8 h time shift to the east. This behaviour can be explained in part by the chosen threshold in Equation 4.8, as it directly impacts the calculation of recovery time. It may also be related to the final points of the core and shell on the phase space, after light therapy. In Figure 5.1 c) and d), the order parameter of the core for an 8 h eastward travel was pushed further the stable point (note the square symbol), contrary to what would occur in the normal recovery case (Figure 4.2), while that of the shell did not change with light therapy. This situation might have caused a longer recovery time of the core in relation to the shell, whose trajectory was not very affected by light therapy. However, this behavior was not reported by the literature to this date and its biological origin is still unclear and needs further detailed analysis.

The second part of this work focused on understanding the mechanism of light therapy and ascertaining its efficacy in reducing the recovery time of the core and shell for a 6/8 h time shift to the east/west. The influence of the light intensity, therapy duration and number of sessions were studied and the optimal parameters were obtained. Next, the main conclusions of this part are presented.

- **Light therapy is more effective for eastward travels.** Continuous bright light accelerates the neuronal rhythms of the core, inducing rapid counterclockwise/positive shifts in the core phase portrait trajectories. Higher light intensity enhances this effect. Thus, for eastward travels, light brings the trajectories closer to the stable point, aiding the escape from the saddle node region. On the other hand, for westward travels, where normal recovery trajectories proceed clockwise to the stable point, light pushes away from the stable point, requiring higher light intensities to get closer to the stable node. Moreover, increasing the therapy duration also increases the phase shift, potentially aiding the recovery from westward travels. When testing the multi-session option, it was observed that increasing the number of therapy sessions prolonged the recovery of the SCN for westward travels, while the recovery times of the shell remain relatively constant and those of the core are slightly increased for eastward travels. Also, the optimal light therapy protocols caused a reduction in the recovery time of the shell in the range of 70-80% for the eastward travels, while for the westward travels this

reduction was only in the range of 20-30%. All these pieces of evidence suggest that light therapy is more effective for eastward travels.

- **Nonlinearity of recovery time with light intensity and duration.** Recovery time shows an oscillating behaviour with increasing light intensity and duration. Hence, for certain light intensities and durations, the recovery time is minimal. This oscillating behaviour occurs due to the phase shift produced by light intensity and duration, which can reach multiples of 2π in the core's phase space, meaning the dynamics have a periodicity. Experimental works have given some insights into this nonlinearity. For example, St Hilaire et al., 2012 proved that the phase-resetting response of the circadian system has a nonlinear relationship with light duration and Zeitzer et al., 2000 verified a nonlinear relationship with illuminance. Although these works didn't prove an oscillating behaviour of the phase-resetting response, it is a first step in proving this phenomenon and more experimental studies of larger arrays of intensities and durations are needed.
- **Light therapy is customisable.** It was shown that duration and light intensity have an inversely proportional relationship, enabling flexibility in achieving the required phase shift for efficient SCN recovery. This ensures that individuals highly sensitive to light can extend treatment duration and reduce light intensity, while those finding therapy burdensome can shorten the duration while increasing light intensity, achieving comparable outcomes. Furthermore, dividing the therapy into various sessions is also nearly as effective as a single session for eastward travels. As a result, light therapy can be tailored even more to individual preferences and needs since people can decide to reduce the duration of each session by extending the therapy over a few days.

6.2 General Conclusion

Circadian rhythms, present in most organisms on Earth, help them to anticipate changes in the environment, thereby increasing their chances of survival. In mammals, the SCN of the brain is responsible for orchestrating these rhythms. It is divided into the core and shell regions and their interplay is crucial for synchronising cellular rhythms. These intricate dynamics can be simulated using mathematical models that explain the synchronisation phenomena in nature in order to tackle health challenges, such as jet lag. This condition, caused by disrupted circadian rhythms due to rapid time zone travel, poses several issues, particularly for individuals who frequently travel, such as flight crews, business people and even astronauts. Bright light therapy for jet lag is already commercialised, though it is based on few experimental studies and its effects on the SCN remain unclear.

Therefore, this work delved into explaining the resynchronisation process during jet lag and the east-west asymmetry in recovery times. It was also possible to model the effect of the light therapy on the SCN and its mechanism was explained. Moreover, the optimal parameters of light therapy for recovering after 6/8 h eastward/westward time shifts were determined. In summary, this work fulfilled its goals, yielding accurate and innovative findings. The findings related to jet lag align with experimental results, and though direct comparisons with existing light therapy outcomes are lacking, this research opens doors for novel experimental protocols.

Furthermore, the new data on jet lag recovery times as well as the new insights on the role of the core-shell organisation advance the knowledge of how the SCN adapts to changes in the LD cycle. The understanding of the jet lag mechanism brings a new perception into potential strategies for its mitigation. Additionally, there was a gap in the knowledge of the effects of light therapy on the SCN, and, hopefully, this work could give more insights about the theme. The found optimal parameters can be easily incorporated into the already-existing light therapy technologies. Thus, one of the most important goals of this research is to aid the medical industry in providing trustworthy jet lag therapies.

In conclusion, this study is a meaningful contribution to the field of chronobiology and jet lag research, paving the way for the widespread use of light therapy in modern healthcare.

6.2.1 Limitations and Future Work

Recognising the study's limitations is fundamental towards a more complete work and future improvement.

First, the light therapy's effect was studied assuming an arrival at 6 a.m., which was considered as the start of the daylight hours at the destination time. More simulations are needed in order to ascertain the effect of arrival time on the recovery time of the SCN.

As seen in Section 2.4.2, the circadian timing at which light therapy is applied is extremely important since the phase shift that light produces in the system depends heavily on it. Therefore, in this work, the influence of the time of the day of light therapy application on recovery time was obtained. The results did not match the experimental observations, although, for a better comparison, the arrival time at the local time zone and the melatonin rhythms might need to be considered. Due to the importance of this light therapy parameter, it is suggested to study its role more thoroughly.

In the future, it would be interesting to choose the threshold in Equation 4.8 based on experimental data of recovery times. Moreover, it should be considered modelling different light frequencies in the spectrum, like blue light and extending the simulations to peripheral tissues coupled to the shell to study their role in the generation of circadian rhythms. Also, modelling the two coupled hemispheres of the SCN would probably improve the accuracy of the model. The role of seasonal variations of LD periods in the resynchronisation of the SCN can also be studied, being the subject of some recent studies (Beurden et al., 2023; Gu et al., 2016; Hannay et al., 2020). Additionally, at the beginning of this work, it was considered modelling the pineal gland to test the melatonin's effect as a jet lag therapy, as well as modelling the influence of blocking arginine vasopressin receptors in the SCN. These alternative jet lag therapies are promising and can be the target of future studies.

References

Acebrón, J. A., Bonilla, L. L., Pérez Vicente, C. J., Ritort, F., & Spigler, R. (2005). The kuramoto model: A simple paradigm for synchronization phenomena [Publisher: American Physical Society]. *Reviews of Modern Physics*, *77*(1), 137–185. https://doi.org/10.1103/RevModPhys.77.137

Antonsen, T. M., Faghih, R. T., Girvan, M., Ott, E., & Platig, J. (2008). External periodic driving of large systems of globally coupled phase oscillators. *Chaos: An Interdisciplinary Journal of Nonlinear Science*, *18*(3), 037112. https://doi.org/10.1063/1.2952447

Arendt, J. (2018). Approaches to the pharmacological management of jet lag. *Drugs*, *78*(14), 1419–1431. https://doi.org/10.1007/s40265-018-0973-8

Asgari-Targhi, A., & Klerman, E. B. (2019). Mathematical modeling of circadian rhythms. *WIREs Systems Biology and Medicine*, *11*(2). https://doi.org/10.1002/wsbm.1439

Ashton, A., Foster, R., & Jagannath, A. (2022). Photic entrainment of the circadian system. *International Journal of Molecular Sciences*, *23*(2), 729. https://doi.org/10.3390/ijms23020729

Beaulé, C. (2008). Aschoff's rules. In *Encyclopedia of neuroscience* (pp. 190–193). Springer, Berlin, Heidelberg. https://doi.org/10.1007/978-3-540-29678-2_383

Becker-Weimann, S., Wolf, J., Herzel, H., & Kramer, A. (2004). Modeling feedback loops of the mammalian circadian oscillator. *Biophysical Journal*, *87*(5), 3023–3034. https://doi.org/10.1529/biophysj.104.040824

Beurden, A. W. v., Meylahn, J. M., Achterhof, S., Meijer, J. H., & Rohling, J. H. T. (2023). Reduced plasticity in coupling strength in the SCN clock in aging as revealed by kuramoto modelling. *Journal of Biological Rhythms*, *38*(5), 461–475. https://doi.org/10.1177/07487304231175191

Bin, Y. S., Postnova, S., & Cistulli, P. A. (2019). What works for jetlag? a systematic review of non-pharmacological interventions. *Sleep Medicine Reviews*, *43*, 47–59. https://doi.org/10.1016/j.smrv.2018.09.005

Boivin, D. B., & James, F. O. (2002). Phase-dependent effect of room light exposure in a 5-h advance of the sleep-wake cycle: Implications for jet lag. *Journal of Biological Rhythms*, *17*(3), 266–276. https://doi.org/10.1177/074873040201700310

Brown, E. N., & Luithardt, H. (1999). Statistical model building and model criticism for human circadian data. *Journal of Biological Rhythms*, *14*(6), 609–616. https://doi.org/10.1177/074873099129000975

Choy, M., & Salbu, R. L. (2011). Jet lag: Current and potential therapies. *P T*, *36*(4), 221–231.

Comtet, H., Geoffroy, P. A., Kobayashi Frisk, M., Hubbard, J., Robin-Choteau, L., Calvel, L., Hugueny, L., Viola, A. U., & Bourgin, P. (2019). Light therapy with boxes or glasses to counteract effects of acute sleep deprivation. *Scientific Reports*, *9*(1), 18073. https://doi.org/10.1038/s41598-019-54311-x

Davidson, A. J., Castanon-Cervantes, O., Leise, T. L., Molyneux, P. C., & Harrington, M. E. (2009). Visualizing jet lag in the mouse suprachiasmatic nucleus and peripheral circadian timing system. *European Journal of Neuroscience*, *29*(1), 171–180. https://doi.org/10.1111/j.1460-9568.2008.06534.x

Dewan, K., Benloucif, S., Reid, K., Wolfe, L. F., Zee, P. C., & Dewan, D. (2011). Light-induced changes of the circadian clock of humans: Increasing duration is more effective than increasing light intensity. *34*(5).

Diekman, C. O., & Bose, A. (2018). Reentrainment of the circadian pacemaker during jet lag: East-west asymmetry and the effects of north-south travel. *Journal of Theoretical Biology*, *437*, 261–285. https://doi.org/10.1016/j.jtbi.2017.10.002

Dunaief, J. (2021, August 20). *Protect your eyes from bright lights, including blue*. Retrieved October 23, 2023, from https://www.brightfocus.org/macular/article/protect-your-eyes-bright-lights-including-blue

Eastman, C. I., & Burgess, H. J. (2009). How to travel the world without jet lag. *Sleep Medicine Clinics*, *4*(2), 241–255. https://doi.org/10.1016/j.jsmc.2009.02.006

Escobar, C., Espitia-Bautista, E., Guzmán-Ruiz, M. A., Guerrero- Vargas, N. N., Hernández-Navarrete, M. Á., Ángeles-Castellanos, M., Morales-Pérez, B., & Buijs, R. M. (2020). Chocolate for breakfast prevents circadian desynchrony in experimental models of jet-lag and shift-work. *Scientific Reports*, *10*, 6243. https://doi.org/10.1038/s41598-020-63227-w

Evans, J. A., Leise, T. L., Castanon-Cervantes, O., & Davidson, A. J. (2013). Dynamic interactions mediated by nonredundant signaling mechanisms couple circadian clock neurons. *Neuron*, *80*(4), 973–983. https://doi.org/10.1016/j.neuron.2013.08.022

Evans, J. A., & Silver, R. (2015). The suprachiasmatic nucleus and the circadian timekeeping system of the body. In *Neuroscience in the 21st century* (pp. 1–49). Springer New York. https://doi.org/10.1007/978-1-4614-6434-1_66-3

Evans, J. A., Suen, T.-C., Callif, B. L., Mitchell, A. S., Castanon-Cervantes, O., Baker, K. M., Kloehn, I., Baba, K., Teubner, B. J. W., Ehlen, J. C., Paul, K. N., Bartness, T. J., Tosini, G., Leise, T., & Davidson, A. J. (2015). Shell neurons of the master circadian clock coordinate the phase of tissue clocks throughout the brain and body. *BMC Biology*, *13*(1), 43. https://doi.org/10.1186/s12915-015-0157-x

Fan, X., Chen, D., Wang, Y., Tan, Y., Zhao, H., Zeng, J., Li, Y., Guo, X., Qiu, H., & Gu, Y. (2022). Light intensity alters the effects of light-induced circadian disruption on glucose and lipid metabolism in mice. *American Journal of Physiology-Endocrinology and Metabolism*, *322*(1), E1–E9. https://doi.org/10.1152/ajpendo.00025.2021

Forbes-Robertson, S., Dudley, E., Vadgama, P., Cook, C., Drawer, S., & Kilduff, L. (2012). Circadian disruption and remedial interventions: Effects and interventions for jet lag for athletic peak performance. *Sports Medicine*, *42*(3), 185–208. https://doi.org/10.2165/11596850-000000000-00000

Forger, D. B., Jewett, M. E., & Kronauer, R. E. (1999). A simpler model of the human circadian pacemaker. *Journal of Biological Rhythms*, *14*(6), 532–537. https://doi.org/10.1177/074873099129000867

Garmin. (2023). *Jet lag adviser*. Retrieved September 22, 2023, from https://www.garmin.com/en-US/garmin-technology/health-science/jet-lag-adviser/

Goltsev, A. V., Wright, E. A. P., Mendes, J. F. F., & Yoon, S. (2022). Generation and disruption of circadian rhythms in the suprachiasmatic nucleus: A core-shell model. *Journal of Biological Rhythms*, *37*(5), 545–561. https://doi.org/10.1177/07487304221107834

Goodwin, B. C. (1965). Oscillatory behavior in enzymatic control processes. *Advances in Enzyme Regulation*, *3*, 425–438. https://doi.org/10.1016/0065-2571(65)90067-1

Green Business Light. (2020). *Lux, lumens and watts: Our guide* [Green business light]. Retrieved October 27, 2023, from https://greenbusinesslight.com/resources/lighting-lux-lumens-watts/

Gu, C., Tang, M., & Yang, H. (2016). The synchronization of neuronal oscillators determined by the directed network structure of the suprachiasmatic nucleus under different photoperiods. *Scientific Reports*, *6*(1), 28878. https://doi.org/10.1038/srep28878

Guevara Erra, R., Perez Velazquez, J. L., & Rosenblum, M. (2017). Neural synchronization from the perspective of non-linear dynamics. *Frontiers in Computational Neuroscience*, *11*, 98. https://doi.org/10.3389/fncom.2017.00098

Gundel, A., & Spencer, M. B. (1999). A circadian oscillator model based on empirical data. *Journal of Biological Rhythms*, *14*(6), 517–524. https://doi.org/10.1177/074873099129000849

Hafner, M., Koeppl, H., & Gonze, D. (2012). Effect of network architecture on synchronization and entrainment properties of the circadian oscillations in the suprachiasmatic nucleus (O. Sporns, Ed.). *PLoS Computational Biology*, *8*(3), e1002419. https://doi.org/10.1371/journal.pcbi.1002419

Hannay, K. M., Forger, D. B., & Booth, V. (2020). Seasonality and light phase-resetting in the mammalian circadian rhythm. *Scientific Reports*, *10*(1), 19506. https://doi.org/10.1038/s41598-020-74002-2

Hastings, M., Maywood, E., & Brancaccio, M. (2019). The mammalian circadian timing system and the suprachiasmatic nucleus as its pacemaker. *Biology*, *8*(1), 13. https://doi.org/10.3390/biology8010013

Herculano-Houzel, S. (2009). The human brain in numbers: A linearly scaled-up primate brain. *Frontiers in Human Neuroscience*, *3*. https://doi.org/10.3389/neuro.09.031.2009

Herzog, E. D. (2007). Neurons and networks in daily rhythms. *Nature Reviews Neuroscience*, *8*(10), 790–802. https://doi.org/10.1038/nrn2215

Hofman, M. A. (2009). Human circadian timing system. In M. D. Binder, N. Hirokawa, & U. Windhorst (Eds.), *Encyclopedia of neuroscience* (pp. 1869–1873). Springer. https://doi.org/10.1007/978-3-540-29678-2_2264

Hu, X., Boccaletti, S., Huang, W., Zhang, X., Liu, Z., Guan, S., & Lai, C.-H. (2014). Exact solution for first-order synchronization transition in a generalized kuramoto model [Number: 1 Publisher: Nature Publishing Group]. *Scientific Reports*, *4*(1), 7262. https://doi.org/10.1038/srep07262

Husse, J., Eichele, G., & Oster, H. (2015). Synchronization of the mammalian circadian timing system: Light can control peripheral clocks independently of the SCN clock: Alternate routes of entrainment optimize the alignment of the body's circadian clock network with external time. *BioEssays*, *37*(10), 1119–1128. https://doi.org/10.1002/bies.201500026

Hussein, L. E. C., Mollard, P., & Bonnefont, X. (2019). Molecular and cellular networks in the suprachiasmatic nuclei. *International Journal of Molecular Sciences*, *20*(8), 2052. https://doi.org/10.3390/ijms20082052

Jewett, M. E., Kronauer, R. E., & Czeisler, C. A. (1994). Phase-amplitude resetting of the human circadian pacemaker via bright light: A further analysis. *Journal of Biological Rhythms*, *9*(3), 295–314. https://doi.org/10.1177/074873049400900310

Juda, M. (2010). *The importance of chronotype in shift work research* [Doctoral Thesis]. LMU München, Faculty of Psychology and Educational Sciences. https://edoc.ub.uni-muenchen.de/11814/1/Juda_Myriam.pdf

Karatsoreos, I., & Silver, R. (2017). Body clocks in health and disease. In *Conn's translational neuroscience* (pp. 599–615). Elsevier. https://doi.org/10.1016/B978-0-12-802381-5.00043-9

Khalsa, S. B. S., Jewett, M. E., Cajochen, C., & Czeisler, C. A. (2003). A phase response curve to single bright light pulses in human subjects. *The Journal of Physiology*, *549*(3), 945–952. https://doi.org/10.1113/jphysiol.2003.040477

Kori, H., Yamaguchi, Y., & Okamura, H. (2017). Accelerating recovery from jet lag: Prediction from a multi-oscillator model and its experimental confirmation in model animals. *Scientific Reports*, *7*(1), 46702. https://doi.org/10.1038/srep46702

Kronauer, R. E., Czeisler, C. A., Pilato, S. F., Moore-Ede, M. C., & Weitzman, E. D. (1982). Mathematical model of the human circadian system with two interacting oscillators. *The American Journal of Physiology*, *242*(1), R3–17. https://doi.org/10.1152/ajpregu.1982.242.1.R3

Kuramoto, Y. (1975). Self-entrainment of a population of coupled non-linear oscillators. In H. Araki (Ed.), *International symposium on mathematical problems in theoretical physics* (pp. 420–422). Springer. https://doi.org/10.1007/BFb0013365

Lara-Aparicio, M., Barriga-Montoya, C., & Fuentes-Pardo, B. (2006). A brief biomathematical history of circadian rhythms: From wigglesworth to winfree. *Scientiae Mathematicae Japonicae*, *64*(2), 357–370.

Li, Y., & Androulakis, I. P. (2021). Light entrainment of the SCN circadian clock and implications for personalized alterations of corticosterone rhythms in shift work and jet lag. *Scientific Reports*, *11*(1), 17929. https://doi.org/10.1038/s41598-021-97019-7

Lu, Z., Klein-Cardeña, K., Lee, S., Antonsen, T. M., Girvan, M., & Ott, E. (2016). Resynchronization of circadian oscillators and the east-west asymmetry of jet-lag. *Chaos: An Interdisciplinary Journal of Nonlinear Science*, *26*(9), 094811. https://doi.org/10.1063/1.4954275

Lucimed. (2023). *Luminette®: Light therapy glasses. official site – myluminette*. Retrieved September 22, 2023, from https://myluminette.com/en-us

Martens, E., Barreto, E., Strogatz, S., Ott, E., So, P., & Antonsen, T. (2009). Exact results for the kuramoto model with a bimodal frequency distribution. *Physical review. E, Statistical, nonlinear, and soft matter physics*, *79*, 026204. https://doi.org/10.1103/PhysRevE.79.026204

Mitchell, P. J., Hoese, E. K., Liwen Liu, Fogg, L. F., & Eastman, C. I. (1997). Conflicting bright light exposure during night shifts impedes circadian adaptation. *Journal of Biological Rhythms*, *12*(1), 5–15. https://doi.org/10.1177/074873049701200103

Moore, R. Y. (1996). Entrainment pathways and the functional organization of the circadian system. *Progress in Brain Research*, *111*, 103–119. https://doi.org/10.1016/s0079-6123(08)60403-3

Morgenthaler, T. I., Lee-Chiong, T., Alessi, C., Friedman, L., Aurora, R. N., Boehlecke, B., Brown, T., Chesson, A. L., Kapur, V., Maganti, R., Owens, J., Pancer, J., Swick, T. J., & Zak, R. (2007). Practice parameters for the clinical evaluation and treatment of circadian rhythm sleep disorders. *Sleep*, *30*(11), 1445–1459. https://doi.org/10.1093/sleep/30.11.1445

Muñoz, M., Peirson, S. N., Hankins, M. W., & Foster, R. G. (2005). Long-term constant light induces constitutive elevated expression of mPER2 protein in the murine SCN: A molecular basis for aschoff's rule? *Journal of Biological Rhythms*, *20*(1), 3–14. https://doi.org/10.1177/0748730404272858

Nagano, M., Adachi, A., Nakahama, K.-i., Nakamura, T., Tamada, M., Meyer-Bernstein, E., Sehgal, A., & Shigeyoshi, Y. (2003). An abrupt shift in the day/night cycle causes desynchrony in the mammalian circadian center. *The Journal of Neuroscience*, *23*(14), 6141–6151. https://doi.org/10.1523/JNEUROSCI.23-14-06141.2003

Nakamura, T., Takasu, N. N., & Nakamura, W. (2016). The suprachiasmatic nucleus: Age-related decline in biological rhythms [Number: 5 Publisher: BioMed Central]. *The Journal of Physiological Sciences*, *66*(5), 367–374. https://doi.org/10.1007/s12576-016-0439-2

Nakamura, W. (2005). Differential response of period 1 expression within the suprachiasmatic nucleus. *Journal of Neuroscience*, *25*(23), 5481–5487. https://doi.org/10.1523/JNEUROSCI.0889-05.2005

Ng, K. (2023, January 17). *How to beat jet lag* [Arcascope]. Retrieved September 22, 2023, from https://www.arcascope.com/how-to-beat-jet-lag/

Ono, D., Honma, K.-i., & Honma, S. (2021). Roles of neuropeptides, VIP and AVP, in the mammalian central circadian clock. *Frontiers in Neuroscience*, *15*, 650154. https://doi.org/10.3389/fnins.2021.650154

ORTOREX. (n.d.). *Lâmpada de terapia com luz SAD*. Retrieved September 22, 2023, from https://ortorex.pt/p/sad-light-therapy-lamp/

Ott, E., & Antonsen, T. M. (2008). Low dimensional behavior of large systems of globally coupled oscillators. *Chaos: An Interdisciplinary Journal of Nonlinear Science*, *18*(3), 037113. https://doi.org/10.1063/1.2930766

Philips. (2023). *Terapia da luz*. Retrieved September 22, 2023, from https://www.philips.pt/c-m-pe/light-therapy

Pietras, B., Deschle, N., & Daffertshofer, A. (2018). First-order phase transitions in the kuramoto model with compact bimodal frequency distributions. *Physical Review E*, *98*(6), 062219. https://doi.org/10.1103/PhysRevE.98.062219

Prabhat, A., Malik, I., Jha, N. A., Bhardwaj, S. K., & Kumar, V. (2020). Developmental effects of constant light on circadian behaviour and gene expressions in zebra finches: Insights into mechanisms of metabolic adaptation to aperiodic environment in diurnal animals. *Journal of Photochemistry and Photobiology B: Biology*, *211*, 111995. https://doi.org/10.1016/j.jphotobiol.2020.111995

Ramkisoensing, A., & Meijer, J. H. (2015). Synchronization of biological clock neurons by light and peripheral feedback systems promotes circadian rhythms and health. *Frontiers in Neurology*, *6*. https://doi.org/10.3389/fneur.2015.00128

Richardson, M. E. S., Parkins, S., Kaneza, I., & Dauphin, A.-C. (2020). Jet lag recovery and memory functions are correlated with direct light effects on locomotion. *Journal of Biological Rhythms*, *35*(6), 588–597. https://doi.org/10.1177/0748730420947589

Roach, G. D., & Sargent, C. (2019). Interventions to minimize jet lag after westward and eastward flight. *Frontiers in Physiology*, *10*, 927. https://doi.org/10.3389/fphys.2019.00927

Rohling, J. H. T., & Meylahn, J. M. (2020). Two-community noisy kuramoto model suggests mechanism for splitting in the suprachiasmatic nucleus. *Journal of Biological Rhythms*, *35*(2), 158–166. https://doi.org/10.1177/0748730419898314

Rohling, J. H. T., vanderLeest, H. T., Michel, S., Vansteensel, M. J., & Meijer, J. H. (2011). Phase resetting of the mammalian circadian clock relies on a rapid shift of a small population of pacemaker neurons. *PLoS ONE*, *6*(9), e25437. https://doi.org/10.1371/journal.pone.0025437

Sakaguchi, H. (1988). Cooperative phenomena in coupled oscillator systems under external fields. *Progress of Theoretical Physics*, *79*(1), 39–46. https://doi.org/10.1143/PTP.79.39

Serkh, K., & Forger, D. B. (2014). Optimal schedules of light exposure for rapidly correcting circadian misalignment (O. Sporns, Ed.). *PLoS Computational Biology*, *10*(4), e1003523. https://doi.org/10.1371/journal.pcbi.1003523

Silver, R. (2018, October 24). Suprachiasmatic nucleus anatomy, physiology, and neurochemistry. In *Oxford research encyclopedia of neuroscience*. Oxford University Press. https://doi.org/10.1093/acrefore/9780190264086.013.27

Sleepopolis Team. (2023, May 4). *Jet lag rooster by sleepopolis* [Sleepopolis]. Retrieved September 22, 2023, from https://sleepopolis.com/calculators/jet-lag/

St Hilaire, M. A., Gooley, J. J., Khalsa, S. B. S., Kronauer, R. E., Czeisler, C. A., & Lockley, S. W. (2012). Human phase response curve to a 1 h pulse of bright white light: PRC to 1 h light pulses in humans. *The Journal of Physiology*, *590*(13), 3035–3045. https://doi.org/10.1113/jphysiol.2012.227892

Strogatz, S. H. (2000). From kuramoto to crawford: Exploring the onset of synchronization in populations of coupled oscillators. *Physica D: Nonlinear Phenomena*, *143*(1), 1–20. https://doi.org/10.1016/S0167-2789(00)00094-4

Strogatz, S. H. (2015). *Nonlinear dynamics and chaos: With applications to physics, biology, chemistry, and engineering* (Second edition). Westview Press, a member of the Perseus Books Group.

Takahashi, T., Sasaki, M., Itoh, H., Sano, H., Yamadera, W., Ozone, M., Obuchi, K., Nishimura, H., & Matsunaga, N. (1999). Re-entrainment of circadian rhythm of plasma melatonin on an 8-h eastward flight. *Psychiatry and Clinical Neurosciences*, *53*(2), 257–260. https://doi.org/10.1046/j.1440-1819.1999.00537.x

Taylor, S. R., Wang, T. J., Granados-Fuentes, D., & Herzog, E. D. (2017). Resynchronization dynamics reveal that the ventral entrains the dorsal suprachiasmatic nucleus. *Journal of Biological Rhythms*, *32*(1), 35–47. https://doi.org/10.1177/0748730416680904

The SciPy community. (2023). *Scipy.integrate.radau — SciPy v1.11.2 manual*. Retrieved September 27, 2023, from https://docs.scipy.org/doc/scipy/reference/generated/scipy.integrate.Radau.html

Timeshifter. (2023). *The jet lag app*. Retrieved September 22, 2023, from https://www.timeshifter.com/

Van Der Pol, B. (1926). On "relaxation-oscillations". *The London, Edinburgh, and Dublin Philosophical Magazine and Journal of Science*, *2*(11), 978–992. https://doi.org/10.1080/14786442608564127

Varadarajan, S., Tajiri, M., Jain, R., Holt, R., Ahmed, Q., LeSauter, J., & Silver, R. (2018). Connectome of the suprachiasmatic nucleus: New evidence of the core-shell relationship. *eNeuro*, *5*(5). https://doi.org/10.1523/ENEURO.0205-18.2018

Yamaguchi, S., Isejima, H., Matsuo, T., Okura, R., Yagita, K., Kobayashi, M., & Okamura, H. (2003). Synchronization of cellular clocks in the suprachiasmatic nucleus [Publisher: American Association for the Advancement of Science]. *Science*, *302*(5649), 1408–1412. https://doi.org/10.1126/science.1089287

Yamaguchi, Y., Suzuki, T., Mizoro, Y., Kori, H., Okada, K., Chen, Y., Fustin, J.-M., Yamazaki, F., Mizuguchi, N., Zhang, J., Dong, X., Tsujimoto, G., Okuno, Y., Doi, M., & Okamura, H. (2013). Mice genetically deficient in vasopressin v1a and v1b receptors are resistant to jet lag. *Science*, *342*(6154), 85–90. https://doi.org/10.1126/science.1238599

Yoon, S., Wright, E. A. P., Mendes, J. F. F., & Goltsev, A. V. (2021). Impact of field heterogeneity on the dynamics of the forced kuramoto model. *Physical Review E*, *104*(2), 024313. https://doi.org/10.1103/PhysRevE.104.024313

Zeitzer, J. M., Dijk, D.-J., Kronauer, R. E., Brown, E. N., & Czeisler, C. A. (2000). Sensitivity of the human circadian pacemaker to nocturnal light: Melatonin phase resetting and suppression. *The Journal of Physiology*, *526*(3), 695–702. https://doi.org/10.1111/j.1469-7793.2000.00695.x

APPENDIX A

Influence of Light Therapy Intensity and Duration on Recovery Time

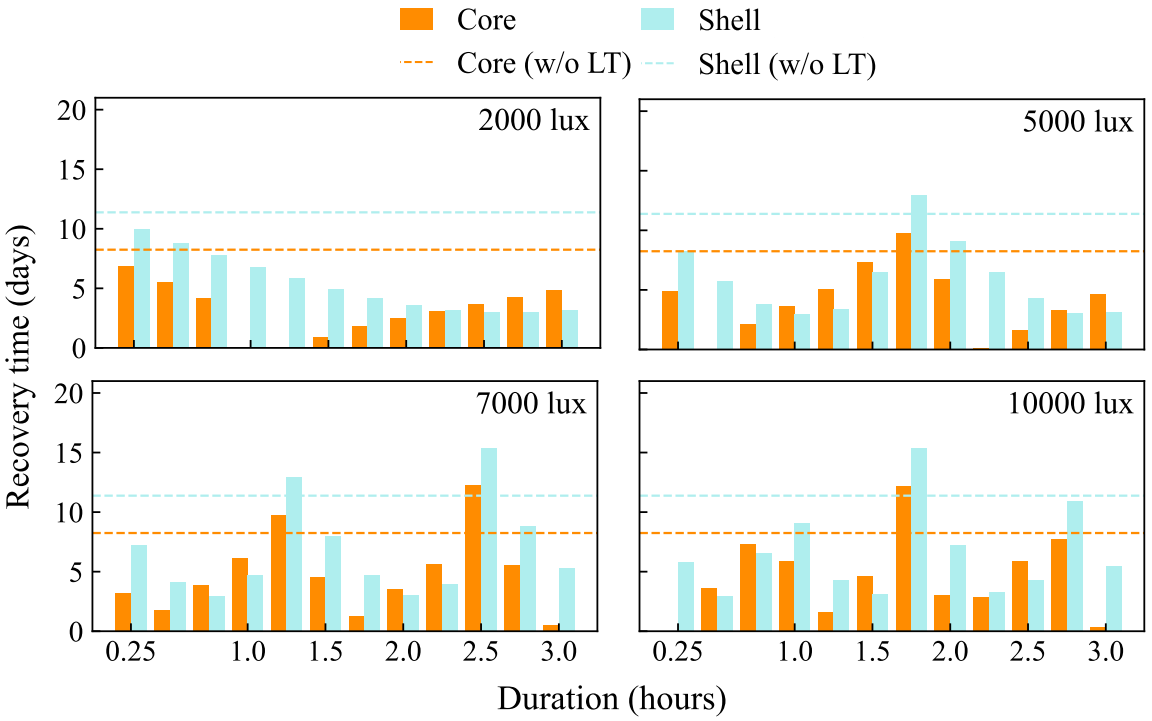

Figure A.1: Recovery times of the core (orange bars) and shell (blue bars) as a function of the LT duration for a 6 h eastward time shift and light intensity of a) 2,000 lux, b) 5,000 lux, c) 7,000 lux and d) 10,000 lux. The parameters used are the same as Figure 5.4. In the absence of the LT, the recovery times are shown by dashed lines.

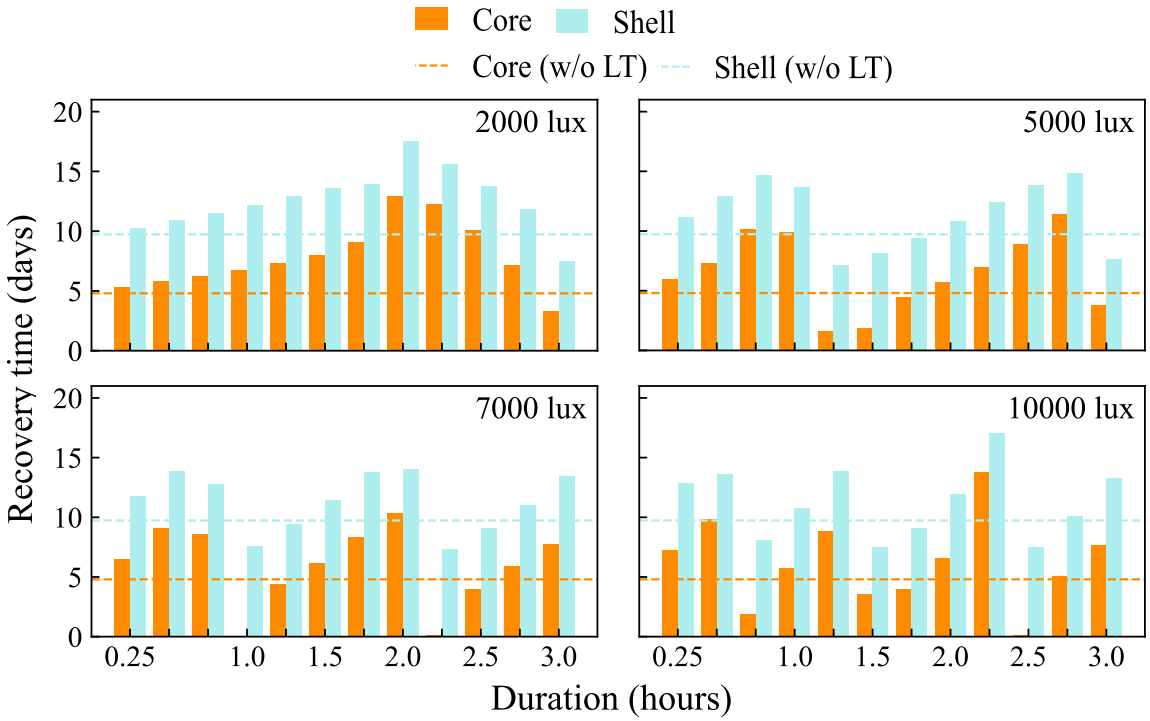

Figure A.2: Recovery times of the core (orange bars) and shell (blue bars) as a function of the LT duration for a 6 h westward time shift and light intensity of a) 2,000 lux, b) 5,000 lux, c) 7,000 lux and d) 10,000 lux. The parameters used are the same as Figure 5.4. In the absence of the LT, the recovery times are shown by dashed lines.

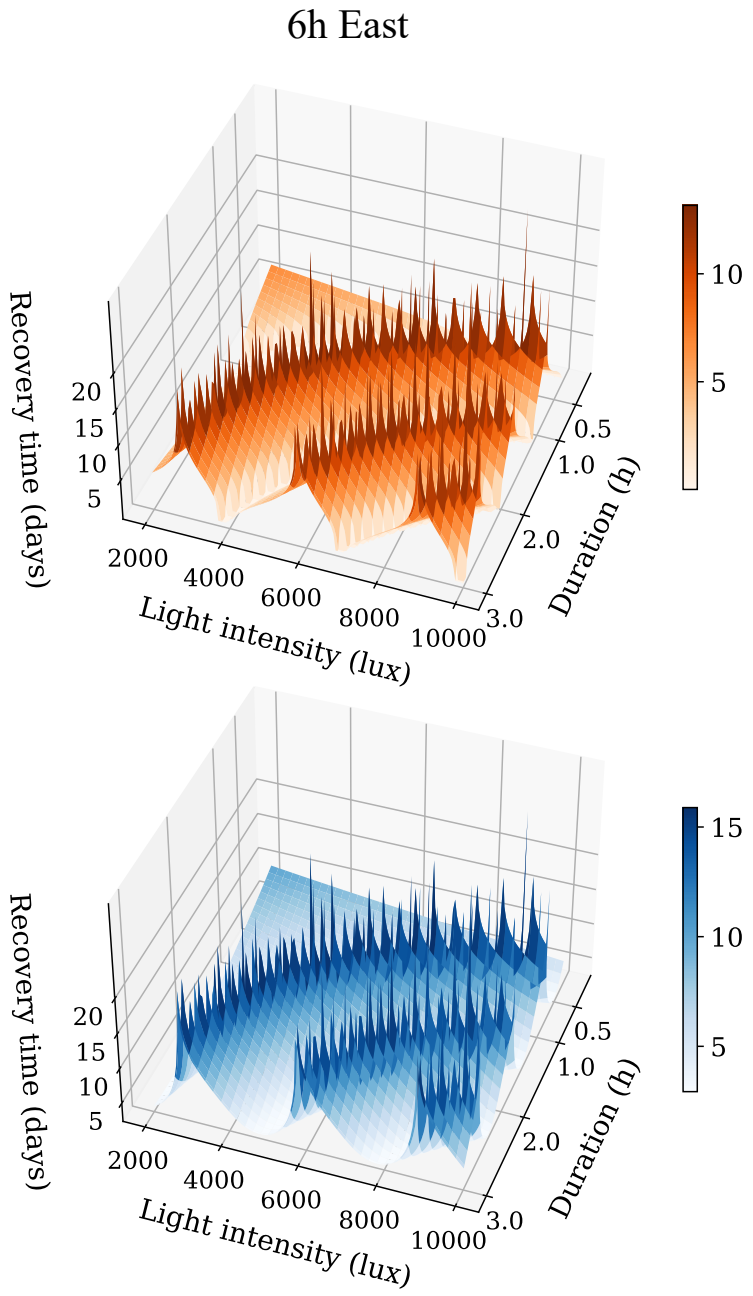

Figure A.3: 3D plots of the recovery time in days for a 6 h time shift to the east versus the LT light intensity and LT duration. The upper orange plot corresponds to the core and the lower blue one to the shell. The simulations were perfomed for $B = [2,000; 10,000]$ (lux), $\Delta B = 50$ (lux) and $D = [15/60; 3]$ h, $\Delta D = 1/60$ h. LT was administered at arrival time ($T = 0$). There is a side colourbar which indicates the correspondence of colour to a recovery time value.

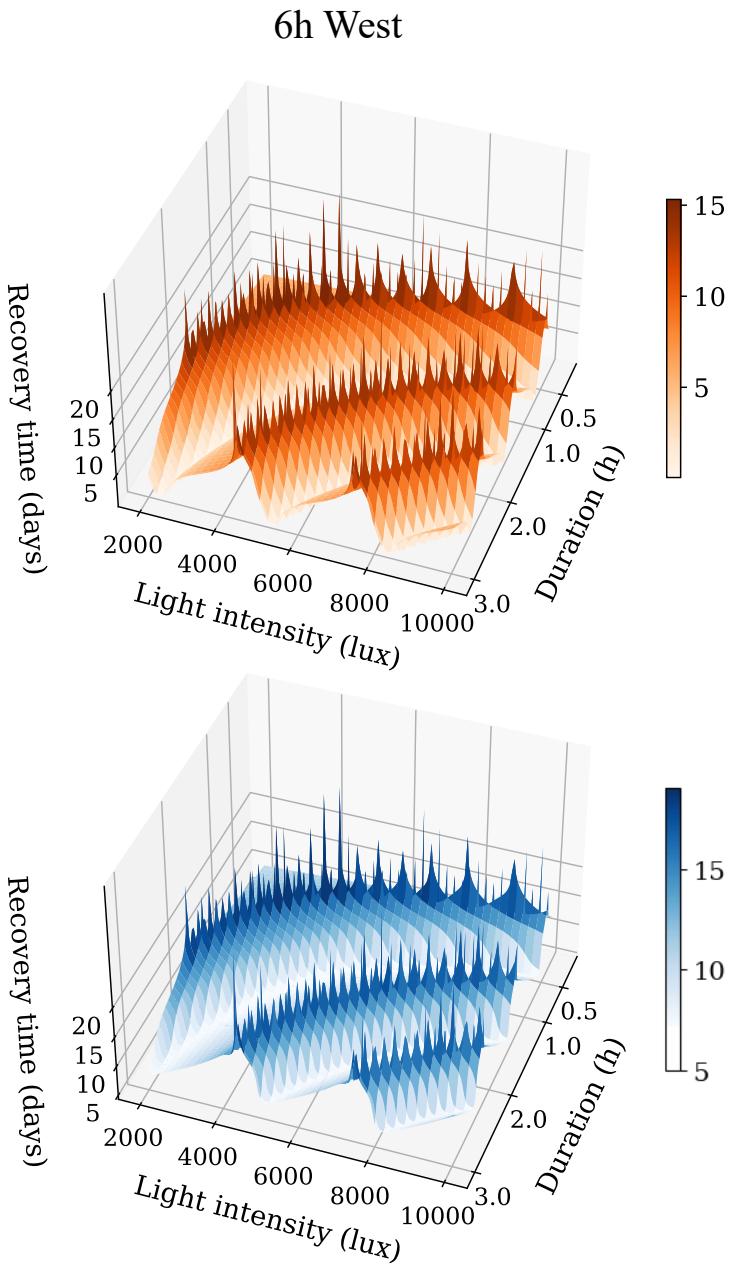

Figure A.4: 3D plots of the recovery time in days for a 6 h time shift to the west versus the LT light intensity and LT duration. The upper orange plot corresponds to the core and the lower blue one to the shell. The simulations were perfomed for $B = [2,000; 10,000]$ (lux), $\Delta B = 50$ (lux) and $D = [15/60; 3]$ h, $\Delta D = 1/60$ h. LT was administered at arrival time ($T = 0$). There is a side colourbar which indicates the correspondence of colour to a recovery time value.

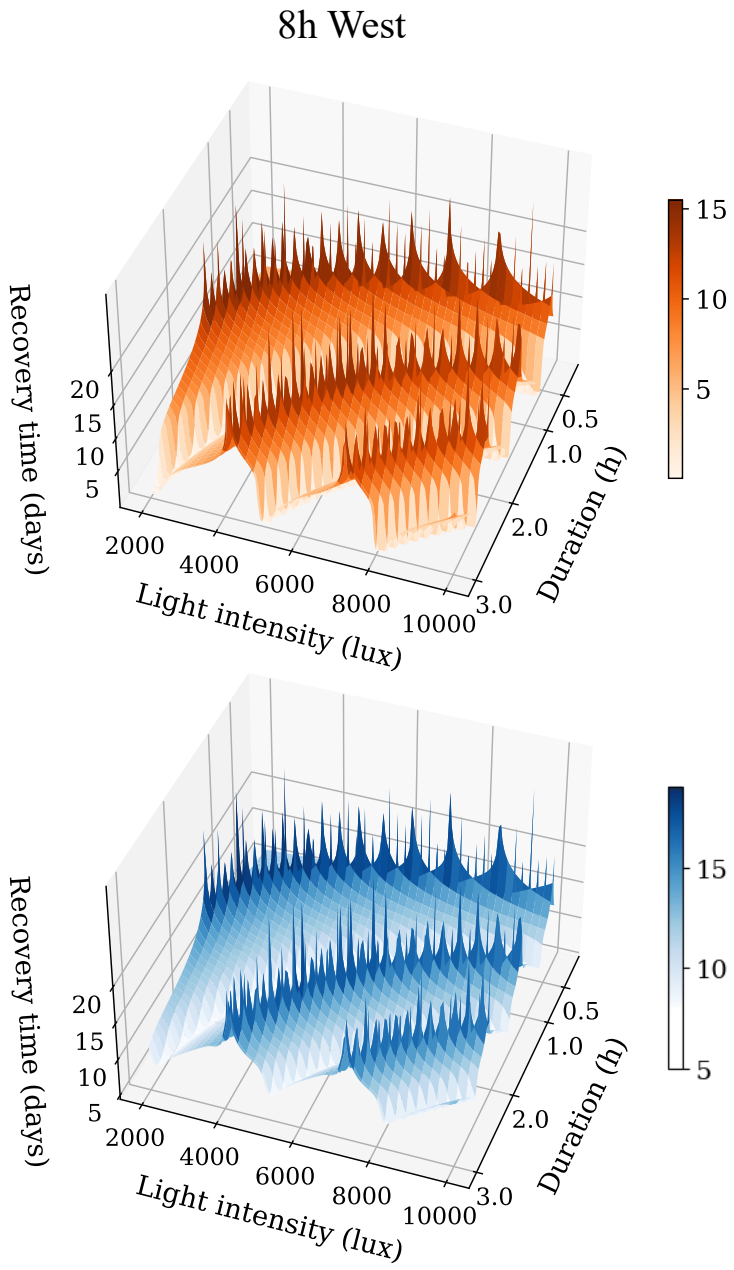

Figure A.5: 3D plots of the recovery time in days for an 8 h time shift to the west versus the LT light intensity and LT duration. The upper orange plot corresponds to the core and the lower blue one to the shell. The simulations were perfomed for $B = [2,000; 10,000]$ (lux), $\Delta B = 50$ (lux) and $D = [15/60; 3]$ h, $\Delta D = 1/60$ h. LT was administered at arrival time ($T = 0$). There is a side colourbar which indicates the correspondence of colour to a recovery time value.